CHARACTERIZATION OF CRAZING PROPERTIES OF POLYCARBONATE

Stephen Brett Clay

Dissertation submitted to the Faculty of the
Virginia Polytechnic Institute and State University
in partial fulfillment of the requirements for the degree of

Doctor of Philosophy
In
Engineering Mechanics

Dr. Ronald G. Kander, Chair
Dr. Edmund G. Henneke
Dr. Norman Dowling
Dr. Brian J. Love
Dr. Surot Thangjitham

August 15, 2000
Blacksburg, Virginia

Keywords: crazing, polycarbonate, technique, mechanical properties, microstructure, Design of Experiments (DOE)

CHARACTERIZATION OF CRAZING PROPERTIES OF POLYCARBONATE

Stephen Brett Clay

(ABSTRACT)

The purpose of this study was to characterize the craze growth behavior of polycarbonate (PC) as a function of stress level, model the residual mechanical properties of PC at various craze levels and strain rates, and determine if the total surface area of crazing is the sole factor in residual properties or if the crazing stress plays a role. To obtain these goals, a new *in-situ* reflective imaging technique was developed to quantify the craze severity in transparent polymers.

To accomplish the goal of craze growth rate characterization, polycarbonate samples were placed under a creep load in a constant temperature, constant humidity environment. Using the new technique, the relative craze density was measured as a function of time under load at stresses of 40, 45, and 50 MPa. The craze growth rates were found to increase exponentially with stress level, and the times to 1% relative craze density were found to decrease exponentially with stress level. One exception to this behavior was found at a crazing stress of 50 MPa at which over half of the samples tested experienced delayed necking, indicating competitive mechanisms of crazing and shear yielding. The draw stress was found to be a lower bound below which delayed necking will not occur in a reasonable time frame.

The yield stress, elastic modulus, failure stress, and ductility were correlated to crazing stress, relative craze density, and strain rate using a Design of Experiments (DOE) approach. The yield stress was found to correlate only to the strain rate, appearing to be unaffected by the presence of crazes. No correlation was found between the elastic modulus and the experimental factors. The failure stress was found to decrease with an increase in relative craze density from 0 to 1%, increase with an increase in crazing stress from 40 to 45 MPa, and correlate to the interaction between the crazing stress and the strain rate. The ductility of polycarbonate was found to

decrease significantly with an increase in relative craze density, a decrease in crazing stress, and an increase in strain rate.

The craze microstructure was correlated to the magnitude of stress during craze formation. The area of a typical craze formed at 40 MPa was measured to be more than 2.5 times larger than the area of a typical craze formed at 45 MPa. The fewer, but larger, crazes formed at the lower stress level were found to decrease the failure strength and ductility of polycarbonate more severely than the large number of smaller crazes formed at the higher stress level.

ACKNOWLEDGEMENTS

I would like to thank several people who have been a great help throughout my academic career. First, thanks are due to my advisory committee which includes Dr. Ronald G. Kander, Dr. Edmund G. Henneke, Dr. Norman Dowling, Dr. Brian J. Love, and Dr. Surot Thangjitham. I would especially like to thank Dr. Ronald Kander, my academic advisory chairman, for his technical support, research advice, and friendship.

I would also like to thank the Air Force Research Laboratory, especially Robert McCarty and the Next Generation Transparency team for making this all possible through funding, technical support, and patience. Dr. Arnold Mayer of the Air Force Research Laboratory is also due thanks for his excellent mentoring and good advice that helped my projects meet the deadlines. Special thanks are due to Chuck Blair for his excellent technical help, especially in designing, building, and troubleshooting equipment.

Several fellow students are due thanks for friendship and research ideas and suggestions. Some of these include Julie Dvorkin, Dr. Jennifer McPeak, Scott Steward, David Brooks, Sumitra Subrahmanyan, Julie Martin, Dr. Mitchell Jackson, Jeff Schultz , Derek Klinedinst, Scott Trenor, Kelly Renshaw, and Dan Esterly. Special thanks are due to Dr. Patricia Dolez for assistance with the TGA, Kelly Renshaw for sharing her DSC expertise, Dr. Yuseung Kim for acquiring GPC results, and Julie Dvorkin and Sumitra Subrahmanyan for editing assistance.

Finally, I would like to thank my Lord Jesus Christ for many answered prayers throughout the years of my research program. Also, my wife, Terry, and my kids, Joshua and Sarah are due thanks for their love, patience, and understanding during the long hours of schoolwork.

TABLE OF CONTENTS

LIST OF FIGURES

LIST OF TABLES

Chapter 1 INTRODUCTION

Polycarbonate (Figure 1) is a transparent thermoplastic with excellent toughness well below its glass transition temperature (T_g) of 145°C. One possible reason for its excellent toughness is the existence of a sub-T_g molecular dissipation mechanism showing up as a broad peak at -100°C in the loss modulus in dynamic mechanical thermal analysis [1].

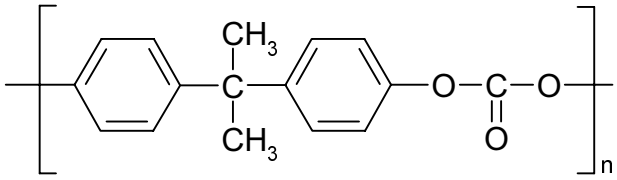

Figure 1: Standard repeat unit of polycarbonate

In the 1970's, the United States Air Force changed the structural ply in some of its advanced fighter and bomber transparency systems from glass and acrylic to polycarbonate. The transition was necessary to increase the capability of the windshield to withstand the high energy impact of birdstrikes. Over the years, one of the most common causes for replacement of the polycarbonate systems was excessive crazing.

The Air Force Research Laboratory (AFRL) is currently sponsoring a program that will revolutionize the manufacturing process for polycarbonate aircraft windshields and canopies. The Next Generation Transparency (NGT) program is developing the technology to injection mold a thick-walled transparency from a single mold (Figure 2). Instead of bolting a metal frame to the canopy perimeter like traditional systems, the new system will have a novel attachment concept, with one possibility for attachment being hardware molded into the thickened edges.

Although NGT will yield many benefits like lower cost, fewer components, improved optics, and significantly shorter change-out time, one concern is that the stress fields which exist on the frameless thermoplastic structure will be different from those experienced in the traditional framed transparency systems. These new stress fields are even more of a concern for

modern fighter and bomber jets which require a relatively large attachment force to ensure the external shape continuity required for stealth. These large attachment forces must be held during all flight hours and create large tensile stresses in certain areas of the transparency. Large tensile stresses often mean large amounts of crazing, but craze prediction models are lacking in the literature. This dissertation will develop a new technique to experimentally measure when and to what extent these stress fields will cause crazing and develop empirical models to predict stress induced crazing.

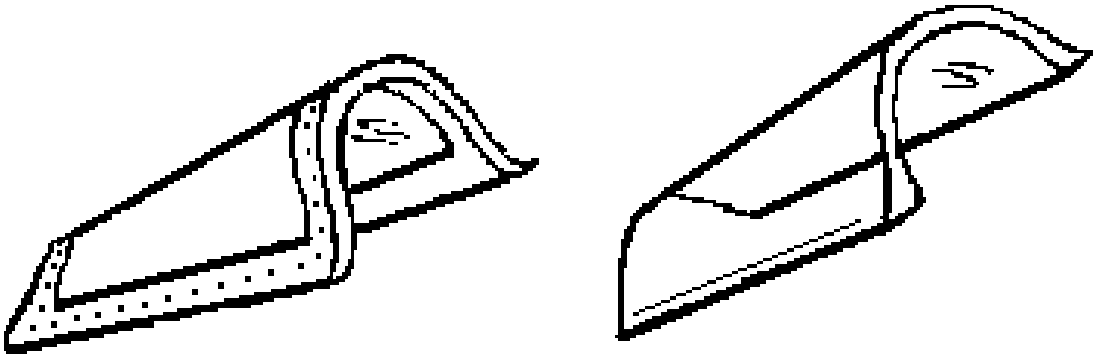

(a) **(b)**

Figure 2: (a) Traditional framed aircraft canopy and (b) frameless aircraft canopy

Crazes, which are crack-like defects in polymers approximately 0.5 μm wide consisting of a web of highly strained microfibrils, have been a subject of investigation for the past 30 years. One reason for such widespread interest is the fact that these defects are likely sites for crack initiation and often cause brittle failure of an otherwise ductile polymer. Crazing is even more prominent as polymers find their way into applications where they are replacing metals. Many of these new service environments contain craze accelerating agents such as solvents, high stresses, high temperatures, and high humidities.

Crazing is a form of localized plastic deformation [2]. Crazes are often mistaken for cracks because of their similarities: they form perpendicular to the principal stress direction, they act as mirrors by reflecting light off of their surfaces, and they fracture if a high enough stress is applied. The major differences between a craze and a crack are as follows: the craze face is covered by a web of microfibrils which bridge the craze surfaces and enable the craze to

carry some load, and intersecting crazes continue to grow, independent of one another instead of joining together [3]. Crazing has been described in literature as a "tortured plastic flow with a large number of voids" [3], "plastic deformation without significant lateral contraction" [3], "highly non-uniform deformation zones" [4], and "unstable local plastic deformation accompanied by volume expansion" [2].

To visually show crazing, two images were taken from the literature (Figure 3). Image (a) is a macroscopic view of crazing around a hole in a poly(methyl methacrylate) (PMMA) sample loaded in tension [5], while image (b) is a transmission electron micrograph of a polystyrene (PS) craze with clearly defined microfibrils spanning the two craze surfaces [6]. The macroscopic craze images to be presented later in this dissertation are very similar to image (a).

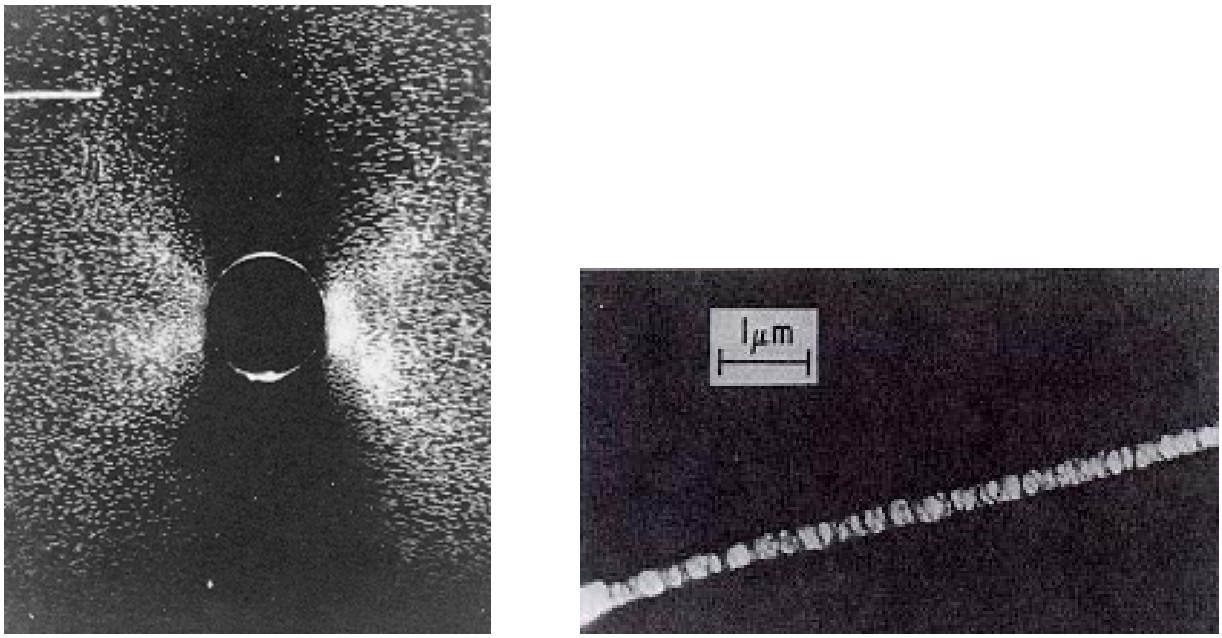

(a) **(b)**

Figure 3: (a) Macroscopic image of crazing around hole in PMMA sample loaded in tension [5], and (b) micrograph of single polystyrene craze with clearly defined fibrils [6]

It has already been stated that crazing is an important process to consider in designing and using a frameless aircraft transparency, especially in a military application where the extreme environments and loading requirements can produce very high stresses. The goals of this dissertation are to (a) characterize the craze growth behavior of polycarbonate as a function

of stress level, (b) model the residual mechanical properties of polycarbonate at various craze levels and strain rates, and (c) determine if the total surface area of crazing is the sole factor in residual properties, or if the crazing stress plays a role. The main steps to attain these goals are to:

1. develop and validate a technique to measure the craze density of transparent polymers,
2. characterize the craze growth behavior of polycarbonate at various crazing stresses,
3. develop a quantitative model of the residual mechanical properties of crazed polycarbonate in terms of crazing amount, crazing stress, and strain rate, and
4. correlate the results to craze microstructure.

Many aspects of polymer crazing are presented in the literature. They are illustrated in Figure 4 as cavitation, craze initiation, single-isolated craze growth, and bulk craze density growth.

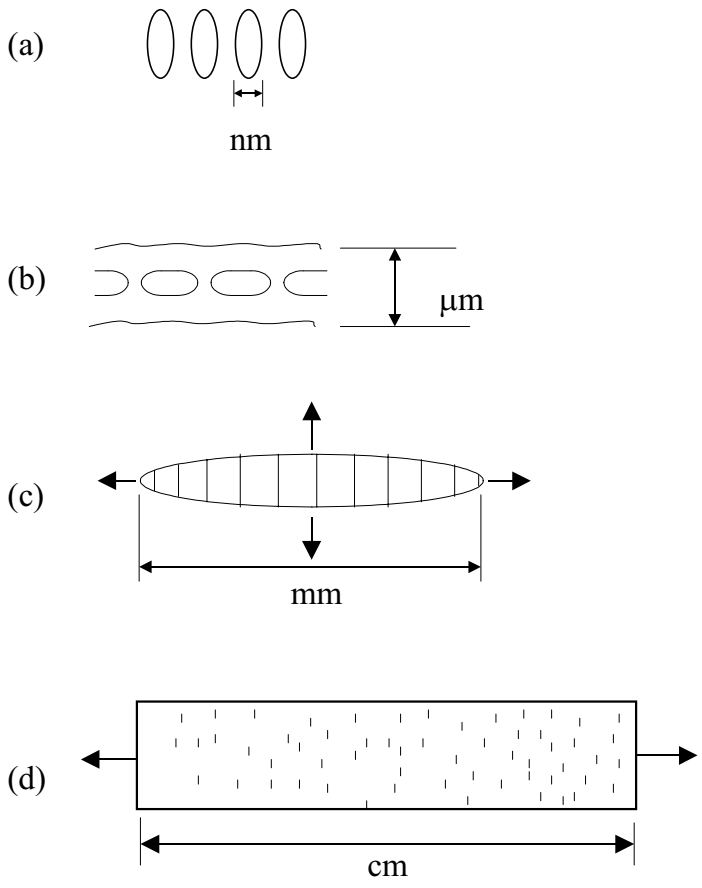

Figure 4: Aspects of craze research: (a) cavitation, (b) craze initiation, (c) single, isolated craze growth, and (d) bulk craze density growth

The majority of the literature discusses single craze initiation and growth, as illustrated in (b) and (c). This dissertation concentrates on the effect of bulk craze density on the mechanical properties of polycarbonate, as illustrated in (d). The bulk craze density growth rate exponentially increased as a function of stress, while the time to reach stable craze initiation decreased exponentially with increasing stress. Increasing the bulk craze density affected the properties related to fracture much more than the elastic or yield properties. For example, the yield stress and elastic modulus were insensitive to the presence of crazing while the failure strength and ductility decreased significantly with increased crazing.

Chapter 2 is a literature review of craze initiation and growth, environmental factors and material properties that affect crazing, and polymer degradation. Chapter 3 describes the development of the new technique to quantify crazing in transparent thermoplastics including the standard operating procedures for craze testing, mechanical property measurement, and thermal characterization. The experimental results for the craze growth rates as a function of stress are presented in Chapter 4. Chapter 5 discusses the effect of crazing on the mechanical properties of polycarbonate, including a quantitative Design of Experiments model. The conclusions and future work are presented in Chapters 6 and 7, respectively.

Chapter 2 BACKGROUND

2.1 Mechanisms of craze initiation and growth

This section of the dissertation will discuss the basic mechanisms believed to be occurring during the formation and development of crazes. The next section of this work will consider the external driving forces and material properties that effect these mechanisms.

2.1.1 Craze Initiation

Many papers have been published in an attempt to explain the initiation of crazes [7, 8], but there is still no universally accepted model for this mechanism. One difficulty in gaining insight to the initiation process is the size scale of crazes. It is believed that the first step is one of main chain motion and the formation of nanovoids that are precursors to crazes [9]. These voids are of the order of 30 nm and often form at stress concentrations like surface flaws or contaminant particles, although this is not always the case [7]. The process of these voids developing into the planar bands called crazes is not well understood. It has been postulated that the stress distribution in the region of one void causes the formation of more voids nearby, perpendicular to the maximum principal stress direction [8].

2.1.2 Craze growth

Craze growth will be discussed in detail in the following section, but an overview is provided here. Growth can be broken up into two components: (1) craze tip advancement and (2) craze thickening or widening [10]. Craze tip advancement probably occurs through the formation of more voids from the stress concentration at the tip. Craze thickening involves the drawing of craze fibrils from bulk polymer [11]. For a fibril to elongate, the polymer chains in the fibrils must experience a combination of chain scission and reptation [12]. This process will be discussed in more detail in the next section.

2.2 Craze growth factors

The crazing rate in polymers is dependent on several factors. Some of the known factors are stress, temperature, humidity, molecular weight, and molecular orientation. These factors

will all be discussed in this chapter but only the effect of stress, temperature, and humidity will be considered experimentally.

2.2.1 Effect of stress

It is commonly accepted that crazing can only occur in the presence of local tensile stress. The magnitude of stress is an important factor in craze behavior. The time to craze initiation decreases with increased stress, making it a viscoelastic property like creep [3]. Also, at low tensile stresses or strain rates, fewer crazes form, but those that do could grow to larger sizes. In contrast, in conditions of higher tensile stresses or strain rates, many smaller crazes form [3]. To illustrate the load-bearing characteristics of a craze, it has been found that crazes in PC can reach strains as high as 200% before fracture [3].

The effect of stress on PC crazing is important in military aircraft transparencies since they experience stress from many different sources, as shown in Figure 5 below. One source of stress during each flight is the pressurization of the cockpit. Stresses also result from extreme temperature fluctuations as the polymer tries to expand and contract more than the metal attachment hardware in a frameless transparency. Aerodynamic forces also produce stress in the windshield, though to a lesser degree.

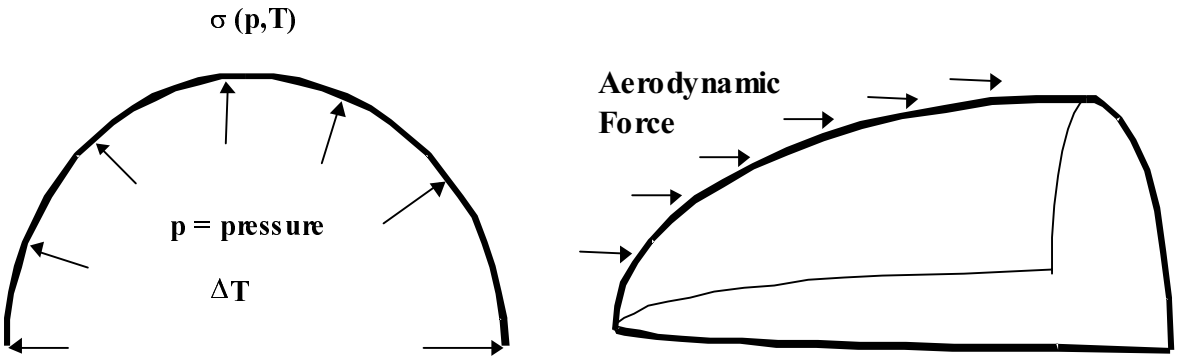

Figure 5: Sources of stress on military aircraft transparencies

Another source of stress in a frameless transparency for stealthy aircraft is the relatively large preload that must be maintained on the transparency to ensure external shape continuity between the transparency and the aircraft body. This stress is illustrated in Figure 6 which depicts the edge of a transparency in the region where it overlaps the airframe.

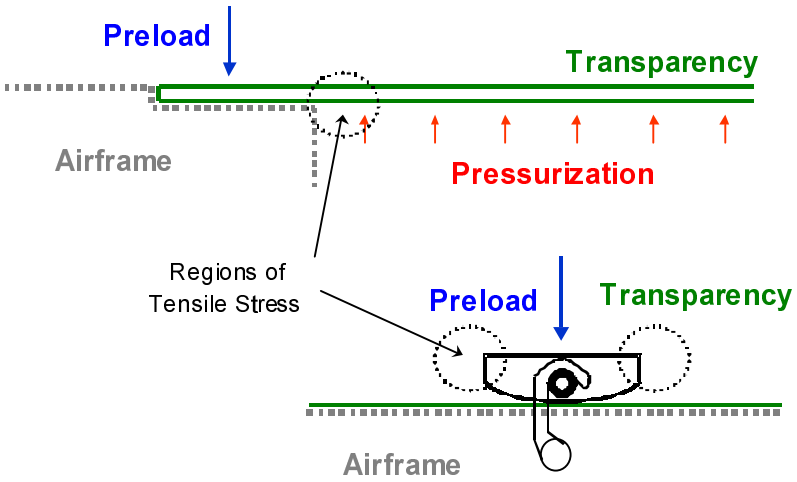

Figure 6: Regions of stress caused by preloading a frameless transparency to ensure external shape continuity

Several stress or strain based craze initiation criteria have been developed. Sternstein and Ongchin [13] produced a stress criterion based on the biaxial loading of PMMA. Their craze envelope is defined by

$$\sigma_b = A(T) + B(T)/I_1 \qquad (2\text{-}1)$$

where $\sigma_b = |\sigma_1 - \sigma_2|$ is the flow stress being twice the maximum shear stress where σ_1 and σ_2 are of opposite sign. $I_1 = \sigma_1 + \sigma_2 + \sigma_3$ is the first stress invariant, and A and B are temperature-dependent constants [13]. One problem with this criterion is that the use of $\sigma_1 - \sigma_2$ implies the direction of maximum shear stress, but crazes form perpendicular to the maximum principal normal stress.

Gent [14] developed a craze initiation criterion based on the assumption that the dilatational stress at a flaw increases the free volume and decreases the local T_g of the material to the temperature of testing, making the stress-softened material unprotected from cavitation. Gent's model is given by

$$\sigma_c/3 = [\beta(T_g - T) + P] / k \qquad (2\text{-}2)$$

where σ_c is the critical applied tensile stress, β is the hydrostatic pressure coefficient of T_g, T is the test temperature, P is the applied hydrostatic pressure, and k is the stress concentration factor relating the applied stress to the micro-stress at the flaw tip.

Crazing has already been categorized as a viscoelastic deformation process like creep and stress relaxation involving multiple localized deformation sites instead of bulk deformation. A theory has been developed in an attempt to describe creep and stress relaxation properties as thermally activated rate processes [5]. It is possible that this theory could also apply to craze growth since similar changes in the polymer must occur in both crazing and creep, only to a smaller degree. The theory begins with the Arrhenius equation, as shown in Equation 2-3, which generally describes how the temperature affects the frequency of thermally activated processes, such as chemical reactions.

$$\nu = \nu_o \exp(-\Delta H / RT) \tag{2-3}$$

where ν is the frequency of the chemical reactions, ν_o is a constant, ΔH is the activation energy required to overcome the potential energy barrier for a given process, R is the gas constant, and T is the absolute temperature. For crazing, the energy barrier comes from the requirement of the polymer molecules to slide past other chains (via reptation) and to undergo conformational changes.

Building on the Arrhenius equation, a model was developed to describe the effect of an applied stress on a thermally activated rate process [5]. The applied stress is believed to produce changes in the potential energy barrier in a way that decreases the height of the barrier in the direction of flow, enhancing reptation and conformational changes necessary for crazing. The changes to the potential energy barrier are shown in Figure 7.

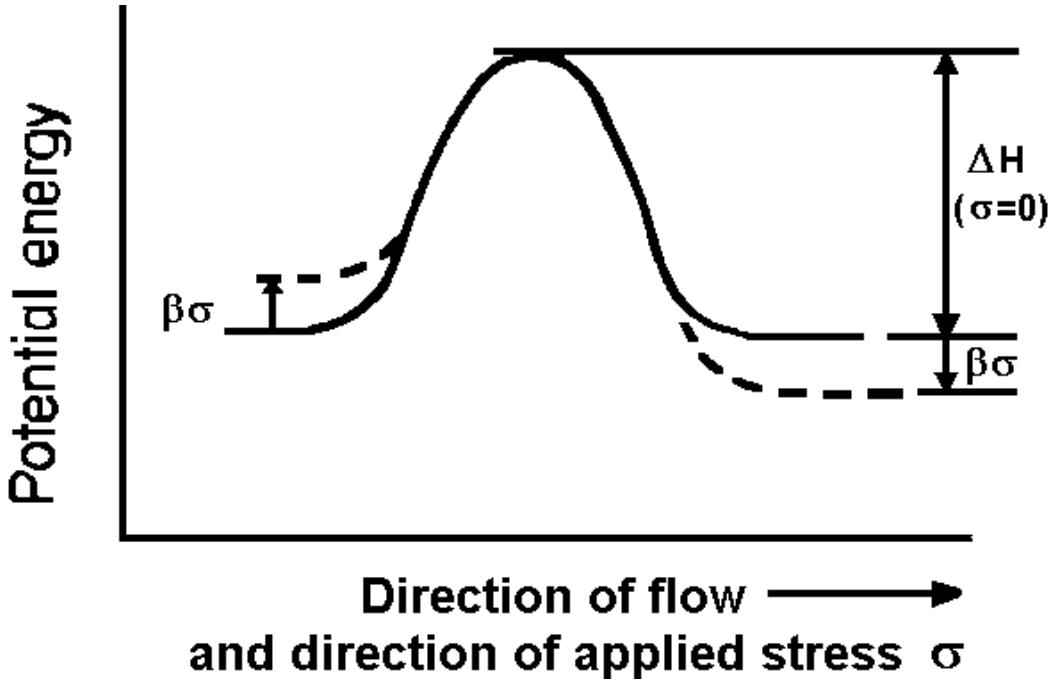

Figure 7: Effect of applied stress to the potential energy barrier of a thermally activated rate process [5]

The Eyring equation was developed to describe the strain rate in the direction of the applied stress in a thermally activated deformation process. The Eyring equation that applies when the term νσ/RT is large is

$$\dot{e} \approx \frac{\dot{e}_o}{2} \exp\left(-\frac{\Delta H - \nu\sigma}{RT}\right) \qquad (2\text{-}4)$$

where $\dot{e}$ is the strain rate, $\dot{e}_o$ is a constant, ν is an activation volume, ΔH, R , and T are defined as above, and σ is the applied stress. This equation mathematically models the changes in the energy barrier due to an applied stress.

Most of the above criteria were developed in the 1960's and 1970's. More recent models of craze behavior will be presented in later sections of this dissertation. The more contemporary criteria include effects of stress, strain, temperature, molecular weight, and entanglement density.

2.2.2 Effect of moisture

Extensive research has been performed to determine the effect of solvent exposure on the craze behavior of polymers [7, 10, 15 - 17]. The time for polymer crazes to initiate decreases in the presence of some vapors or liquids. Two possible explanations for this relationship are that the small molecules of the solvent weaken the intermolecular forces of the polymer chains and the surface energy is lower in the presence of the liquid [7, 16 - 19],. The general conclusions for the first explanation are that the liquid diffuses into flaws and plasticizes the polymer, making it vulnerable to cavitation [20]. For the second possible explanation, the reasoning is that lowering the surface energy makes void formation easier [7].

The most widely accepted theory of craze initiation and growth in the presence of a solvent is called the meniscus instability model. It was developed by Argon and Salama [9 - 11]. The principle of meniscus instability is the phenomenon that occurs with a climbing liquid in a capillary tube. In a craze, the material in the tip is plastically deformed and acts as the liquid in the meniscus model. The surface energy of the interfaces governs the instability. The interfacial surface energy decreases if a solvent enters the craze and replaces the air, causing the instability to increase and the craze to grow at a higher rate. This explanation agrees with experimental evidence.

Craze thickening can also be explained with meniscus instability[10]. The model describes a region of material a few nanometers thick between the fibrillated and bulk polymer. A series of menisci are formed in this region from negative hydrostatic tension. This process describes the formation of surface drawn fibrils. Craze growth kinetics are related to the magnitude of the hydrostatic tension.

This study will not consider the typical organic solvents that have been frequently cited [7, 10, 15 - 17, 19, 20]. The assumption is that exposure to common craze accelerating solvents will be limited in application, and that their effects are already well documented. This study will concentrate on the effect of moisture on the craze behavior of polymers. Previous research has

concluded that moisture produces changes in the crazing rate similar to organic solvents, but to a lesser degree [16, 21, 22].

Arnold [16] studied the effect of water absorption on the strength of poly(methyl methacrylate) (PMMA). She found that the failure stress decreased after being immersed in water, similar to the effect of exposure to ethylene glycol. Another observation reported by Arnold was that craze initiation was longer for samples that were immersed in water for longer amounts of time prior to loading. Two possible reasons for this behavior are that (1) during the long immersion times, the absorbed water blunts the flaws, or (2) the surface eventually develops compressive stresses, making it more difficult for crazes to form.

Josserand, et al. [21], studied the effect of moisture on the fracture of PMMA. They found that the diffusion of water into PMMA is governed by Fick's law, but state that the time to diffuse into the fibrils could be much faster than the time to saturate the bulk polymer since the craze fibrils have such a large surface-to-volume ratio. In their study, water behaved like a plasticizer by lowering the glass transition temperature (T_g), tensile modulus, and yield strength of the polymer. They found that the lifetime of a craze fibril immersed in water was three orders of magnitude lower than that in dry air.

Notomi et al. [22] found similar results for PS and styrene/acrylonitrile (SAN). They concluded that the absorption of moisture decreased the stress required for crazing, causing increased amounts of crazing compared to dry polymers.

2.2.3 Effect of temperature

It is very important for military aircraft transparencies to determine the temperature effect on PC craze. Military aircraft are stationed all over the world in a wide variety of climatic exposures. Also, during flight, the transparency experiences extreme temperature fluctuations ranging from exposure to very cold air at high altitudes to aerodynamic heating effects at supersonic speeds. A calculated temperature profile for a typical Mach 2.5 flight is shown in Figure 8 below.

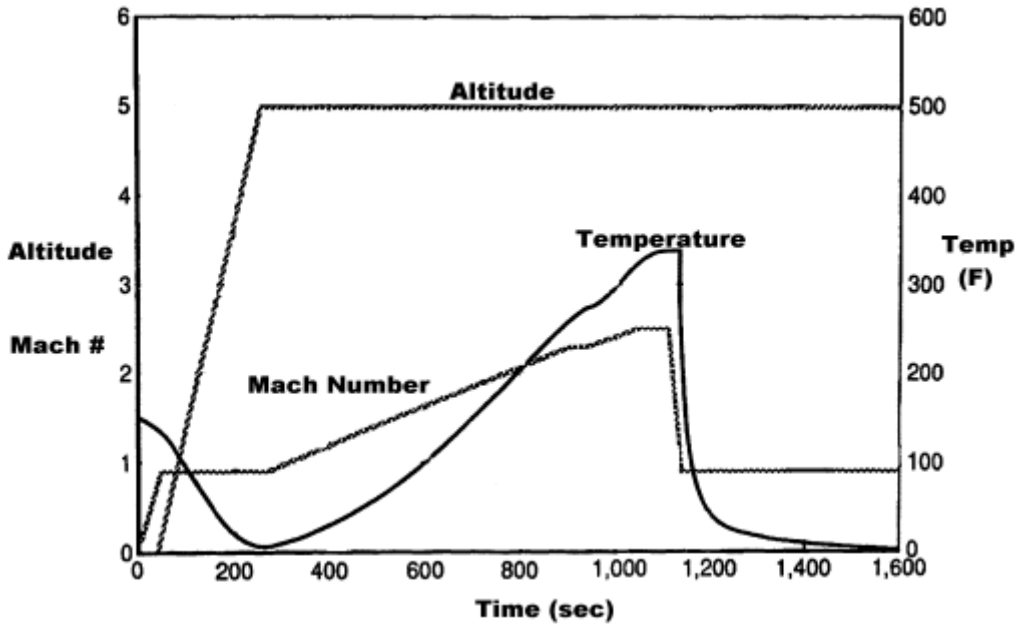

Figure 8: Mach 2.5 thermal profile of transparency skin temperature

Figure 8 shows that the temperature ranges from 0°F up to a maximum of about 330°F. The calculated maximum temperature on the graph is slightly above the T_g of PC (≈300°F), but the transparency only experiences this temperature for a very short period of time. The graph shows that as the altitude increases, the temperature begins to decline. This continues until the aerodynamic friction from the increased speed dramatically increases the skin temperature of the transparency.

Increased temperature has been found to increase the crazing rate of polymers. Devins and Reed [23] found that the critical strain for initiation of craze linearly declined to near zero as the temperature was increased to near T_g. Their model showed that the stress (or strain) required for craze initiation is a function of temperature.

In the study in which Iisaka [20] exposed PC to di-n-octylphthalate and adipic acid polyester, it was found that the time to initiate craze at a given strain decreased as the temperature rose. When the craze initiation time was very long, the lower limit for the critical craze initiation strain approached the same value at all temperatures. This result is similar to a previous study where the estimated minimum surface energy required for various solvents to propagate a void decreased with increasing temperature until a characteristic temperature, T_c, was reached. Above T_c the minimum surface work remained constant.

Other studies have shown that a temperature gradient through the thickness of a polymeric part can cause the residual stresses on the surface of injection molded parts to become less compressive and possibly even become tensile [24 - 26]. This change drastically increases the crazing rate in a polymer since crazing occurs in the presence of tensile stress.

2.2.4 Effect of molecular weight

One of the most important factors affecting craze behavior is intermolecular entanglements. Entanglements refer to the interaction between long polymer molecules which limit chain mobility. In contrast to crosslinking, no primary chemical bond exists at the entanglement point. The ability of a polymer to form entanglements depends on molecular weight. Each polymer has a critical entanglement molecular weight (M_e), below which the chains are too short to entangle. If the modulus of the rubbery plateau in a modulus/temperature plot is not a function of molecular weight, then it can be assumed that the entanglement molecular weight is also independent of the bulk molecular weight [2]. The entanglement density is defined as the number of entanglement points per unit volume. PC has a high entanglement density due to its stiff molecules containing benzene rings in the chain backbone.

Many recent studies have determined that entanglements play a dominant role in craze resistance. To form the microstructure of a craze, the polymer must undergo entanglement loss, either by chain scission or disentanglement [4]. Ishikawa found that the critical stress to initiate crazing is directly proportional to molecular weight. He related this finding to the fact that the melt viscosity increases with increased molecular weight due to a greater amount of intermolecular interactions. He concluded that crazing involves disentanglement due to the slippage of polymer molecules from the high dilatational stresses present [2].

McLeish [4] also determined that entanglements play a role in crazing from the fact that critical molecular weights have been found below which stable crazes cannot form. These critical craze molecular weights are on the same order of magnitude as the entanglement molecular weight. The model developed by McLeish consists of a segment of a long polymer chain anchored on a growing craze fibril. As the fibril grows, it pulls on this chain segment forcing the long polymer chain to disentangle along its contour. The expression for this model is given below by

$$S_c \approx [\sigma_{yd0}(T)\,(M/M_e)\,(\dot{\varepsilon}/\dot{\varepsilon}_c)^{1/n}\,\Gamma_d]^{1/2} \qquad (2\text{-}5)$$

where S_c is the bulk crazing stress, σ_{yd0} is the yield stress for molecules of entanglement molecular weight M_e, M is the molecular weight, $\dot{\varepsilon}_c$ is the critical local deformation rate, $\dot{\varepsilon}$ is the local strain rate at the critical stress, n is a scaling parameter, and Γ_d is the surface energy for a disentanglement-dominated craze. Γ_d is defined as

$$\Gamma_d = \gamma + w\,(\dot{\varepsilon}/\dot{\varepsilon}_c)\,(M/M_e)^{3/2}\,d\,\nu_e \qquad (2\text{-}6)$$

where γ is the van der Waals surface energy, w is the contribution of single entanglement length to the disentanglement dissipation, ν_e is the entanglement density, and d is the spatial separation of linked entanglements. The authors claim that, since PC has a high entanglement density, γ is negligible and $S_c \approx M^{5/4}$.

Plummer and Donald [27], looked at shear deformation and crazing of PC that was aged for various amounts of time at 130°C. They defined the localized shear deformation as deformation zones (DZ). They found the following relationships:

(1) A transition from DZ's to crazing occurs with increasing temperature.
(2) Critical strain for craze initiation does not depend on aging time.
(3) The DZ/craze transition temperature is inversely proportional to aging time.
(4) The critical craze strain increases with molecular weight at a given temperature just above the transition temperature.
(5) The transition temperature is independent of molecular weight and weakly dependent on temperature in higher temperature regions.
(6) Decreasing the strain rate lowers the critical strain for craze initiation and the transition temperature.

The authors noted that the crazes in low molecular weight material became unstable at low strain rates near the T_g by forming cracks soon after initiation. They measured the craze extension ratio, λ_{craze}, and found it to be constant along the length of the craze. They concluded that craze widening, which involves the formation and extension of fibrils, is brought about by

drawing the bulk polymer instead of by fibril creep. If fibril creep occurred, then the extension ratio of the fibrils formed first would eventually be greater than the newly formed fibrils. Also, for PC, which has a high entanglement molecular weight, experimental evidence shows a molecular weight dependence of crazing. Since disentanglement is expected to depend on molecular weight while chain scission and shear flow are not, they believe that PC exhibits disentanglement-dominated craze growth.

2.2.5 Effect of molecular orientation

Shonaike and Reed [28] conducted a study to determine the effect of cold rolling on the crazing rate of polycarbonate. They began with 25 mm thick material and continuously cold-rolled the plates until a thickness of 1 mm was obtained. This processing caused the polymer molecules to align in the direction of rolling. Their results showed that between 0% and 50% pre-orientation, the crazes found in samples after uniaxial failure in a cold environment showed higher length and density for lower pre-orientation. For samples pre-oriented 75%, no evidence of crazing was seen.

Similar to cold-rolling, some pre-orientation is expected for injection molded parts since polymer chains in the softened resin passing through the injection gate align in the direction of flow. Therefore, similar results are expected in an injection molded transparency as found in the study cited above. Specifically, it is believed that tensile stresses in the mold flow direction should give rise to lower crazing rates compared to stresses in the transverse direction.

2.3 Crazing versus Shear Yielding

The normal deformation mechanism for polycarbonate is shear yielding. Shear yielding is a ductile process involving large scale molecular motion during which the bulk polymer necks down to a significantly smaller cross sectional area [5]. During this process, polycarbonate generally elongates to approximately 110% of its original length. In contrast to shear yielding, polycarbonate also crazes, which involves only very localized plastic deformation zones as described above. A craze-dominated failure will exhibit more brittleness than the typical yielding behavior. It has been found that crazing and shear yielding are competing mechanisms in polycarbonate and govern whether the failure mechanism is ductile or brittle [5, 6, 29].

2.4 Mechanical Properties of Crazed Material

The crazing literature concentrates on the initiation and growth of crazes, but is incomplete in the area of determining the effect of crazes on the mechanical properties of polymers. One obvious reason for this void is the absence of a universally accepted technique to measure the amount of crazing on a polymeric sample. Since this dissertation is devoted to measuring the residual mechanical properties of crazed polycarbonate, a technique to quantify the amount of crazing was developed as described in Chapter 3.

One attempt to predict the effect of crazing on the mechanical properties of polystyrene (PS) was presented by Tang and coworkers [30]. They used the finite element method (FEM) to predict the elastic modulus in the craze fibril direction (E_1), the elastic modulus perpendicular to the fibril direction (E_2), the shear modulus (G_{12}), and Poisson's ratio (ν_{12}) of crazed PS.

In their model, they could only consider uniform, low density crazes due to software limitations. Specifically, Tang, et al., found that crazed polymers have lower strength since crazes have a lower modulus and higher porosity than the undamaged bulk polymer. They found that E_1 decreased significantly, ν_{12} and G_{12} decreased slightly, and E_2 was not affected. These results show that the properties perpendicular to the crazes are most affected, which could be expected. For this reason, all of the results reported in this dissertation are in the direction perpendicular to the craze surfaces.

2.5 Polymer Degradation

To ensure that the reduced mechanical properties were actually due to the crazes and not a result of polymer degradation due to physical aging or chemical reactions, differential scanning calorimetry (DSC), thermogravimetric analysis (TGA), and gel permeation chromatography (GPC) experiments were conducted before and after the craze growth tests.

2.5.1 Differential scanning calorimetry

DSC is a thermal technique commonly used to measure transitions in polymers like the glass transition temperature and melting temperature [31]. In its most common uses, polycarbonate is an amorphous thermoplastic with a glass transition temperature around 145°C.

The free volume theories used to explain the physical aging process of polymers indicate that when aging occurs, the free volume in the polymer decreases. With lower free volume there

is a decrease in molecular mobility which leads to changes in mechanical properties of the polymer and an increase in the glass transition temperature [5, 6, 32]. This occurs because the polymer needs to reach a higher temperature to produce large scale molecular motion when less free volume is available for chain movement. Thus, changes in the T_g provide important information for the detection of physical aging, and DSC was used to measure shifts in the T_g.

A general description of the DSC technique is given by considering the meaning of each of the three words. (1) Calorimetry implies the measurement of heat capacity (C_p). (2) Scanning implies that a temperature range is being scanned, making sure to include the desired transition temperature. (3) Differential describes the process since it looks at the difference between the heat capacity of an empty pan and the heat capacity of a pan/sample combination [33].

The glass transition is seen as a characteristic jump in the heat capacity. This is because the heat capacity in the rubbery state (above T_g) is larger than the heat capacity in the glassy state (below T_g). The rubber has a larger heat capacity since it includes rotational, vibrational, and conformational contributions while the glass heat capacity only includes contributions from rotations and vibrations (Figure 9). The absence of conformational energy in the glass is due to the fact that below the glass transition, the conformational changes of the polymer are negligible since the energy level is too low to permit the cooperative motion of a large number of chain segments [33].

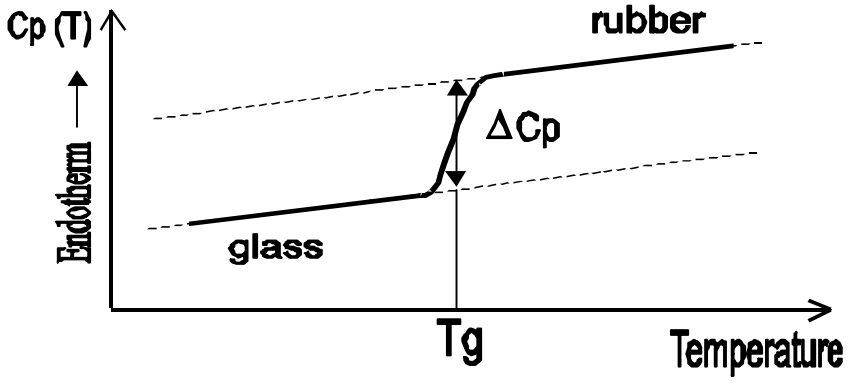

Figure 9: Conceptual graph of DSC scan

2.5.2 Thermogravimetric analysis

TGA is another thermal technique commonly used to characterize polymers. In contrast to DSC, thermal transitions are not detected in TGA, but chemical reactions that could cause degradation [6, 34]. A TGA analysis is performed by placing the polymeric sample in the furnace and measuring the mass loss with a sensitive balance as the temperature is increased [31]. The experiment is complete when no more changes are observed. A difference in a TGA scan between the as-received material and post-test material could show that degradation has occurred that may not be attributed to crazing.

2.5.3 Gel permeation chromatography

GPC is a size exclusion technique commonly used to characterize the molar mass distribution of polymers[6]. The popularity of GPC comes from its simplicity and the fact that an entire molar mass distribution can be obtained rather than just an average. A GPC experiment is performed by passing a polymer in solution through a stationary column containing various sized pores. As the polymer passes through the pores, the smaller molecules take longer to reach the end of the column since they are able to travel through many more of the smaller pores than the larger molecules. A detector at the end of the column measures the concentration of the solution as a function of time. The retention time gives a distribution of molecular weight relative to the polymer used for calibration[6].

As mentioned before, degradation involving chemical reactions could be occurring like molecular rearrangement or chain scission. Shifts in the molecular weight distribution between the as-received and post test material could indicate that such changes have taken place.

2.6 Humidity Control

One technique to control the humidity is to place saturated salt solutions in a closed environment. The control variable of relative humidity (RH) is defined by Equation 2-7 as the vapor pressure of water divided by the saturation vapor pressure over water at a given temperature [35]. As the temperature increases, the air is able to hold more water. Therefore, for a given mass of water vapor in the chamber, the RH changes with changes in temperature.

$$RH = \frac{P_w}{P_{ws}} \times 100 \tag{2-7}$$

An environment in equilibrium with a salt solution has a different RH level than an environment in equilibrium with pure water because the concentration of water vapor in the air is lower. This is due to the lower chemical potential of water in the aqueous salt solution [36].

Greenspan [37] published experimental RH results of 28 different saturated solutions of binary salts ranging from RH values of 3.39% to 97.88% at 25°C. Two salts commonly used to calibrate RH sensors are lithium chloride (11.30% RH at 25°C) and sodium chloride (75.29% RH at 25°C) [35].

Some advantages and disadvantages of using salt solutions will now be considered. The main advantages include simplicity, cost, no chance of equipment malfunction, and little change in RH with changes in temperature, as shown in Table 1.

Table 1: Effect of temperature on RH values of salt solutions [37]

Temperature (°C)	Lithium Chloride (%RH)	Sodium Chloride (%RH)
10	11.29 ± 0.41	75.67 ± 0.22
15	11.30 ± 0.35	75.61 ± 0.18
20	11.31 ± 0.31	75.47 ± 0.14
25	11.30 ± 0.27	75.29 ± 0.12
30	11.28 ± 0.24	75.09 ± 0.11

The primary disadvantages are accidental splashing on samples that causes salt absorption which could affect polycarbonate properties, poor dehumidification, and long RH equilibration time after each opening of the environmental chamber.

Chapter 3 EXPERIMENTAL

3.1 Development of a technique to measure the craze density of transparent polymers

Previously, a wide variety of techniques have been employed to study crazing behavior in polymers. The most basic detection method that has been used is visual observation [38 - 40]. This approach yields a good qualitative approximation of craze initiation in cases of exposure to certain organic solvents that cause extreme amounts of crazing in a short period of time. Many studies have also made use of microscopic techniques, both *in-situ* [41 - 43] and post-test [28, 39, 44, 45]. The *in-situ* observations typically yield a qualitative result while some of the post-test studies report quantitative crazing data on the failed samples.

Hockings and Task [46, 47] have separately attempted to quantify the damage on a crazed surface by detecting the amount of a directional test light reflected by the craze openings. The resulting "craze index" has been shown to be a good method of comparison, but has not been correlated to the craze density. Some limitations to this method are the ineffectiveness in measuring low amounts of crazing and the need to place the instrument in close contact with the surface being measured. Placing the measurement device close to the test specimen limits the testing environment since the sensitive instrumentation cannot survive extreme conditions of temperature and humidity.

Another technique, known as "departure points", has been used effectively to detect craze initiation during solvent-stress testing [48, 49]. Constant strain rate tests and creep tests were performed in both air and a testing solvent. The point where the solvent tests diverged from the tests in air was determined to be the point of craze initiation. Although this method is valuable to measure craze initiation behavior, it yields no information about craze propagation.

In 1995, Volynskii and Bakeev [10] published an entire book devoted to solvent crazing of polymers. One reason that they avoided studying dry crazing was that the standard experimental procedure involved the use of transmission electron microscopy (TEM). The major drawback was that the preparation and procedure for TEM is complicated and requires extremely thin samples (0.5-1.0 μm) which do not necessarily represent the behavior of bulk polymer.

It is necessary to develop a new method to detect and measure crazing in a more quantitative way to be able to develop a failure criterion based on craze severity instead of just craze initiation. The technique to be developed in this study is an *in-situ*, quantitative, non-subjective, direct measurement of relative craze density (amount of surface crazing per unit surface area). Since the measurement instrumentation is located outside of the environmental chamber, the only restrictions on the testing environment are those related to the limiting of visibility. This combination of traits permits a quantitative measurement of the rate of increase in craze density as a function of various testing parameters.

The new technique developed is conceptually simple. A polycarbonate sample, in the form of an ASTM D638 type III tensile bar (Figure 10), is placed under a constant load at constant temperature and relative humidity. While under load, a reflective imaging craze measurement system (Figure 11) is used to measure the crazing in the gage section at a pre-determined sampling rate. The measurement system consists of a CCD camera integrated with a Matrox Meteor frame grabber board and Visual Basic control software. The maximum image acquisition rate, without interruption of other data acquisition and control, was found to be 0.1 Hz. The images are monitored real-time, stored, and analyzed after testing.

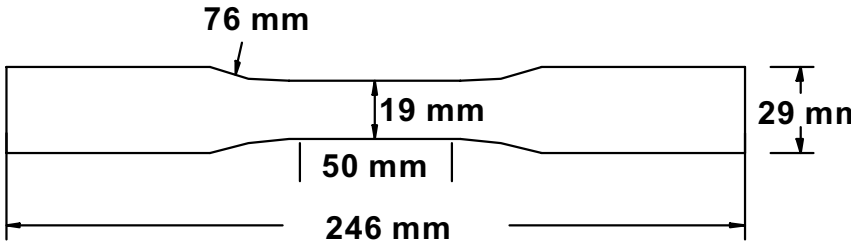

Figure 10: ASTM D638 type III tensile specimen geometry [50]

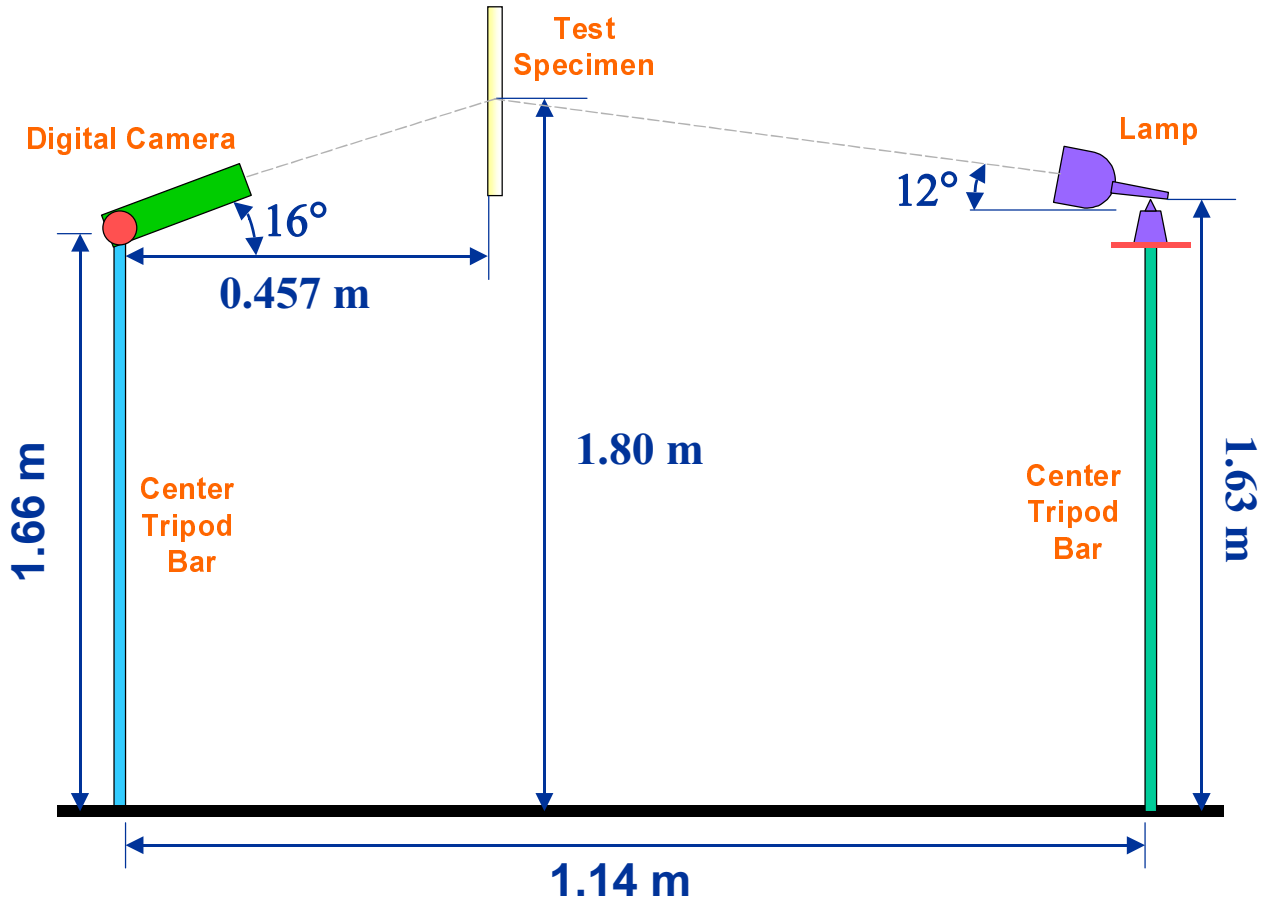

Figure 11: Reflective imaging craze measurement system

The concept is that the crazes on the sample surface act as tiny mirrors and reflect the light. The reflections are detected by the CCD camera. A typical image of crazed polycarbonate is shown in Figure 12.

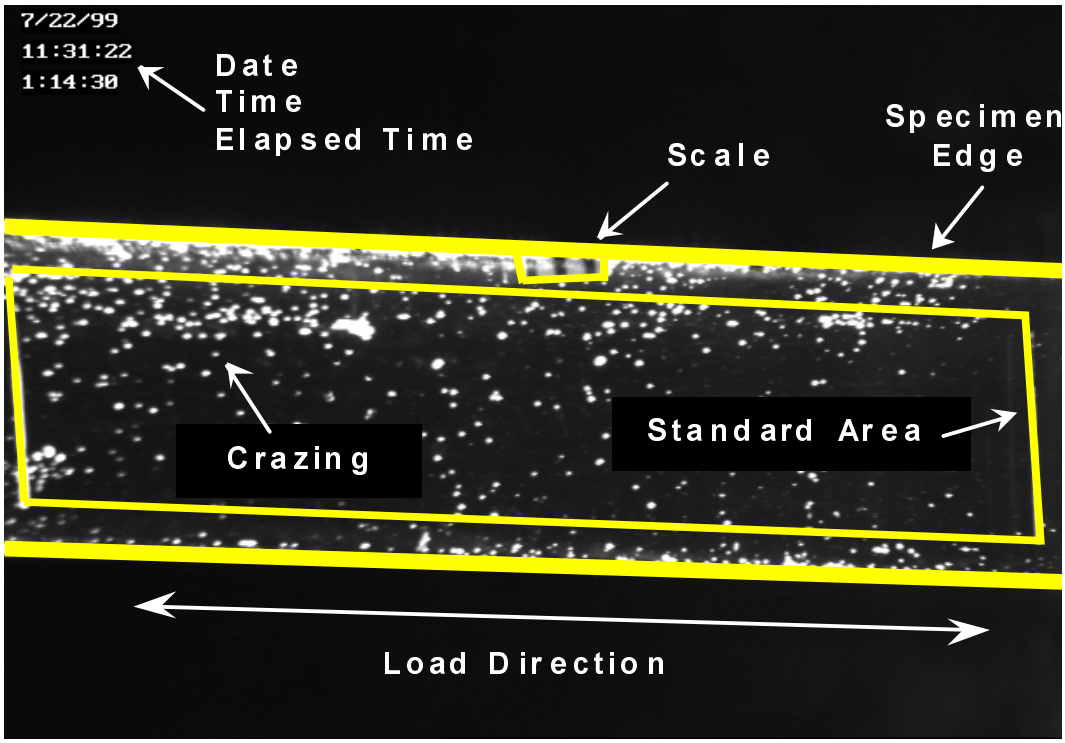

Figure 12: Typical image of crazed polycarbonate

After the images are collected, they are analyzed using SigmaScan Pro™ image analysis software to calculate the craze density for various times at each test condition. Any equivalent image analysis software may be used. To enhance reproducibility, each image is "masked" to the region inside the marked standard area (shown in Figure 12). "Masking" essentially sets each pixel outside of the selected area to an intensity of zero, which is black in color [51]. Next, the image is "thresholded" (Figure 13) to false color the crazed region taken to be the intensity range from 127 - 255 [51]. Finally, SigmaScan Pro™ is used to measure the craze density of the thresholded image by dividing the area of the thresholded crazed region by the standard area.

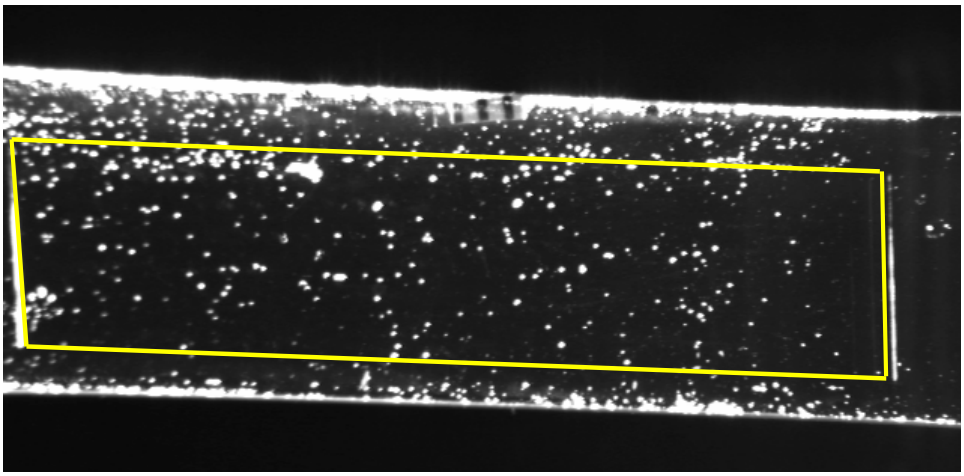

(a)

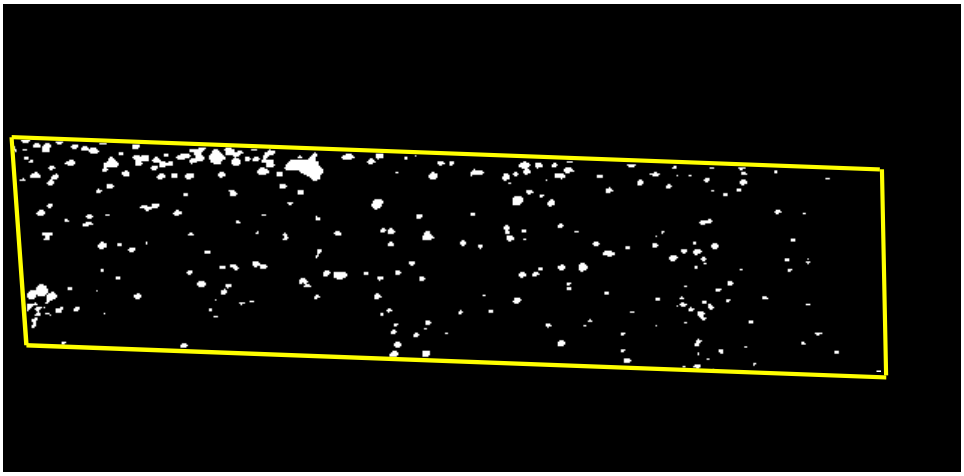

(b)

Figure 13: Typical image of crazed polycarbonate (a) before and (b) after thresholding

To visually describe relative craze density, several images are displayed in Figure 14 at various levels, ranging from 0.10% to 9.4%. This range covers most of the data recorded in this dissertation. Since some glaring occurred at the specimen edges, the craze densities were only measured from the central region without glare.

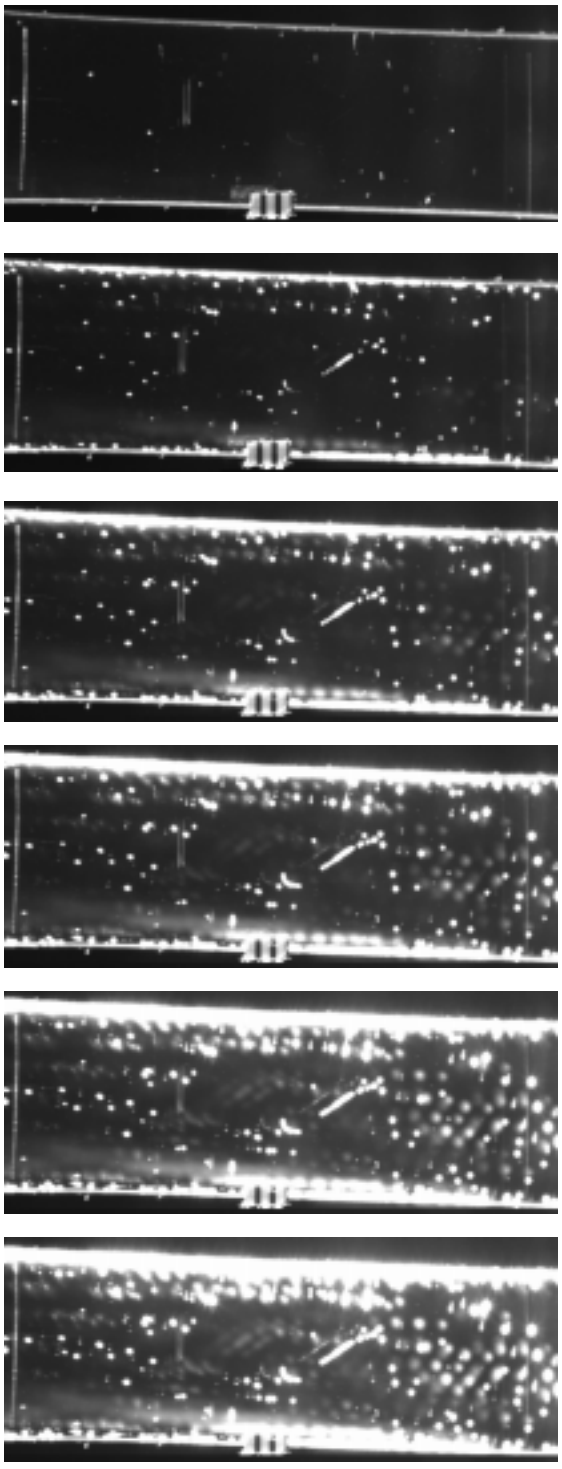

Figure 14: Pictorial description of relative craze density

3.2 Design and fabrication of equipment

The new craze measurement technique required testing equipment solely devoted to this project since each test could last several weeks depending on the magnitudes of stress, temperature and relative humidity. To accommodate this requirement, a creep tester with an environmental control system was designed and fabricated.

3.2.1 Load frame

The first component designed and fabricated was the welded load frame, made from 3”x3”x1/4” square tubing of ASTM A500 gr. B steel (Figure 15). The load frame was designed to hold four hydraulic cylinders on the bottom cross beams and four ¾” diameter loading rods on the top cross beams.

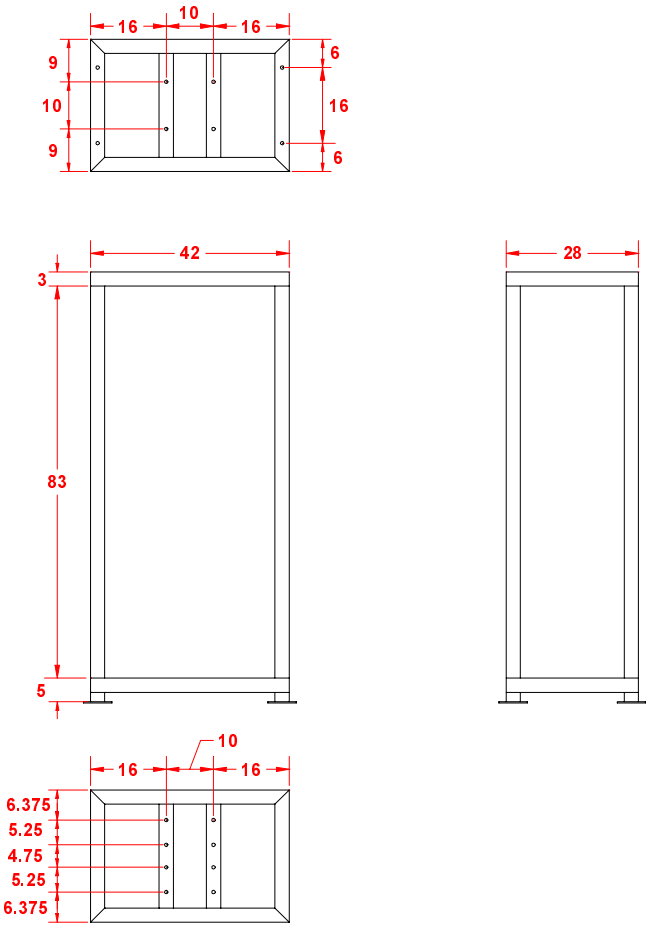

Figure 15: Load frame (units are inches)

3.2.2 Hydraulic load application system

The next step was to design and build a hydraulic load application system that could maintain loads up to 5000 lb. A simplified schematic of the final design for the loading system is shown in Figure 16.

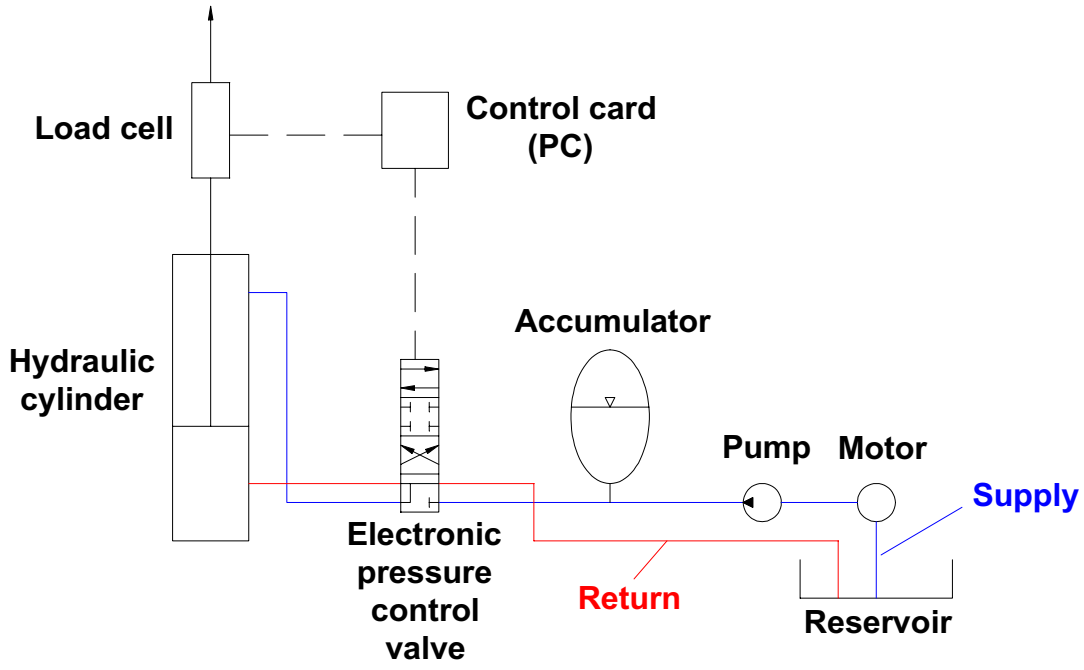

Figure 16: Simplified schematic of hydraulic load application system

The critical component of the hydraulic system is the electronic pressure control valve manufactured by Bosch. This valve receives a user-defined setpoint for pressure (P_{set}) and flow rate (Q_{set}) from the control card. It simultaneously receives the actual load magnitude from a Sensotec in-line tension load cell. The system is flow rate controlled until the actual load reaches the load at the setpoint pressure. At this point, the control valve maintains the desired pressure.

3.2.3 Gripping system

The ASTM specimen was then attached to the hydraulic cylinder. A schematic and photograph of the final design for the gripping system is shown in Figure 17. The gripping design consists of a grip attachment which connects to the loading rod and the grips which are

attached directly to the specimen. Once in the grips, the specimen rests on the top and bottom grip attachment.

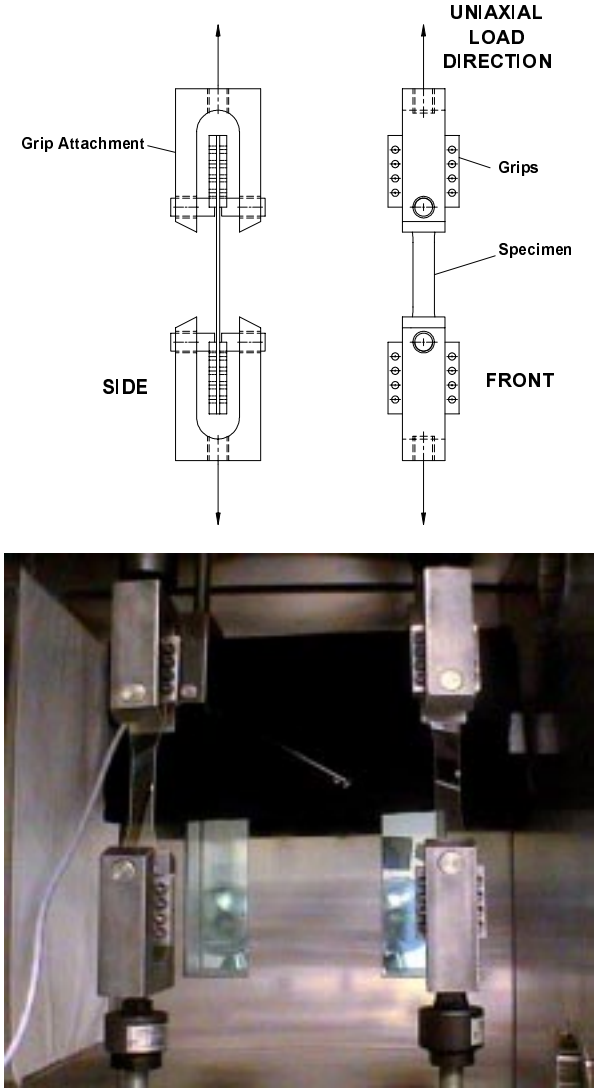

Figure 17: Grip/sample assembly

3.2.4 Environmental control system

The last necessary major component is the environmental control system. AFRL already owned a Cincinnati Sub-Zero remote conditioning unit capable of delivering a controlled environment in the range of -73 to +177°C (± 1°C) and 10 to 95% rh (± 4% rh). To use this equipment for craze testing, an environmental chamber needed to be designed and fabricated to integrally fit into the load frame with access for the hydraulic load application system. The final

design is shown in Figure 18. The chamber was manufactured by Russells Technical Products. It consists of two hinged doors on opposite sides, four glass viewports (two in each door), eight load train ports (four in the top, four in the bottom), one instrumentation port (in the side), and two duct ports (for the CSZ ducts).

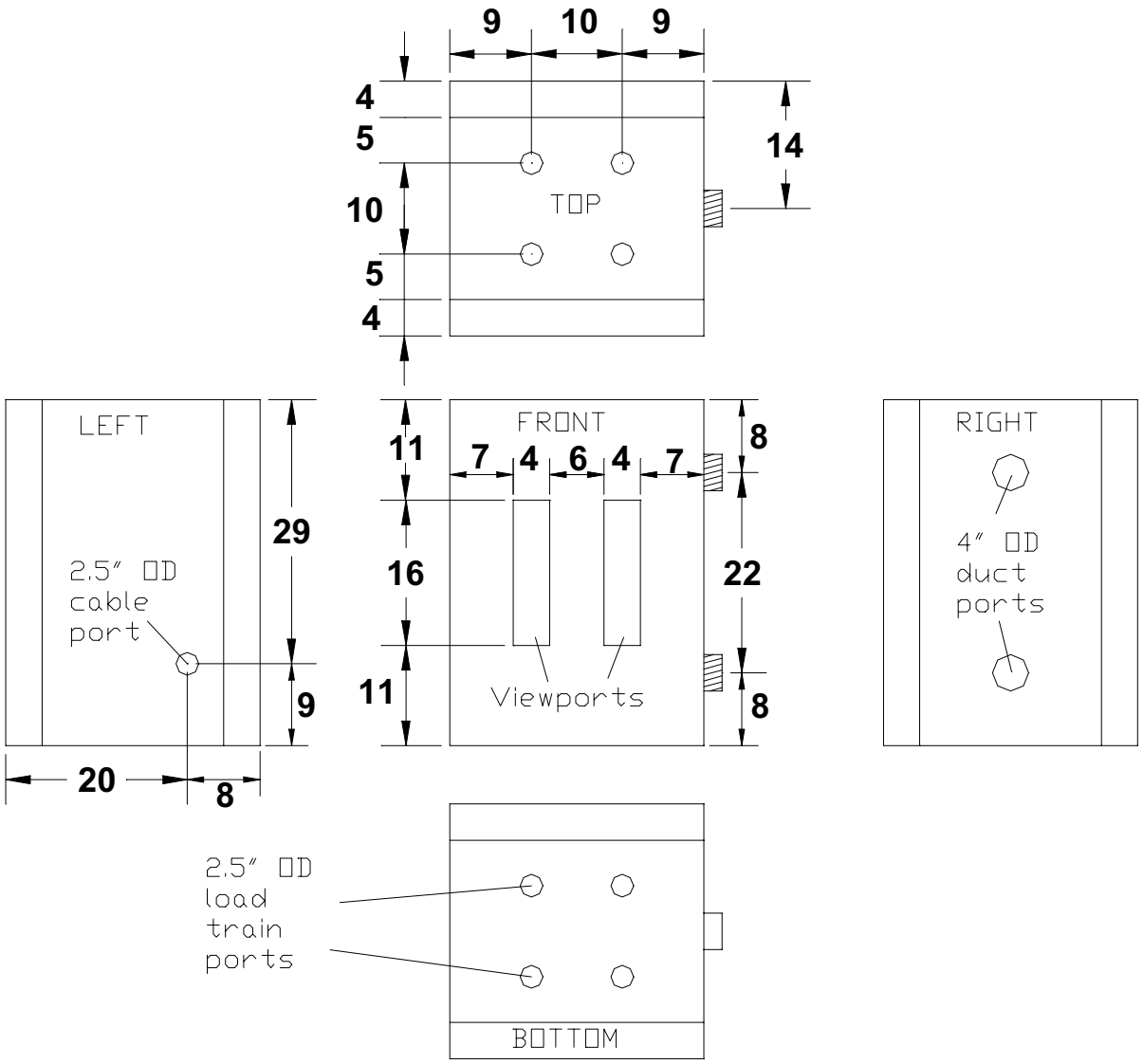

Figure 18: Environmental testing chamber

The experimental setup was integrated into what is seen in Figure 19. The system consists of a steel load frame, hydraulic load application unit, environmental conditioning system, and imaging equipment.

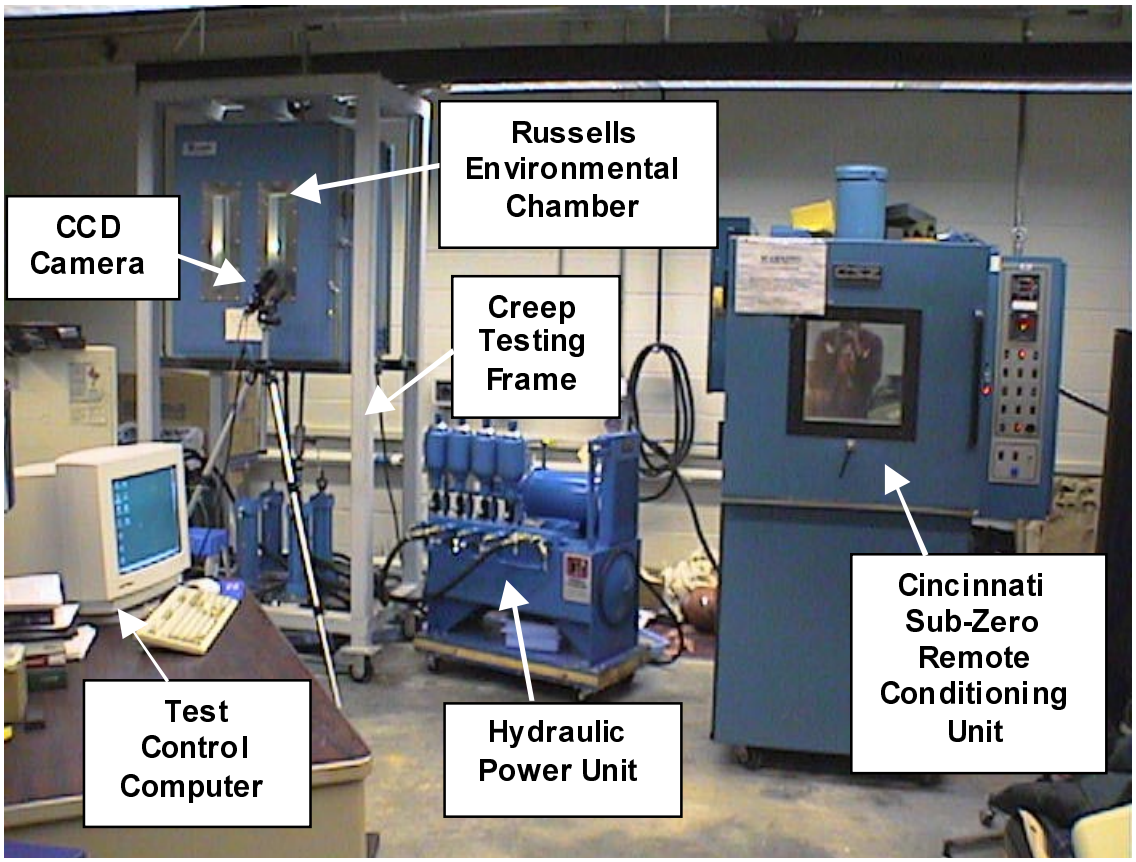

Figure 19: Creep tester and environmental conditioning system

3.3 Materials

Two different grades of bisphenol-A polycarbonate were used for this dissertation. Both materials were obtained commercially and contain common additives such as UV stabilizers. The new technique to measure the rate of change of craze density was validated with aircraft grade polycarbonate panels obtained from Rohm and Haas, known as Tuffak W. Aircraft grade material differs from normal commercial grade material in that it has improved optics due to better purification and color balancing. The material was melt calendared to 3 mm thick. The relative molecular weight as measured by gel permeation chromatography (GPC) was 55,000

g/mol. This value is believed to be near the geometric mean of M_n and M_w [6]. The glass transition temperature determined from the peak of the loss modulus in dynamic mechanical analysis at a heating rate of 1°C/min was found to be 156°C. The yield stress was measured to be 62 MPa while the elastic modulus was found to be 2.3 GPa [52].

The material that was used for the main model development was a commercial grade 6 mm thick polycarbonate sheet supplied by McMaster Carr. The number average molecular weight as measured by GPC was 19,450 g/mol with a polydispersity index of 2.2. The glass transition temperature determined from DSC was found to be 147°C. The yield stress and elastic modulus were measured to be 65 MPa and 2.3 GPa, respectively.

3.4 Humidity Control

Due to the temporary malfunction of the environmental control system, an alternative technique to control the humidity had to be used for some of the crazing tests. An attempt was made to control the humidity by placing saturated salt solutions of lithium chloride and sodium chloride in the Russells environmental chamber as described in Chapter 2. It was found that the volume of the chamber was too large for the lithium chloride solution to dehumidify, especially during the summer months when the ambient humidity was very high. Rather than totally ignore relative humidity, all of the experiments were performed in the presence of a distilled water bath in the sealed chamber. Theoretically, the equilibrium relative humidity for this case is 100%, but the measured relative humidity was 85±5% rh due to the frequent opening of the chamber door.

After each sample was crazed to the desired level, it was equilibrated in a small dessicator to 11.3% rh in the presence of lithium chloride. The samples were then placed in airtight sample bags and transported to the Instron universal testing machine. The residual mechanical properties were measured immediately upon removal from the sample bags.

3.5 Standard operating procedure

Since a universally accepted procedure does not exist for the newly developed craze density measurement technique, it is important to explicitly define the setup and step-by-step procedure used to obtain the data reported in this dissertation. It should be noted that using a different setup and measurement procedure, especially for the optical craze measurement, will most assuredly result in different relative craze densities. Data obtained from a different setup

can be compared to the results in this work if an appropriate correlation factor is determined and applied to the data.

3.5.1 Sample preparation

It has been found that sample preparation is a very important step in obtaining consistent, accurate data. Improper handling and preparation could result in scratches, rough edges, skin oil exposure, and other solvent exposure that could accelerate crazing in polycarbonate. The following is the recommended procedure for sample preparation:

(1) Handle test material with care to avoid scratching the surface and minimize skin contact with gage section to reduce skin oils affecting craze growth.
(2) With a band saw, cut a 33.5 mm x 267 mm rectangle from the plate to fit into the template for the TensilkuT ASTM dumbbell cutting machine.
(3) Cut the rectangle into an ASTM D638 Type III dumbbell specimen (Figure 10) with continuous, smooth motion with maximum cutting depth per stroke of 0.4 mm until the final few strokes during which cut < 0.1 mm deep.
(4) Remove the protective paper, if applicable.
(5) Rinse the specimen with water to remove loose grit and wipe with a soft clean cloth.
(6) Sufficiently sand the edges with 100 grit sandpaper.
(7) Re-rinse the sample and wipe with a soft, clean cloth.
(8) Sand the edges with 400 grit sandpaper until smooth.
(9) Re-rinse the sample and wipe with a soft, clean cloth.
(10) Measure and record the gage section thickness and width to the nearest 0.05 mm, being careful not to scratch the surface.
(11) Equilibrate the ASTM sample to the testing environment.
(12) Place squarely in grip plates (Figure 17) and torque all socket head cap screws to 12 N-m.

3.5.2 Craze testing

The recommended craze testing method is as follows:

(1) Place the top specimen grip plates on the top load frame grip pins.

(2) Start the Visual Basic main application and select the "Move" menu to move the cylinder so the bottom cylinder grip is about 75 to 100 mm above the bottom specimen grip plates (see Figure 17 for component identification).

(3) Move the cylinder down as slowly as possible until the cylinder grip screws engage the specimen grip plates. At this point, a constant load of approximately 220 N will automatically be held on the specimen.

(4) Place the polarizing filters around the pre-loaded specimen and gently twist the top and/or bottom grips to achieve a constant color throughout the gage section of the test specimen, indicating a constant stress.

(5) From the test control window select the appropriate station number and Image. The screen will display a real-time continuous grab from the digital camera.

(6) Turn on the light source and align the camera and light source according to the standard setup shown in Figure 11.

(7) Turn the camera's light adjustment knob to the maximum position and focus the camera on the sample surface.

(8) Input the test parameters into the Visual Basic application from the "Setup" menu.

(9) Press the "Start" button on the test control window to apply the load and start the image acquisition timer.

(10) Monitor the real-time test parameters and image shown on the display screen to check for errors in stress level or image acquisition.

(11) After the first image is saved, turn the light adjustment knob on the camera to the center notched position.

(12) Once the test has reached the desired craze level, press the "Stop" button on the test control window and unload the specimen.

3.5.3 Image analysis

The following procedure has been developed to reduce the subjectivity and increase the repeatability for analyzing the test images.

(1) Open the first test image with SigmaScan Pro [51] and record the start time and date.

(2) Calibrate the distance using the known width of the gage section and record the calibration ratio (pixels:mm).

(3) Graphically mark the standard area of the gage section (≈ 15mm x 50 mm).

(4) Mask the image with the marked area [51].

(5) Measure and record the masked area. This value will be used as the standard area.

(6) Open the test image to be analyzed and record the elapsed time

(7) Copy the distance calibration information from the original image to the test image.

(8) Copy and paste the mask layer on the 1st image to the new test image to be analyzed.

(9) Mask the test image to be analyzed.

(10) From the "Transforms – Lookup Table" menu, select the rectangular monochrome LUT with one cycle [51]. This lookup table converts every pixel with an intensity from 0 to 126 to black and every pixel with an intensity from 127 to 255 to white. The white pixels are considered to be the crazes.

(11) Threshold the transformed image to an intensity range of 250-255.

(12) Measure the craze area and count the number of objects with the "Tools- Measure Defined" menu.

(13) View the column statistics in the image analysis spreadsheet with the F6 function key to obtain the total craze area (make sure the count value is correct).

(14) Record the filename, elapsed time, number of objects, and total area.

(15) Divide the craze area by the standard area to get the relative percent area crazed.

3.5.4 Residual mechanical property measurement

The following procedure outlines the general steps to follow to measure the residual mechanical properties of crazed samples.

(1) Conduct constant strain rate tensile tests to failure at the rate specified in the test matrix for a given sample.

(2) Measure the yield stress, failure stress, elastic modulus and elongation for each sample.

When plotting the engineering stress (load divided by original cross sectional area) versus engineering strain (displacement divided by original gage length), polycarbonate initially deforms in a linear manner. It then exhibits a maximum at the initiation of macroscopic shear deformation. After yielding is established, polycarbonate draws at a relatively constant draw stress. The stress finally increases as the entire gage section becomes plastically deformed and the polymer chains are generally oriented in the maximum stress direction. The yield stress, failure stress, and modulus line are shown in Figure 20 to illustrate the measurement of the mechanical properties.

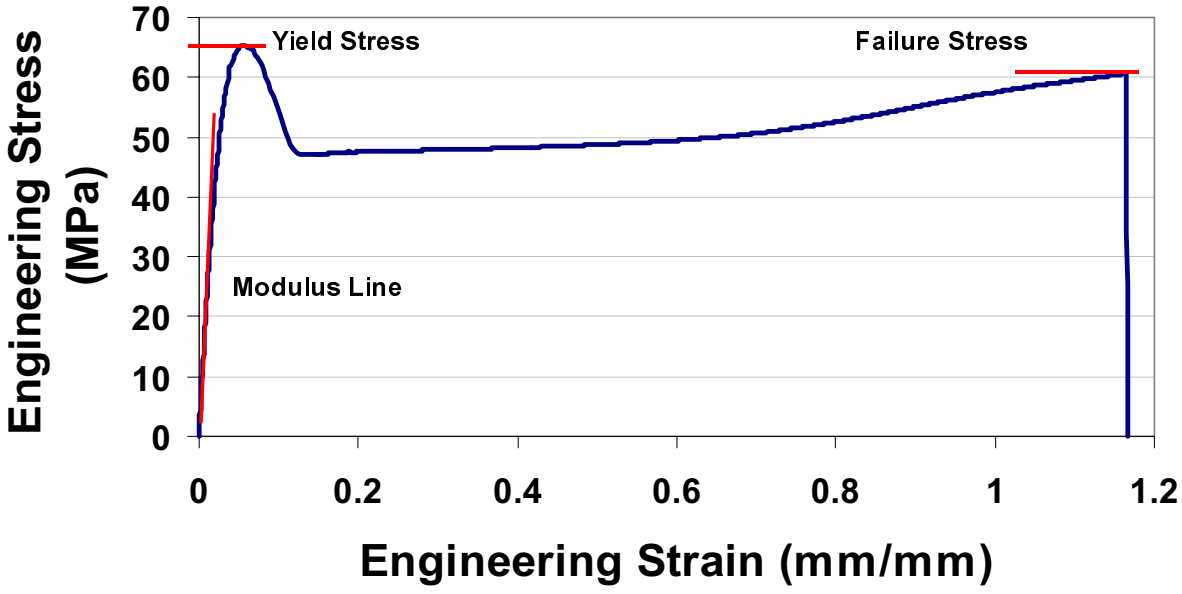

Figure 20: Typical stress-strain curve for polycarbonate

For this dissertation, the yield stress was taken to be the maximum magnitude of stress before the constant drawing region. The failure stress was measured as the maximum stress obtained by the polycarbonate just prior to fracture. The elastic modulus was calculated by measuring the slope of the initial linear portion of the curve. The measure of ductility was taken to be the final length of the necked portion of the gage section after fracture normalized to the gage section of 50 mm. This region is illustrated in Figure 21.

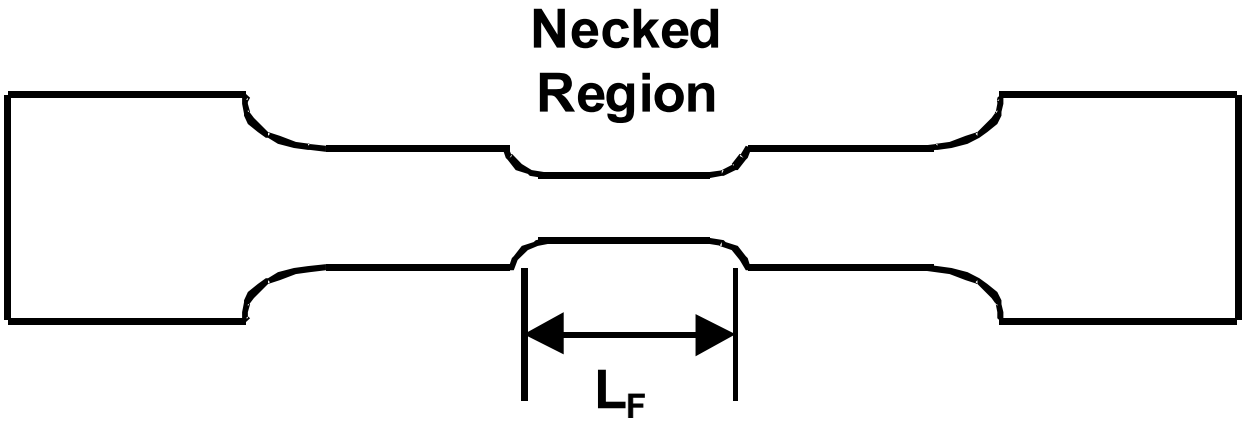

Figure 21: Drawing of ASTM dogbone sample with necked gage section

3.6 Design of Experiments (DOE)

One of the goals of this research study is to correlate the residual mechanical properties of crazed polycarbonate samples to crazing stress, relative craze density, and strain rate. Limited material with a large number of factors makes it difficult to obtain meaningful results using only the traditional approach of changing one variable at a time. It is believed that more valuable modeling results will be obtained by taking advantage of a designed experiment with an mathematically orthogonal test matrix. The designed experiment approach requires more pre-experiment planning than traditional techniques, but increases the chances of obtaining a valid model that assigns the response to the proper input variables or interaction between input variables. The steps for methodically setting up a properly designed experiment have been well documented [53].

Following the procedures outlined in the literature, a test matrix with three input variables, each tested at two levels, was selected. The factors and levels are shown in Table 2.

Table 2: Designed experiment factors and levels

Factors	Low	High
(A) Stress (MPa)	40	45
(B) Relative Craze Density (%)	1	10
(C) Strain Rate (min^{-1})	0.2	2

The ranges for the factors shown in Table 2 were selected with several things in mind. The stress range was selected to grow crazes in a time frame on the order of hours to days since a typical flight for a military aircraft is on the order of hours. The relative craze density and rate ranges were selected to provide an envelope spanning an order of magnitude.

With three factors in the DOE approach, it is best to conduct a full-factorial test matrix, i.e., to test every possible combination of variables. This results in having to complete 8 runs. Each test condition will be repeated three times for a total of 24 required tests [53]. For full factorial designs, no "aliasing" exists, which means that all two-way and three-way interactions are evaluated. The tests to be conducted are shown below in Table 3.

Table 3: Designed experiment 3 factor - 2 level – full factorial test matrix

Run	Stress (MPa)	Relative Craze Density (%)	Strain Rate (min^{-1})
1	40	1	0.2
2	40	1	2
3	40	10	0.2
4	40	10	2
5	45	1	0.2
6	45	1	2
7	45	10	0.2
8	45	10	2

Both graphical and statistical analyses are performed on the results of the above test matrix. The first analysis technique is to derive a predictive equation for the response using average effects of each factor. Next, a Pareto diagram will be plotted to graphically show the importance of each factor. Finally, interaction plots will be developed to determine if there are any strong interactions between two factors.

3.6.1 Predictive equation derivation

A fictitious data set is given in Table 4 for a two factor, two level full factorial design to illustrate the process of determining the predictive equation. The two experimental factors are labeled A and B. The +1's and –1's represent the high and low levels for factors A and B. To keep the test matrix orthogonal, the interaction column is calculated by multiplying column A by column B.

Table 4: Fictitious data DOE data set to illustrate calculations

Run	Factor A	Factor B	Interaction AxB	Average Response, Y_{avg}
1	-1	-1	+1	20
2	-1	+1	-1	16
3	+1	-1	-1	40
4	+1	+1	+1	34

The first step in determining the predictive equation is to calculate the average of the response column as shown in Equation 3-1.

$$\mathbf{(Y_{avg})_{avg} = (20 + 16 + 40 + 34) / 4 = 27.5} \quad (3\text{-}1)$$

Next, the differential effect from the high setting to the low setting of each factor is determined. For example, the differential effect of factor A is found by averaging the response of A at the high setting and subtracting the average response of A at its low setting, as shown in Equation 3-2.

$$\mathbf{\Delta A = (A_{+})_{avg} - (A_{-})_{avg} = [0.5 \times (40 + 34)] - [0.5 \times (20 + 16)] = 19} \quad (3\text{-}2)$$

where ΔA is the differential effect of factor A, $(A_{+})_{avg}$ is the average response of A at its high setting and $(A_{-})_{avg}$ is the average response of A at its low setting. Similarly, the differential effects of B and the interaction between factor A and factor B (AxB) are found to be –5 and -1, respectively.

Finally, the values calculated above are used to formulate the predictive equation as shown in Equation 3-3.

$$\begin{aligned} \mathbf{Y_{pred}} &= \mathbf{(Y_{avg})_{avg} + (\Delta A/2)\, A + (\Delta B/2)\, B + (\Delta AB/2)\, AB} \\ &= \mathbf{27.5 + 9.5\, A - 2.5\, B - 0.5\, AxB} \end{aligned} \quad (3\text{-}3)$$

where Y_{pred} is the predicted response, $(Y_{avg})_{avg}$ is the average of the response column, ΔA is the differential effect of factor A, ΔB is the differential effect of factor B, and ΔAB is the differential effect of the interactions between factors A and B.

3.6.2 Pareto diagram formulation

The next step in analysis is to develop a Pareto diagram, graphically showing the importance of the differential effect of each factor found in Equation 3-3. The absolute value of half of each differential effect is simply plotted as a function of its corresponding factor, as shown in Figure 22. Half of the effect is plotted instead of the entire differential effect since the constant in the predictive equation represents the average predicted value and increasing by half of the total effect represents the maximum value, while decreasing by half of the total effect represents the minimum predicted value for the response. The half effect is shown in the predictive equation (Equation 3-3) as the coefficient of each factor ($\Delta X/2$).

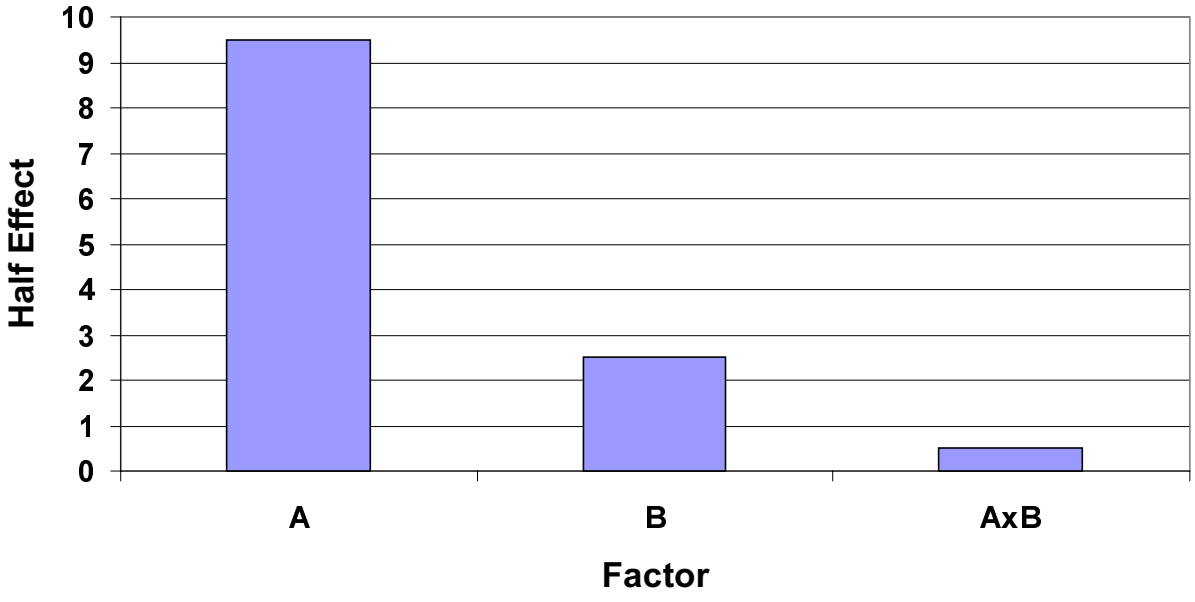

Figure 22: Pareto diagram of half effects of sample data set

It is obvious from Figure 22 that the most significant factor is A. It is not obvious from the Pareto diagram whether terms B or AxB should be included in the model at all. The statistical software used in the analysis section of this dissertation calculates the probability of

placing an insignificant term in the predictive model. This probability is the variable *p(2-tail)* and is shown in the confidence equation below.

Confidence term belongs in model = (1 – *p(2-tail)*) * 100% (3-4)

The rule of thumb given in the literature is that if the value of *p(2-tail)* for a given factor is less than 0.10 then the term should be included in the model. The *p(2-tail)* cannot be calculated for the sample data set above since the calculation requires multiple repetitions for each run.

3.6.3 Interaction diagram development

One major advantage to using DOE analysis is the ability to assign the response to an interaction between two main factors. An interaction diagram is a graphical way to determine if an interaction is significant. The diagram is developed by plotting the average response for each level of factor B as a function of factor A. The interaction diagram for the sample data set in Table 4 is shown in Figure 23.

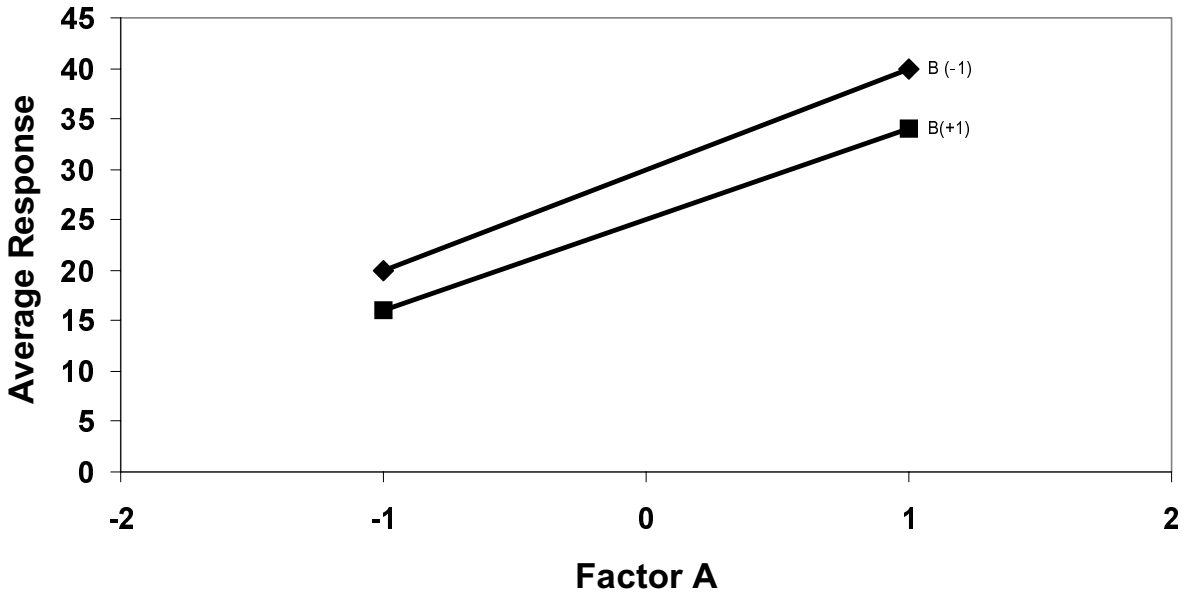

Figure 23: Interaction diagram for sample data set showing no interaction

Figure 23 shows that a significant increase occurs in the average response with an increase in A, only a slight decrease occurs in the average response with an increase in B, and the curve for B(-1) is approximately parallel to the curve for B(+1) indicating no interaction between factors A and B. This result graphically verifies Equation 3-3. An interaction diagram with a strong interaction between factors A and B would show intersecting lines, rather than parallel.

3.7 Polymer degradation

As mentioned in Chapter 2, differential scanning calorimetry (DSC), thermogravimetric analysis (TGA), and gel permeation chromatography (GPC) experiments were conducted before and after the craze growth tests to ensure that the reduced mechanical properties were actually due to the crazes and not a result of polymer degradation due to physical aging or chemical reactions.

3.7.1 Differential scanning calorimetry

The DSC used for this study was a Perkin Elmer Delta Series DSC7 power compensation DSC (Figure 24) with a maximum temperature range of -170°C to +730°C (±0.1°C) and heating rates from 0.1°C to 200°C/min [54].

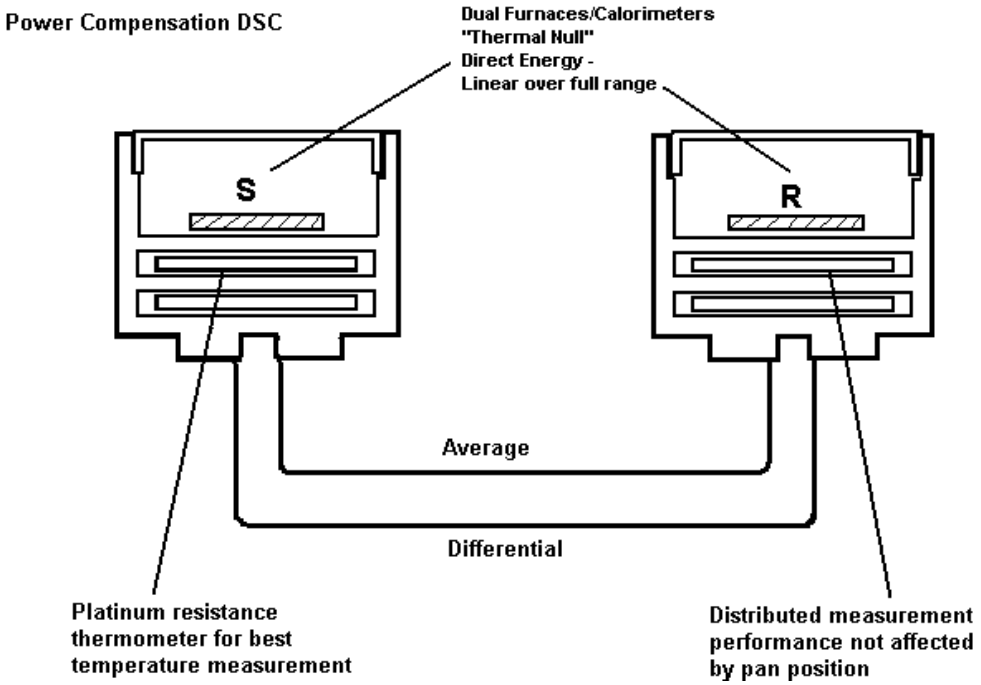

Figure 24: Schematic of Perkin Elmer Delta Series DSC7 power compensation DSC [55]

A simplified outline of the procedure for performing DSC thermal characterization with the Perkin Elmer Delta Series DSC is as follows:

(1) a 5 to 10 mg sample is cut from the tensile sample, weighed, and placed in the DSC pan,

(2) both the sample pan and a reference pan are placed in the instrument,

(3) the DSC is programmed to scan a temperature range from 100 to 200°C at a heating rate of 10°C/min,

(4) the differential heat capacity is measured and plotted as a function of temperature, and finally,

(5) the T_g is taken from the scan as the temperature at which 50% of the change in differential heat capacity has occurred [6].

3.7.2 Thermogravimetric analysis

The TGA used for this study was a Perkin Elmer TGA7 with a temperature range of ambient to 1000°C (±0.1°C) and heating rates from 0.1 to 200°C/min [56]. The ultramicrobalance measures changes in weight as small as 0.1 μg with an accuracy of 0.1%. The suggested sample size for the TGA7 is from 2 to 50 mg.

All of the tests for this dissertation were performed under identical conditions. The initial temperature was 100°C and the final temperature was 900°C with a heating rate of 20°C/min. The sample size varied from 10 to 15 mg. All tests were performed in an atmosphere of air.

The initial and final temperature of the transition were measured using the double tangent technique. An example measurement is shown in Figure 25.

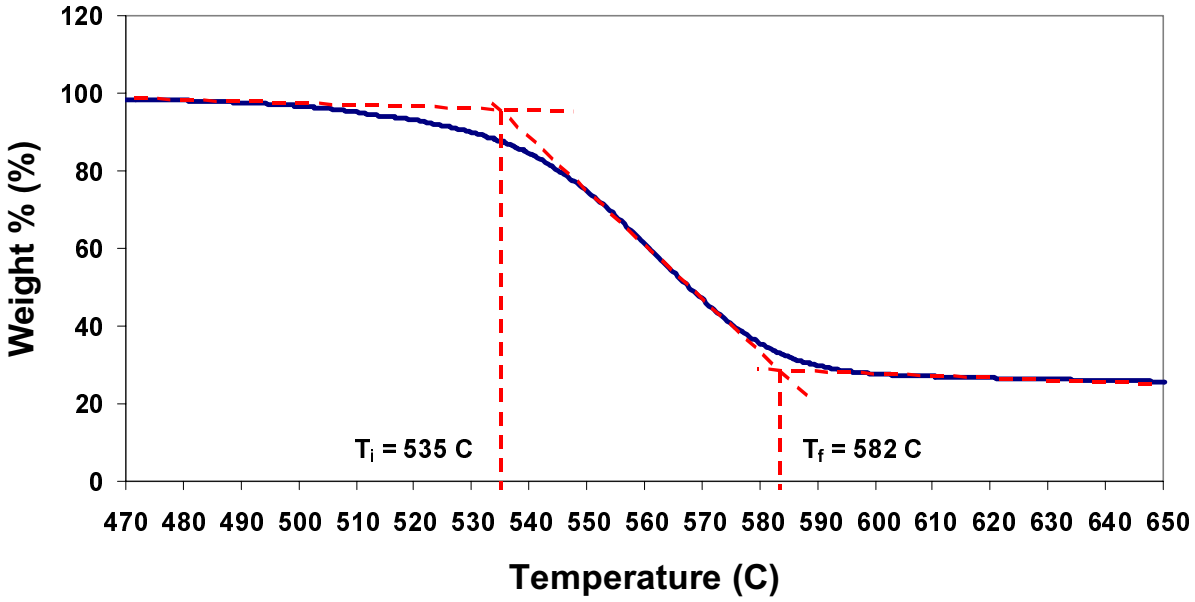

Figure 25: Double tangent technique to measure the initial and final transition temperatures for a thermogravimetric analysis of polycarbonate

3.7.3 Gel permeation chromatography

The GPC used for this study was a Waters 2690 gel permeation chromatograph. The solvent that was used was chloroform with a concentration of approximately 3 mg/mL, flow rate

of 1.000 mL/min, injection volume of 100.0 μL, inlet pressure of 89.160 KPa, and input mass of approximately 0.3 mg.

The general procedure is as follows:

(1) dissolve a polymer sample in a solvent,

(2) inject the solution into the separation column,

(3) measure the output of the column as a function of time with an ultraviolet or infrared detector, low angle light scattering, or viscometer,

(4) correlate the output to a measured standard. Extreme caution should be taken when analyzing the output of a GPC. Some common errors have been documented in the literature [57, 58].

Following the GPC run, the number average, weight average, and z average molecular weights were calculated with the use of a universal calibration.

Chapter 4 RESULTS

4.1 Validation of experimental technique

Checking the validity of a new technique is an important step prior to data publication. The two main techniques for validation were measuring the precision and comparing results to expected trends. The panels used in the validation study were an aircraft grade polycarbonate known as Tuffak W. The material description is given in Chapter 2.

4.1.1 Repeatability assessment

To assess the repeatability of the image analysis procedure, three craze growth charts were generated at three different times using the same raw images. Figure 26 shows the results of the assessment.

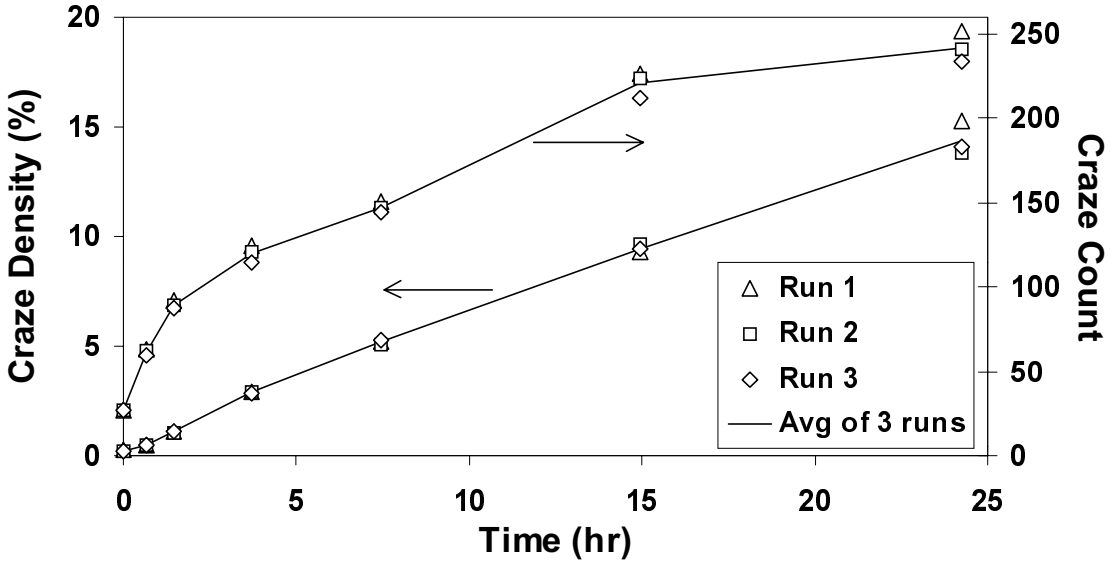

Figure 26: Results of image analysis repeatability study using same raw images at three different times

The results displayed in Figure 26 indicate that the image analysis process is very repeatable. For this study, edge initiated crazes were eliminated from the analysis area since the bulk surface crazing is of greatest concern. When edge crazing exists at higher craze levels,

there is some subjectivity in selecting the appropriate area to measure and the variability will increase slightly.

It is also important to realize that the craze density measurement is a function of measurement stress. To show this dependence, the craze density was measured on six samples at three different stress levels. Figure 27 displays the results at 3.5, 7, and 14 MPa.

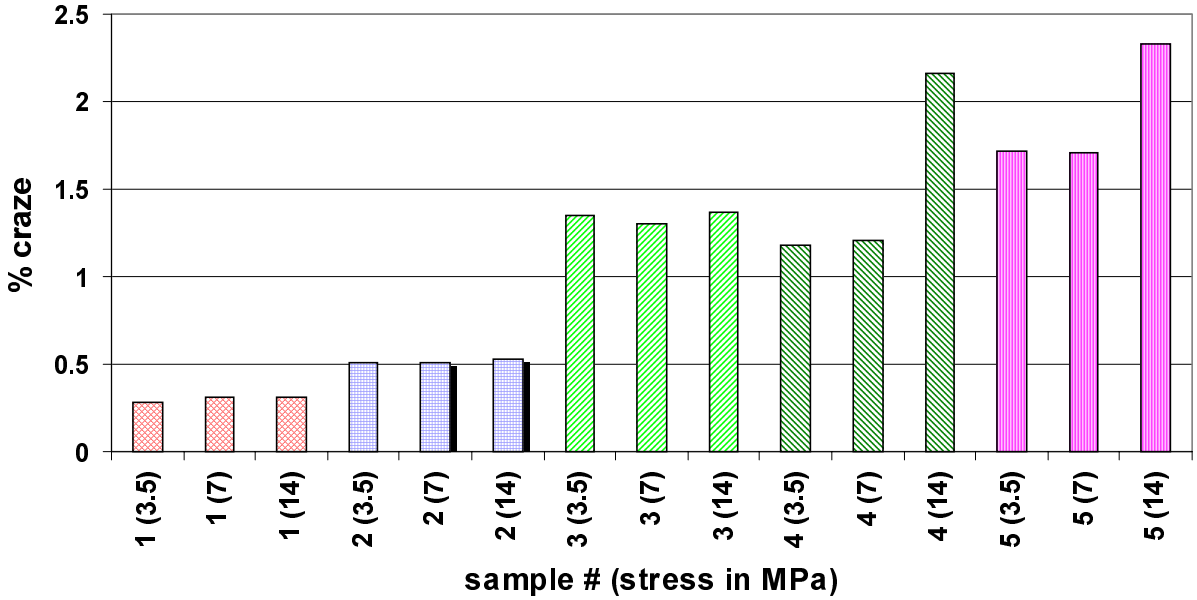

Figure 27: Effect of stress level on craze density measurement

It can be concluded that the effect of stress level on the craze density measurement is very small at low craze levels. Also, at craze levels larger than one percent, the stress effect becomes significant between 7 and 14 MPa. For this reason, any craze density measurement reported using this technique must include the measurement stress level to be useful. In this report, all craze densities were measured at 14 MPa unless otherwise stated.

4.1.2 Comparison with theoretical trends

Craze experiments were performed on polycarbonate tensile bars under creep stresses of 28 and 34 MPa at standard conditions of 21°C and 46% relative humidity. The craze density,

shown as a percent of the total standard area, is shown as a function of time in Figure 28. The data consists of four tests at 28 MPa and five tests at 34 MPa.

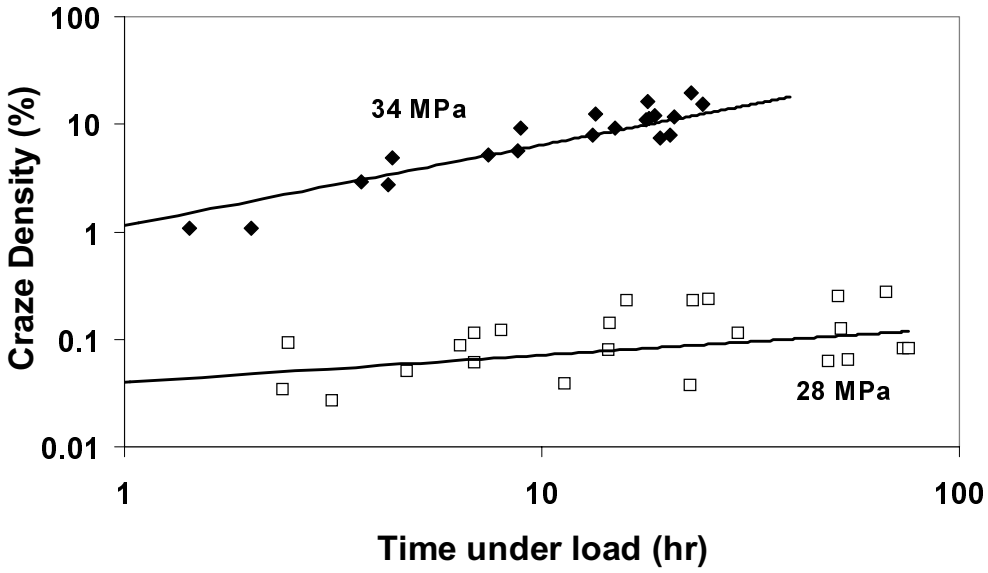

Figure 28: Effect of stress level on the crazing rate of polycarbonate at standard laboratory conditions

As expected, the craze damage increases with increased stress. One test was also performed at 21 MPa, with no crazing seen after 500 hours under load. These results show that differences in the data produced at 21, 28, and 34 MPa are statistically significant.

Linear regression was performed on each test shown in Figure 28, and the craze density was found as a function of time. To quantitatively demonstrate the effect of stress on the crazing rate of polycarbonate, the time to reach one percent craze density was found for each test. The average time to reach one percent craze density at 28 MPa was found by extrapolation to be 500 hr with a standard deviation of 430 hr. The 34 MPa tests produced an average time to one percent craze density of 1.4 hr with a standard deviation of 0.85 hr.

To further assess the craze quantification capabilities, tests were performed at three different temperatures, knowing that increasing the temperature should increase a polymer's crazing rate [3]. Four tests were conducted at 38°C, 28 MPa and 50% rh, and three tests were

performed at 54°C, 28 MPa, and 50% rh. Figure 29 compares the tests conducted at 21, 38, and 54°C.

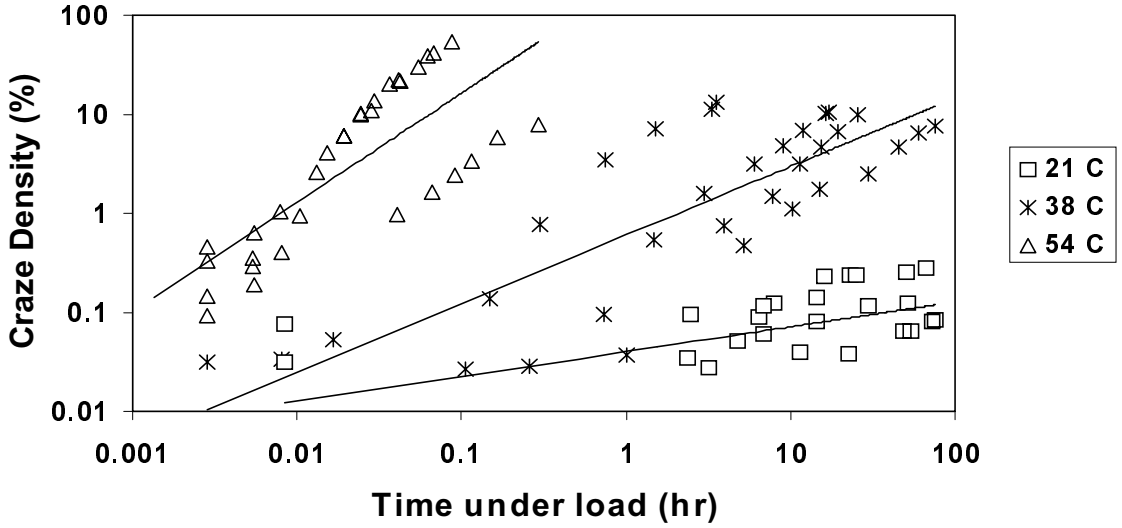

Figure 29: Effect of temperature on the crazing rate of polycarbonate held under 28 MPa creep load

Figure 29 shows the dramatic increase in the crazing rate of polycarbonate due to an increase in temperature. To quantify the change, linear regression was performed on each of the tests, and the time to obtain one percent craze density was determined. For the 21°C tests, the average time to one percent craze density was found by extrapolation to be 500 hr with a standard deviation of 430 hr. The average time to one percent craze density at 38°C was found by interpolation to be four hours with a standard deviation of four hours. Finally, the 54°C average time to one percent craze density was found by interpolation to be 0.008 hr with a standard deviation of 0.00035 hr. For all practical purposes, the highest temperature tests obtained one percent craze density immediately upon loading.

4.1.3 Lessons learned

Through the validation process, several lessons were learned. Four craze accelerating factors were identified that were not originally considered. The first one is skin oils. It was observed that the samples that were excessively handled in the gage section crazed at a much higher rate than the ones that were kept free from skin oils. This was quite evident during

experiments in which the dust was wiped from the gage section immediately before applying the creep load. It is believed that the skin oils act as a plasticizing agent, increasing molecular mobility on the sample surface.

The other three crazing agents found were the adhesive on electrical tape, the adhesive on measurement calibration tape, and rubberbands. Both the electrical tape and rubberbands were used to hold a cardboard template in place in the gage region so the standard image area would be the same for each test. It is believed that both of the adhesives also act as surface plasticizing agents. The rubberband could also have transferred some plasticizer onto the polycarbonate surface. Also, it was relatively tight around the gage section creating a compressive force in the direction perpendicular to the creep load which, through the Poisson effect, would create additional tensile stress in the creep direction. This increased stress, along with any plasticizer, would increase the crazing rate in this region.

The crazing agents listed above show that the crazing behavior of polycarbonate is very sensitive to what is happening on the surface. For this reason, it is believed that complete saturation of the bulk polymer is not necessary to study the effect of moisture on craze resistance.

4.2 Molecular orientation

As discussed in Chapter 2, molecular orientation in a polymer is believed to play a role in the rate of craze growth. For this reason, the molecular orientation of both the 3 mm and 6 mm polycarbonate described in Chapter 3 was characterized. The technique to characterize the molecular orientation was to measure the elastic modulus for three samples cut in both the direction used for craze testing and the direction perpendicular to the craze samples. The results are shown in Table 5 with longitudinal referring to the direction of the craze test samples.

Table 5: Values of elastic modulus of longitudinal and transverse samples of polycarbonate

	3 mm		6 mm	
Direction	Avg Modulus (MPa)	St Dev (MPa)	Avg Modulus (MPa)	St Dev (MPa)
Longitudinal	2104	60.4	2222	56.9
Transverse	2132	37.4	2235	41.3

Large amounts of molecular orientation in a polymer show up as changes in the elastic modulus. For instance, applying a uniaxial stress aligned with the preferred molecular direction would result in a higher elastic modulus than if the stress was applied perpendicular to the molecular orientation. Table 5 shows that the elastic modulus in both the craze sample direction and perpendicular to the craze sample direction are the same, within experimental scatter. This leads to the conclusion that significant molecular orientation does not exist.

4.3 Craze growth rates

The material used in this portion of the dissertation was the McMaster Carr 6 mm thick polycarbonate described in Chapter 3. In an attempt to build a model to predict the residual mechanical properties of crazed polycarbonate, several samples were crazed to a relative craze density of 10%. The relative craze densities are shown as a function of time under load in the log-log plot of Figure 30.

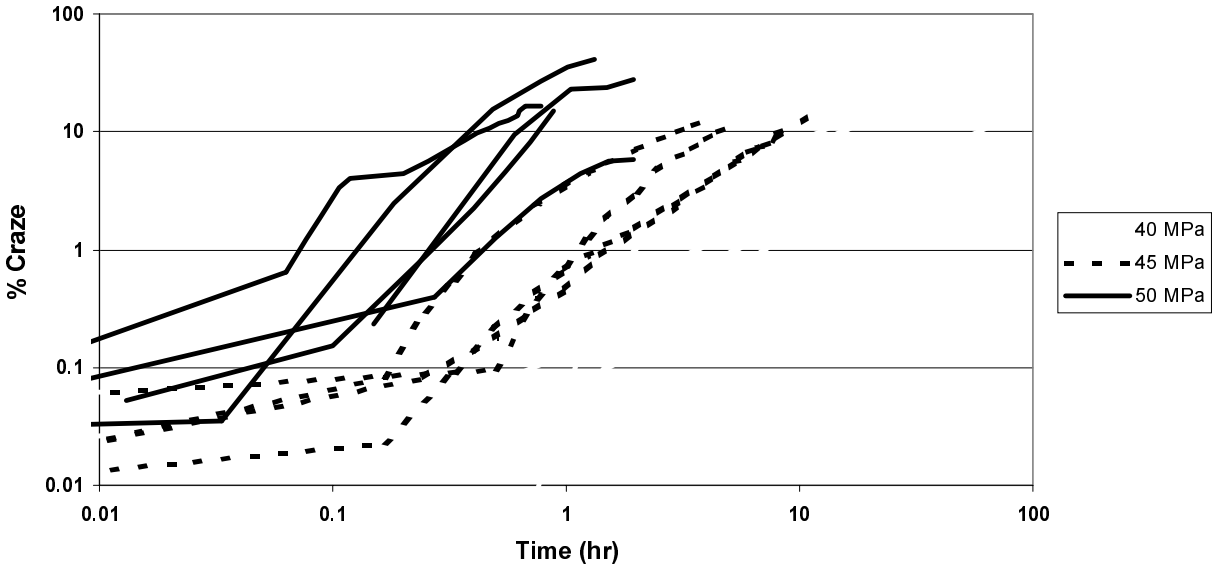

Figure 30: Relative craze density as a function of time under load for various stress levels at 24°C and 85% rh

Similar to Figure 28 in the validation study, a lower stress produces a lower crazing rate. Figure 30 shows that the data at 40, 45, and 50 MPa are statistically different. The graph is generally qualitative, showing the overall crazing behavior of polycarbonate. To better quantify the effect of stress level on crazing rate, the growth rates for the data obtained in Figure 30 were measured by calculating the slope of the linear part of the craze growth curve once stable craze growth was established. These data are plotted as a function of stress in Figure 31 with error bars showing one standard deviation.

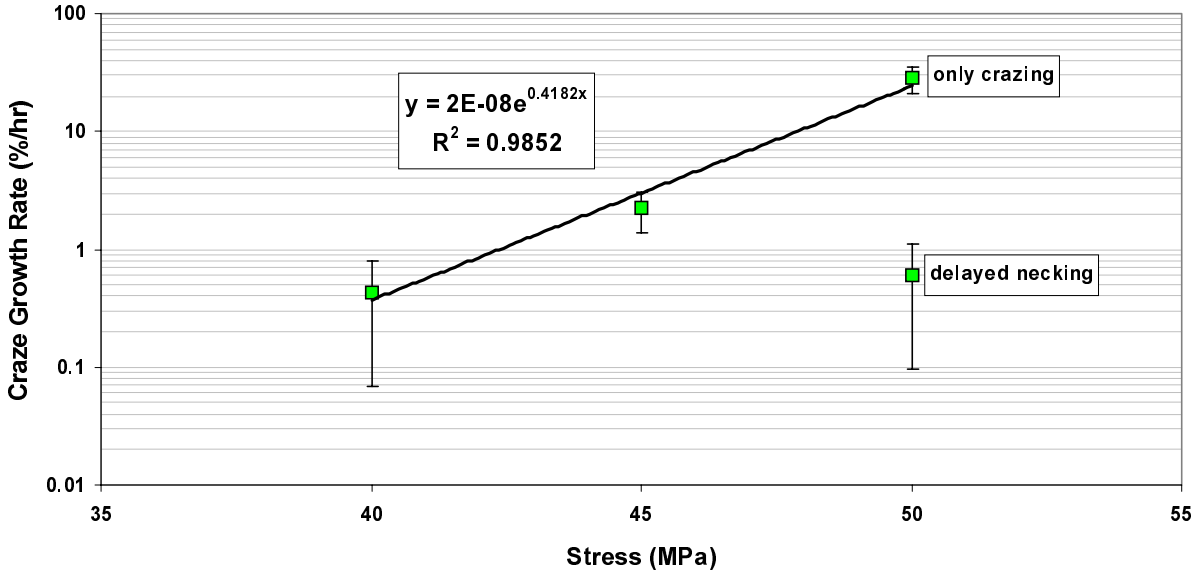

Figure 31: Effect of stress level on craze growth rate (24°C, 85% rh)

Two things are apparent from the above graph: (1) the craze growth rate increases exponentially with stress at 24°C and 85%rh as shown in Equation 4-1, and (2) a competition between crazing and shear yielding exists at a crazing stress of 50 MPa.

$$\mathbf{R(\sigma) = (2x10^{-8})\ e^{0.4182\sigma}} \qquad (4\text{-}1)$$

where R(σ) is the craze growth rate in %/hr and σ is the crazing stress in MPa.

The former observation shows that once the applied stress is high enough to produce crazing in a reasonable time frame, increasing the stress by only 5 MPa could increase the crazing rate by an order of magnitude. Given the range of crazing stress in this dissertation, there is no clear evidence of a minimum stress below which crazing will not occur.

Also, the Eyring stress-rate theory presented in Chapter 2 shows that if crazing can be represented as a thermally activated rate process, then the effect of stress on the crazing rate would be of the general form

$$\dot{e} \approx \frac{\dot{e}_o}{2} \exp\left(-\frac{\Delta H - \nu\sigma}{RT}\right) \qquad (4\text{-}2)$$

Comparison of Equations 4-1 and 4-2 shows that they are of the same form, indicating that changes in the growth rate of bulk craze density can be represented by the Eyring model of thermally activated processes in the presence of an externally applied stress.

The latter observation is the phenomenon described in Chapter 2. When a high enough energy level exists, large scale macrodeformation occurs in the form of shear yielding. Over half of the polycarbonate samples tested at 50 MPa initially showed a lower than expected craze growth rate, and after one to four hours, the measured craze density decreased as the sample began to neck (Figure 32). An uncharacteristically low crazing rate exists because most of the energy is being absorbed by large scale motion rather than by the localized plastic deformation that occurs in crazing. The measured decrease at long times is only an apparent decrease in craze growth resulting from the crazes deforming due to large scale motion in the vicinity of the craze. As the shape of the craze changes, the craze surfaces reflect less light directly to the CCD camera, resulting in a decreased measurement of relative craze density.

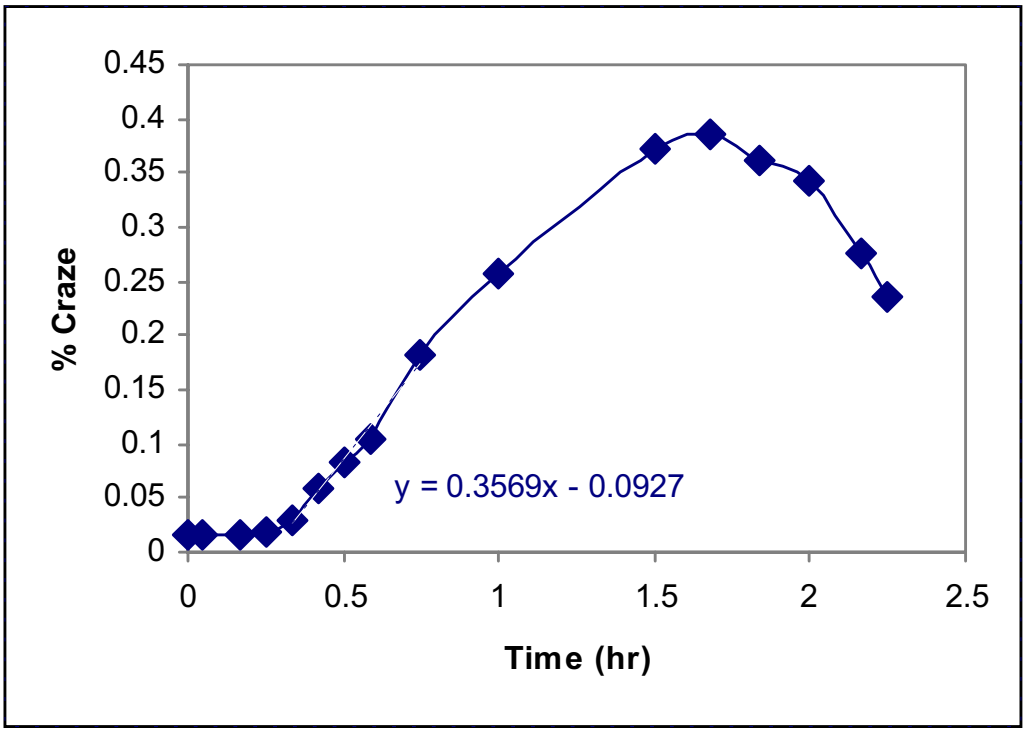

Figure 32: Typical apparent craze growth curve for sample that experienced delayed necking.

The stress-strain curve for this material exhibits a yield stress around 65 MPa when tested at a strain rate of 0.2 min^{-1} and shows a draw stress between 46 and 48 MPa as shown in Figure 33. These results indicate that the draw stress acts as a lower bound below which delayed necking will not occur in a reasonable time frame since many of the 50 MPa tests yielded and none of the 45 MPa tests did.

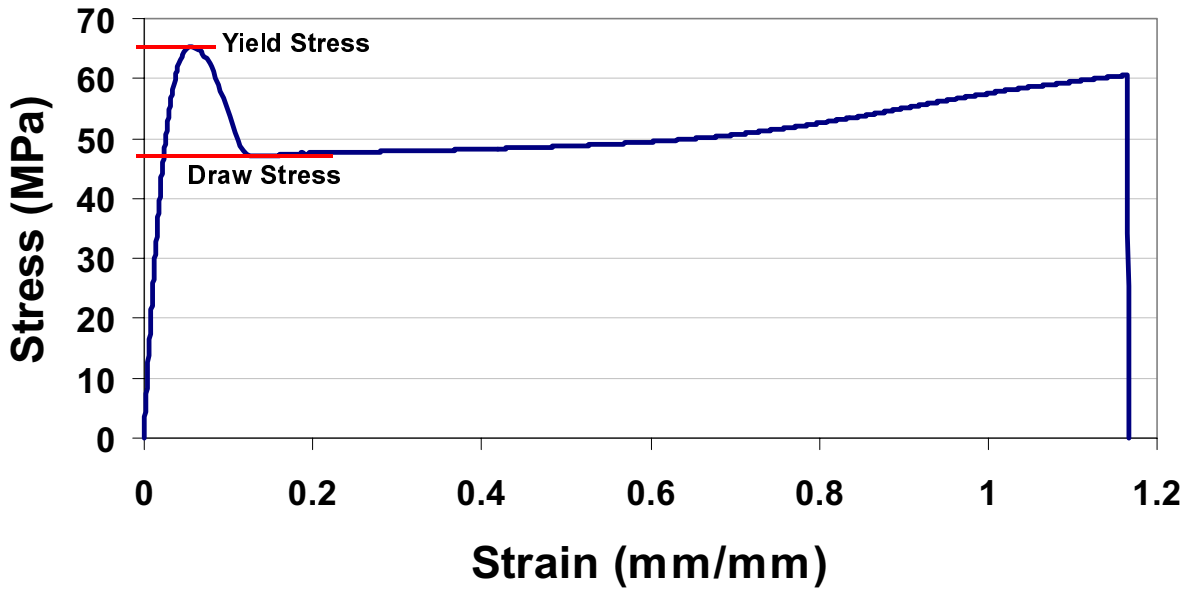

Figure 33: Stress-strain curve of as-received polycarbonate tested at 0.167 min^{-1}, 24°C, and 85% rh

Besides the growth rate, another important characteristic to measure is the time to craze initiation. The time to stable craze growth was measured for each data set shown in Figure 30 and plotted as a function of stress level in Figure 34 with error bars showing one standard deviation.

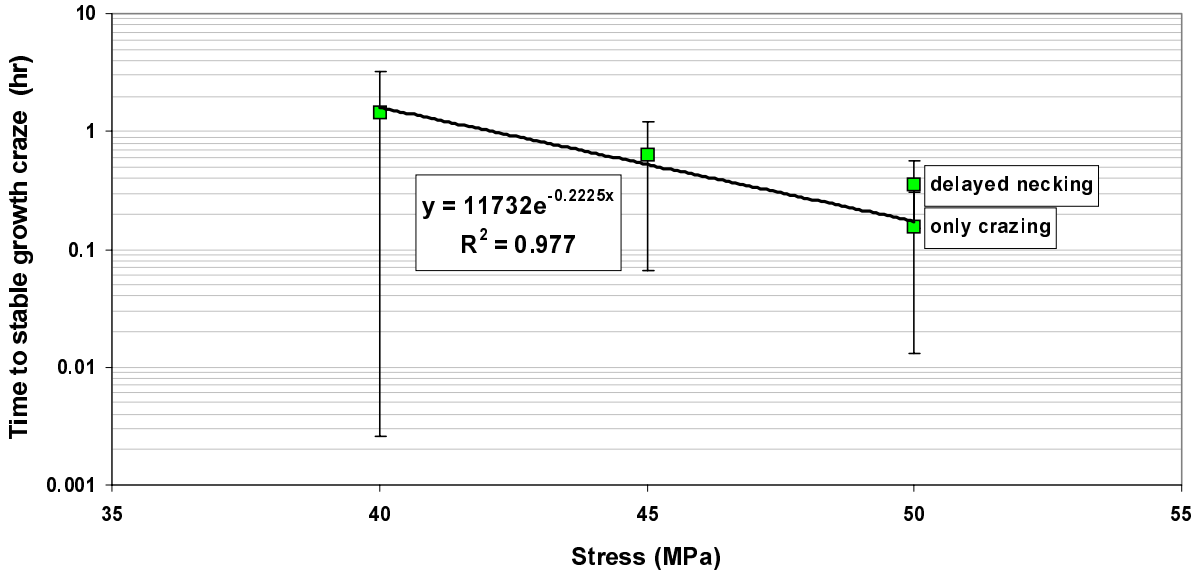

Figure 34: Effect of stress level on craze initiation time (24°C, 85% rh)

As expected, the time to craze initiation decreases with increasing stress level at 24°C and 85% rh according to Equation 4-3. One exception to this behavior is the delayed necking samples in which the craze initiation time was higher for the same reasons the craze growth rates were lower in Figure 31.

$$t_{c0}(\sigma) = 11{,}732\ e^{-0.2225\sigma} \qquad (4\text{-}3)$$

where $t_{c0}(\sigma)$ is the time to stable craze growth initiation in hr, and σ is the crazing stress in MPa.

It is obvious from Figure 34 that the scatter in the craze initiation data is too large to put much faith in Equation 4-3. The reason for the large scatter is that in the range of stress tested, craze initiation begins in a very short time scale. For this reason, the time to reach 1% relative craze density was measured for each data set in Figure 30 and plotted as a function of crazing stress in Figure 35 with error bars showing one standard deviation.

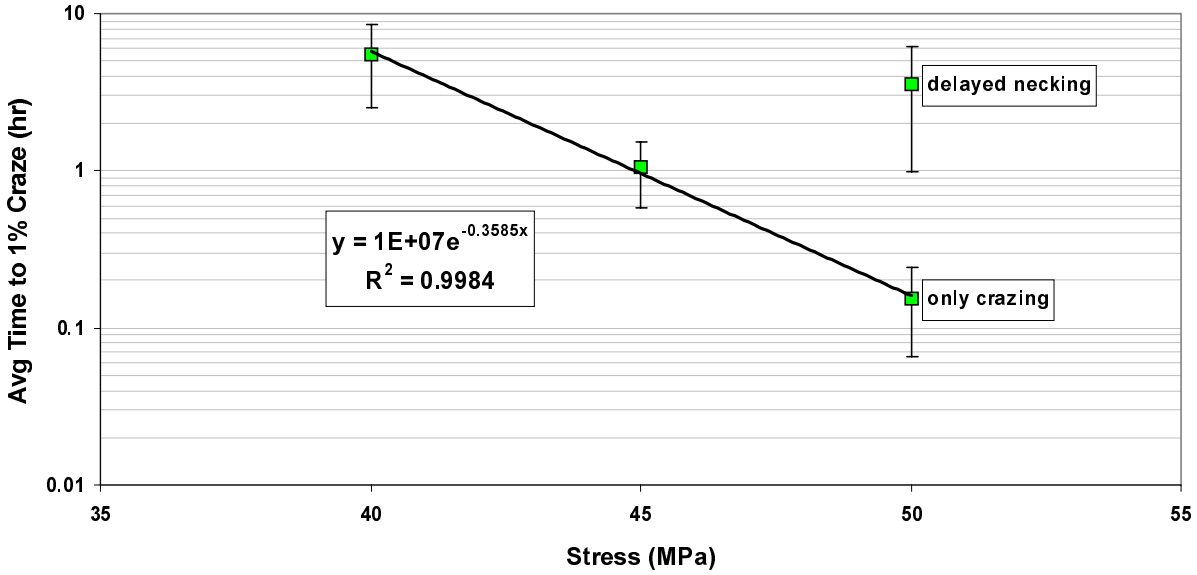

Figure 35: Effect of stress level on time to 1% relative craze density (24°C, 85% rh)

Figure 34 displays a much improved metric for the viscoelastic nature of crazing of the test material than craze initiation. It is shown that the time to 1% relative craze density decreases exponentially with crazing stress at 24°C and 85% rh with the relationship given as

$$t_{c1}(\sigma) = 1x10^{7}\, e^{-0.3585\sigma} \qquad (4\text{-}4)$$

where $t_{c1}(\sigma)$ is the time to 1% relative craze density in hr and σ is the crazing stress in MPa.

Once again, the samples that experienced delayed necking do not obey Equation 4-4 since an entirely different mechanism exists. The time to 1% craze density was much higher for the samples that yielded than for the samples that only crazed for the same reasons that the craze initiation time was higher and the craze growth rate was lower.

Mathematically, Equation 4-1 represents the slope of a craze growth chart while Equation 4-4 is a point on the craze growth curve. Equation 4-5 incorporates these two expressions into a single equation that can be used to predict the craze growth chart for the test material as a function of stress between 40 and 50 MPa.

$$D(\sigma, t) = R(\sigma)\,[t - t_{c1}(\sigma)] + 1 \qquad (4\text{-}5)$$

where D(σ, t) is the relative craze density in %, R(σ) is the craze growth rate as a function of stress as shown in Equation 4-1, t is the time under load in hrs, and $t_{c1}(\sigma)$ is the time to reach 1% relative craze density as a function of stress as shown in Equation 4-4. Figure 36 graphically shows the goodness of fit for Equation 4-5.

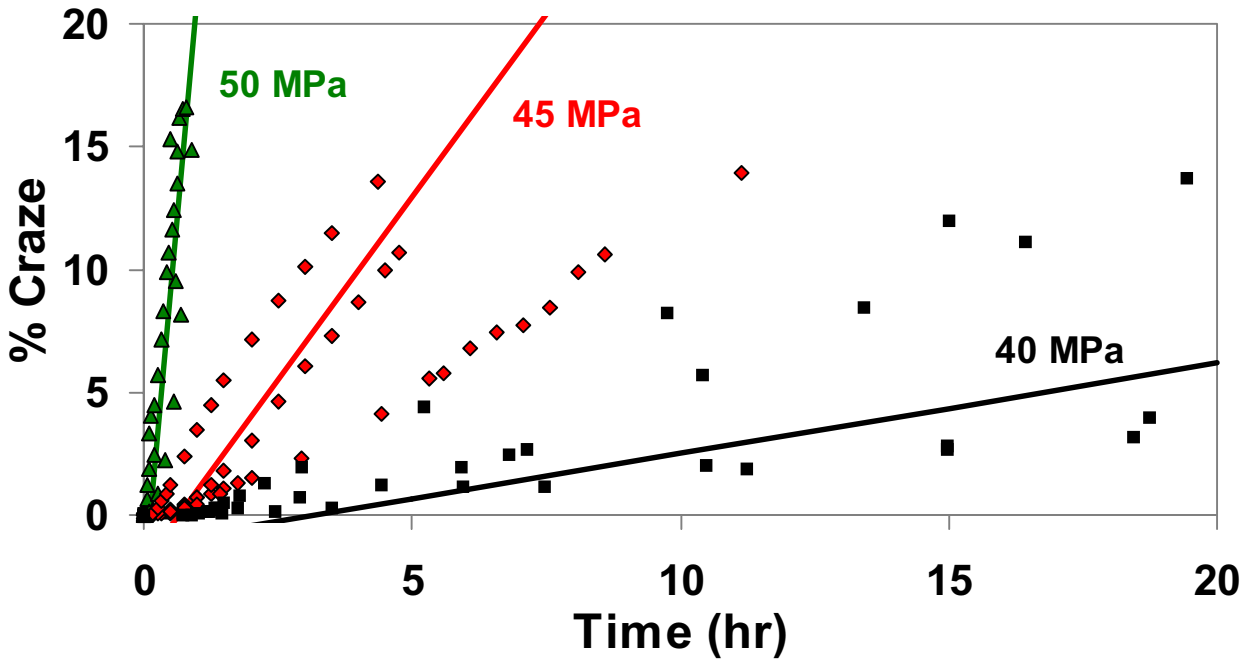

Figure 36: Craze growth prediction of Equation 4-5 with experimental data at 40, 45, and 50 MPa

Chapter 5 DISCUSSION

5.1 Qualitative analysis of the effects of crazing stress, relative craze density, and strain rate on mechanical properties

This section of the dissertation is dedicated to graphically interpreting the effects of crazing stress, crazing amount, and strain rate on the yield stress, elastic modulus, failure stress, and ductility of polycarbonate. First, the effects of moisture and strain rate on the mechanical properties of as-received polycarbonate are determined. These results are used as a baseline for the crazing effects. Next, the effects of the crazing stress and crazing amount on the mechanical properties of polycarbonate are investigated. Finally, the residual mechanical properties as a function of strain rate are graphically interpreted. The next section of the dissertation is dedicated to developing a quantitative model to predict the effects of crazing stress, crazing amount, and strain rate on the mechanical properties of polycarbonate.

5.1.1 Effect of moisture and strain rate on the mechanical properties of as-received samples

Figure 37 through Figure 40 are presented to determine the effect of moisture and strain rate on the yield stress, elastic modulus, failure stress, and ductility of as-received polycarbonate. These results will be used as a baseline in determining the behavior of polycarbonate that had been crazed to various levels at various magnitudes of crazing stress. The material used for this section was the McMaster Carr 6 mm thick polycarbonate sheet described in Chapter 3.

5.1.1.1 Effect of moisture and strain rate on the yield stress of as-received polycarbonate

According to the theory presented in Chapter 2, moisture has a plasticizing effect on polymers, resulting in increased molecular mobility [6]. When plasticization occurs, the yield stress decreases since less energy is required to bring about the large scale molecular motion required for plastic deformation.

Changes in the mechanical behavior of polymers with respect to strain rate have to do with the time available for polymer chains to respond to the applied stress. Relaxation is the

response of polymer molecules to changes in temperature and stress. When the load is applied at a very high rate, the polymer molecules do not have sufficient time to relax, resulting in an increase in the yield stress [6]. Figure 37 shows the yield stress results.

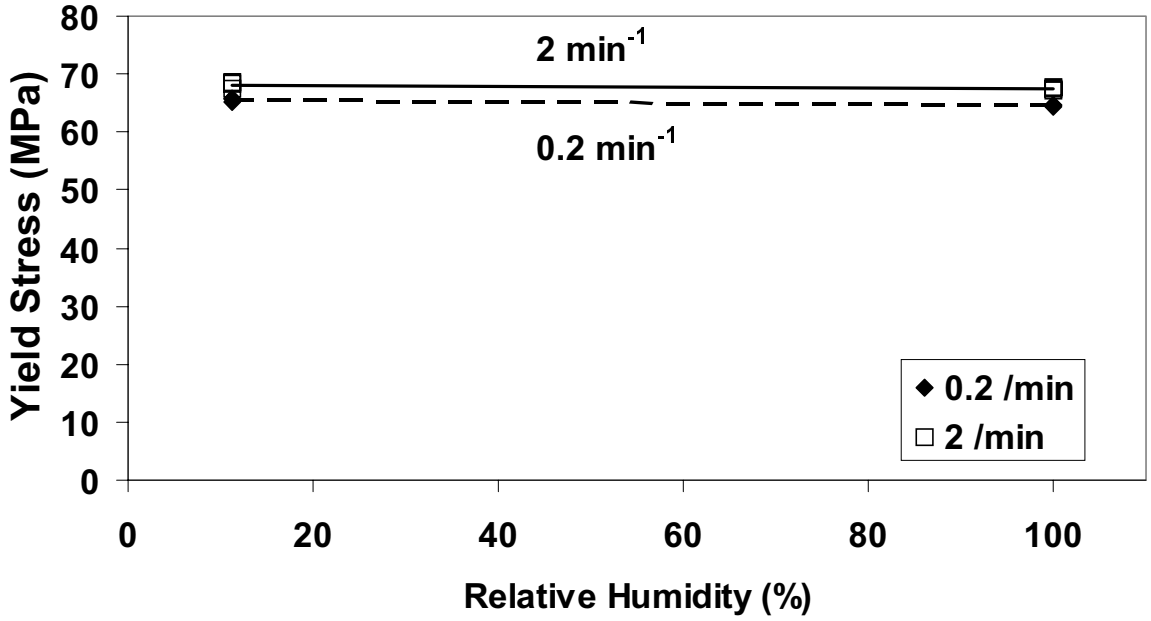

Figure 37: Effect of rh and strain rate on the yield stress of as-received polycarbonate

Three very clear conclusions about the yielding behavior of polycarbonate that can be drawn from Figure 37 are:

(1) the yield stress decreases with increasing moisture content,
(2) the yield stress increases with increasing strain rate, and
(3) the rate of decrease with rh is approximately the same for both testing rates.

These conclusions follow the theories of plasticization and relaxation time. Increasing the humidity from 11.3% rh to 100% rh decreased the yield stress approximately 1 MPa, while increasing the strain rate from 0.2 min^{-1} to 2 min^{-1} increased the yield stress on the order of 3 MPa.

5.1.1.2 Effect of moisture and strain rate on the elastic modulus of as-received polycarbonate

Figure 38 shows the response of the elastic modulus of polycarbonate at two humidities and two strain rates.

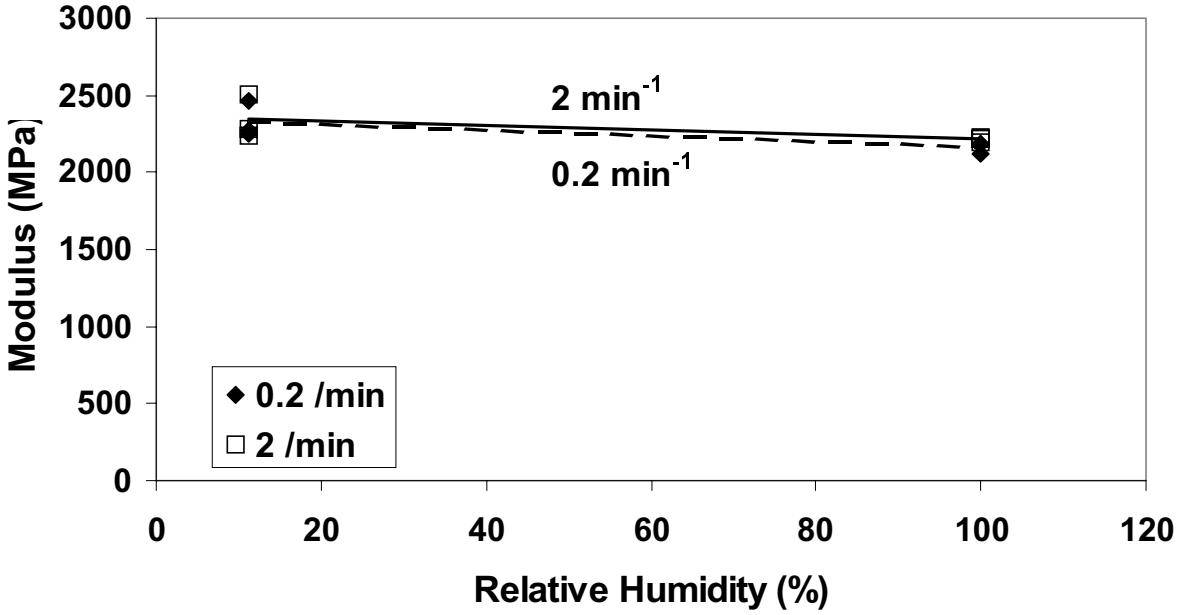

Figure 38: Effect of rh and strain rate on the elastic modulus of as-received polycarbonate

The conclusions that can be drawn about the effect of moisture and strain rate on the elastic modulus are:

(1) the elastic modulus decreases with increases moisture content, and
(2) the changes in the elastic modulus for strain rates of 0.2 and 2 min^{-1} are negligible.

The moisture effect is assumed to be the result of plasticization, similar to the yield stress response. For a given magnitude of stress, a plasticized material would exhibit a higher strain than an unplasticized material due to increased molecular mobility. This would decrease the elastic modulus.

5.1.1.3 Effect of moisture and strain rate on the failure stress of as-received polycarbonate

Yield stress and elastic modulus are elastic properties while failure stress and final elongation are failure properties. Theory suggests that both humidity and strain rate would effect the elastic properties more than failure properties since the elastic properties are governed by chain mobility while failure is governed by the statistical distribution of flaws. Figure 39 shows the failure stress of polycarbonate at two humidities and two strain rates.

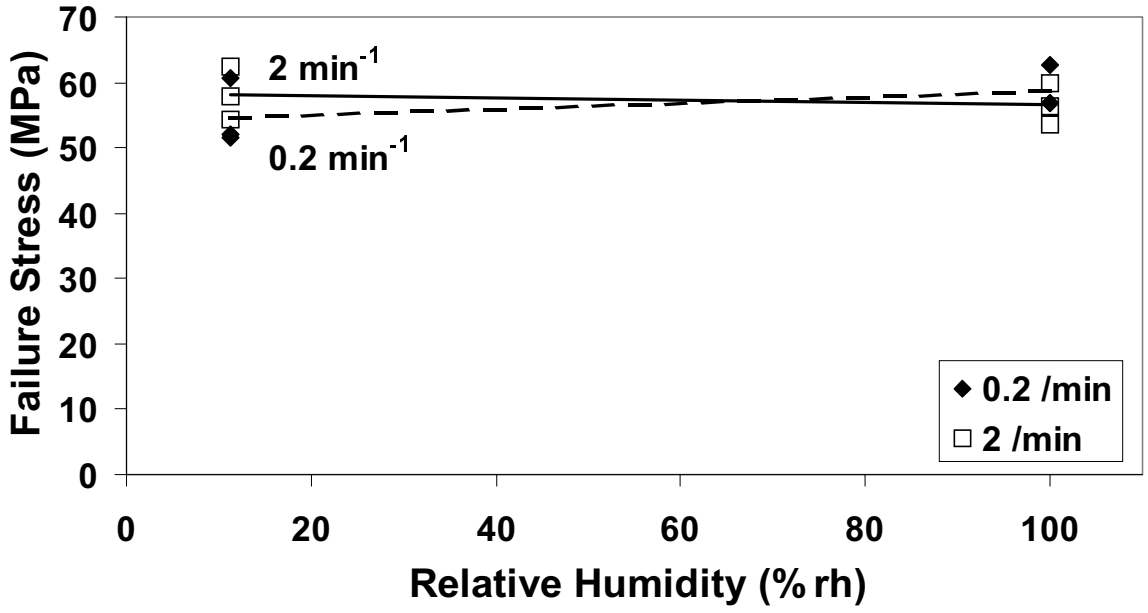

Figure 39: Effect of rh and strain rate on the failure stress of as-received polycarbonate

The conclusions that can be drawn about the effect of moisture and strain rate on the failure stress of polycarbonate are:

(1) the changes in the failure stress between humidities of 11.3 and 100% rh are negligible, and
(2) the changes in the failure stress between strain rates of 0.2 and 2 min^{-1} are negligible.

These conclusions show that any effect of strain rate on the failure stress of crazed samples implies an interaction between failure stress and crazing.

5.1.1.4 Effect of moisture and strain rate on the elongation of as-received polycarbonate

As mentioned above, the final elongation of polycarbonate is a failure property and should not be affected by moisture or strain rate to a large degree. The failure is governed by flaw distribution rather than chain mobility. Figure 40 shows the final length of the plastically deformed neck normalized to the gage length as a function of relative humidity and strain rate.

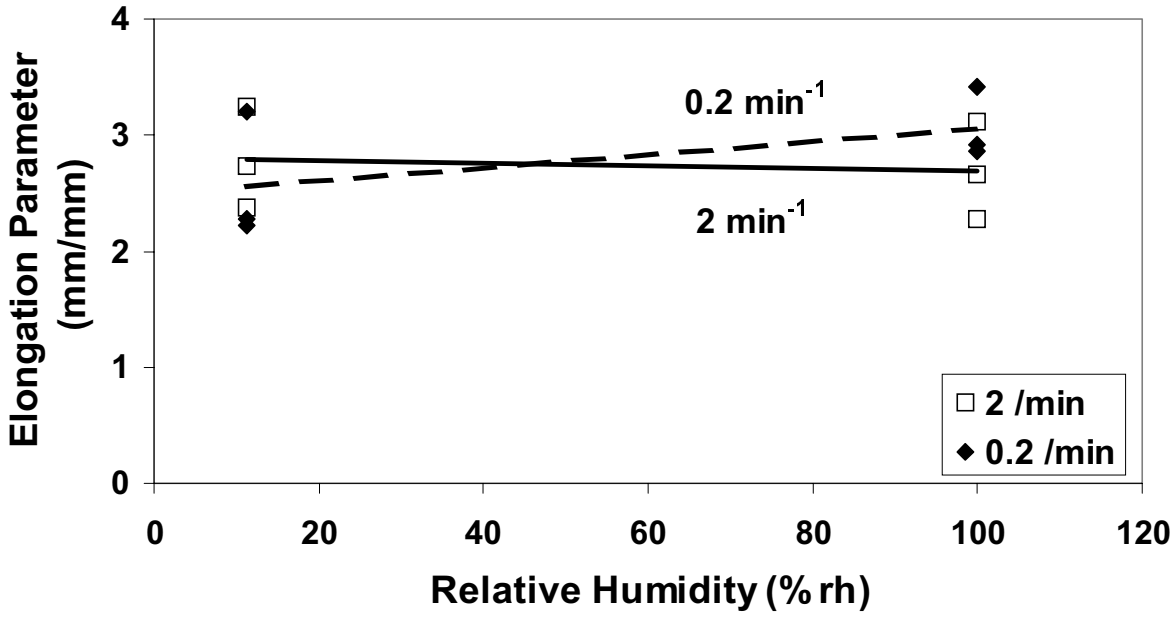

Figure 40: Effect of rh and strain rate on the ductility of as-received polycarbonate

Two conclusions that can be drawn about the effect of moisture and strain rate on the final elongation of polycarbonate are:

(1) the changes in the final elongation between humidities of 11.3 and 100% rh are negligible, and

(3) the changes in the final elongation between strain rates of 0.2 and 2 min^{-1} are negligible.

These conclusions show that any effect of strain rate on the final elongation of crazed samples implies an interaction between ductility and crazing.

5.1.2 Effect of relative craze density

The material used for this section of the dissertation was the 3 mm thick melt-calendered polycarbonate obtained from Rohm and Haas described in Chapter 3. The data shown in Figure 41 were obtained from samples crazed in various environments and possessing a variety of relative craze densities (all greater than 10%). The purpose of this graph is to try to generally show which mechanical properties are affected most by crazing.

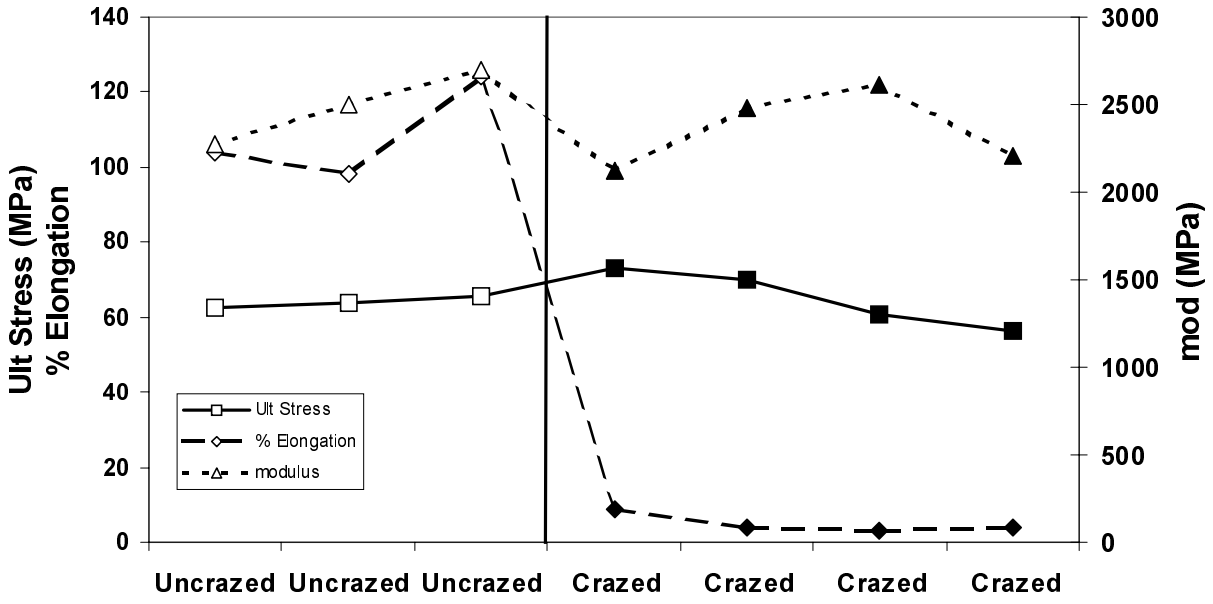

Figure 41: Effect of relative craze density on residual mechanical properties of 3 mm thick Rohm & Haas polycarbonate

It can be seen from the above graph that the ultimate stress and elastic modulus are apparently unaffected by crazing for the 3 mm thick polycarbonate samples, but the ductility decreases significantly. During testing, the crazed samples failed in a very brittle, glass-like manner with small fragments of polycarbonate projecting outward from the sample. For this material, these results indicate that large amounts of crazing greatly decrease the toughness of

the material. A highly crazed aircraft transparency made from this material would most assuredly fail during a birdstrike, even with a relatively low momentum.

The remainder of the results displayed in this dissertation are from the 6 mm polycarbonate samples obtained from McMaster Carr as described in Chapter 3. It will be shown that for this material, even at craze levels on the order of 10% and lower, the strength, stiffness, and ductility are all affected by crazing to a certain extent.

5.1.3 Effect of crazing stress on pre-crazed polycarbonate

The data presented in Figure 42 through Figure 48 have been organized in a way to try to show the effect that the magnitude of crazing stress and relative craze density have on the yield stress, elastic modulus, failure stress, and ductility. These effects will then be correlated to the microstructure of the crazes at each stress level.

5.1.3.1 Effect of crazing stress on the yield stress of pre-crazed polycarbonate

Figure 42 shows the effect that the magnitude of crazing stress and relative craze density have on the yield stress of polycarbonate. The data from the two different strain rates are plotted on separate graphs to decouple the effects of crazing stress and strain rate.

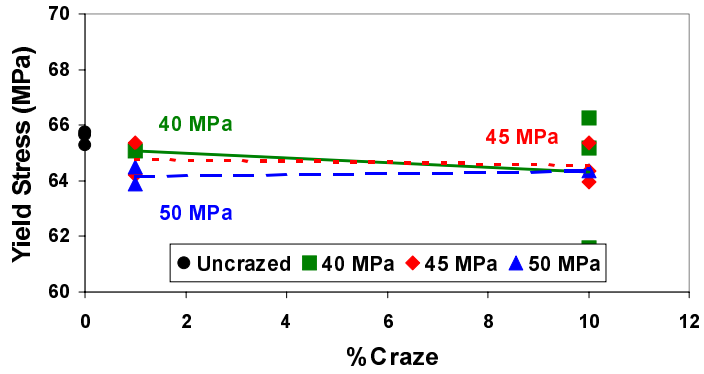

(a)

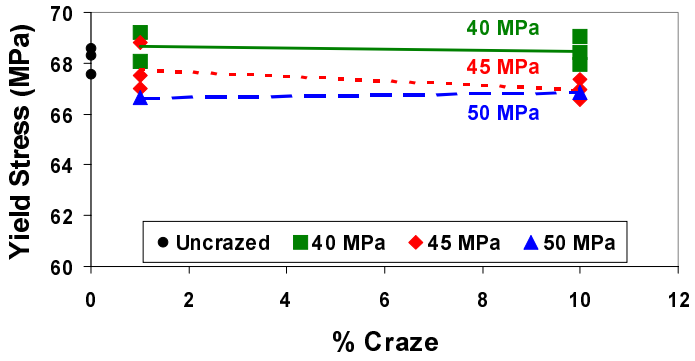

(b)

Figure 42: Effect of crazing stress and relative craze density on the yield stress of polycarbonate tested at (a) 0.2 min^{-1} and (b) 2 min^{-1} strain rates

These results show that the yield stress is not significantly affected by the crazing stress or relative craze density in the range tested. Although the differences in yield stress are not of a large magnitude, some general conclusions that can be drawn are:

(1) the yield stress decreases slightly with increasing craze density, and

(2) the yield stress decreases with increasing magnitude of crazing stress.

The first conclusion can be drawn from observing the yield stress of the uncrazed samples and the linear fit to the data. It should be noted that the effect is small, but can be seen for even a craze density as low as 1% for the 0.2 min^{-1} curve.

The second conclusion comes from comparing the curves from both strain rates and observing that the same trend exists in crazing stress. For both curves, the yield stress is highest for a crazing stress of 40 MPa and lowest for a crazing stress of 50 MPa.

The fact that the changes in yield stress are small is not surprising. Crazes are basically surface flaws that make up a very small part of the total volume of material, while the yield stress is an elastic property that involves energy being absorbed by the entire bulk sample. Flaws effect failure much more than elastic properties since failure often initiates at flaws.

5.1.3.2 Effect of crazing stress on the elastic modulus of pre-crazed polycarbonate

Figure 43 shows the effect that the magnitude of crazing stress and relative craze density have on the elastic modulus of polycarbonate. The data from the two different strain rates are plotted on separate graphs to decouple the effects of crazing stress and strain rate.

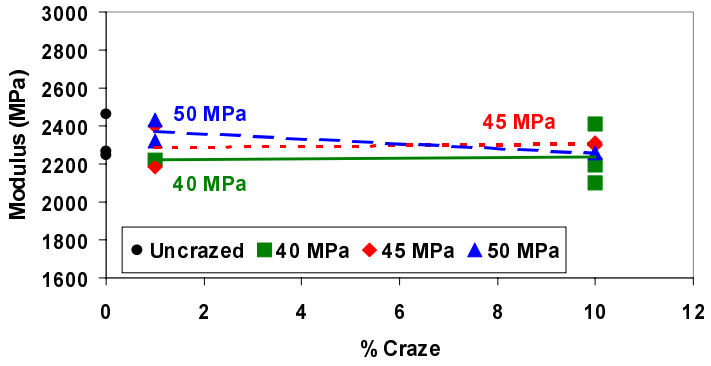

(a)

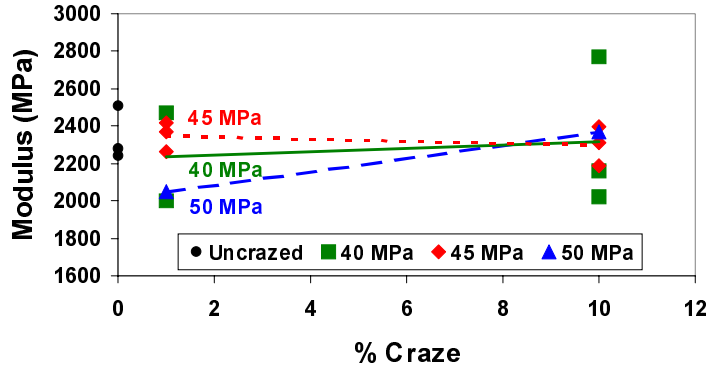

(b)

Figure 43: Effect of crazing stress and relative craze density on the elastic modulus of polycarbonate tested at (a) 0.2 min^{-1} and (b) 2 min^{-1} strain rates

The results shown in Figure 43 show that the elastic modulus is not affected by the magnitude of crazing stress and relative craze density. Once again, this conclusion is logical since the elastic modulus is an elastic property involving contributions from the entire bulk material of which the crazes are only a small part.

5.1.3.3 Effect of crazing stress on the failure stress of pre-crazed polycarbonate

Figure 44 shows the effect that the magnitude of crazing stress and relative craze density have on the failure stress of polycarbonate. The failure stress was taken as the final stress

obtained prior to fracture as described in Chapter 3. In an attempt to separate the effects of crazing stress and strain rate, the data from the two different strain rates are plotted on separate graphs.

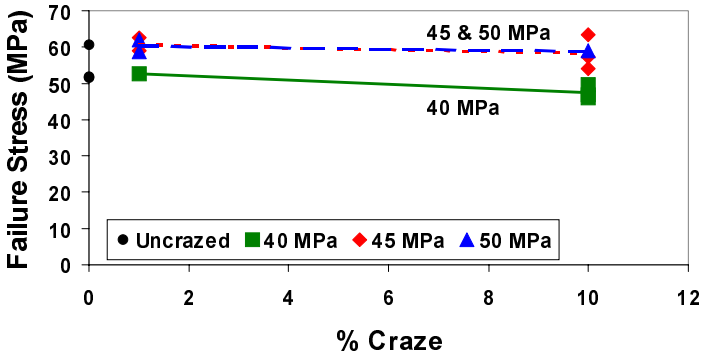

(a)

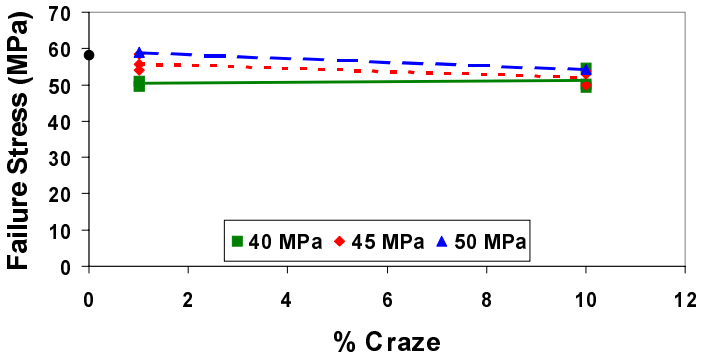

(b)

Figure 44: Effect of crazing stress and relative craze density on the failure stress of polycarbonate tested at (a) 0.2 min^{-1} and (b) 2 min^{-1} strain rates

It can be concluded from Figure 44 that the failure stress is affected by both the magnitude of crazing stress and relative craze density. Two conclusions that can be drawn from these results are:

(1) the failure stress increases with increasing crazing stress, and

(2) the failure stress decreases slightly with increasing amounts of crazing.

The reason for the first conclusion is not obvious without further investigation. More explanation is provided below in the correlation between the crazing stress and craze microstructure.

As mentioned above, the failure of polycarbonate should be more affected by crazing than the elastic behavior. The second conclusion agrees with this theory. Failure initiates at flaws, and a surface with a higher craze density contains more and/or larger flaws.

5.1.3.4 Effect of crazing stress on the ductility of pre-crazed polycarbonate

Figure 45 shows the effect that the magnitude of crazing stress and relative craze density have on the ductility of polycarbonate. The measure of ductility was taken to be the final length of the plastically deformed neck normalized to the gage length. This metric was chosen rather than % elongation since the deformation process is non-affine, consisting of a necked region and a non-plastically deformed region that have extremely different properties. The data from the two different strain rates are plotted on separate graphs to decouple the effects of crazing stress and strain rate.

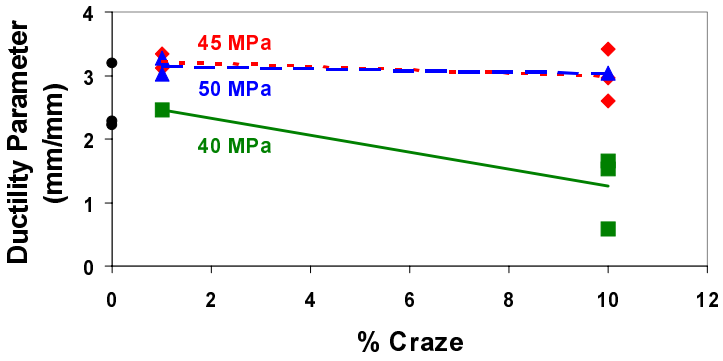

(a)

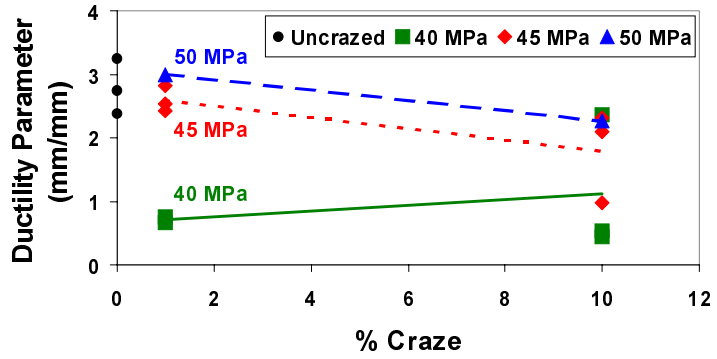

(b)

Figure 45: Effect of crazing stress and relative craze density on the ductility of polycarbonate tested at (a) 0.2 min^{-1} and (b) 2 min^{-1} strain rates

The final neck length on a failed polycarbonate sample is a failure property (post-yield) and not an elastic property. As mentioned above, failure properties are expected to be affected by crazing to a much greater extent than elastic properties. The results shown in Figure 45 show that this expectation is fulfilled. Two conclusions that can be drawn are:

(1) the ductility of polycarbonate decreases with increasing amount of crazing, and
(2) the ductility of polycarbonate crazed at 40 MPa is much lower than the ductility of polycarbonate crazed at 45 or 50 MPa.

The first conclusion follows the idea that the failure process is controlled by the density of flaws and correlates well with the reduction in ductility shown above for the 3 mm polycarbonate samples (Figure 41). A general comparison of the 3 mm and 6 mm thick samples show that the 3 mm thick samples showed a much sharper decrease in ductility, but they also contained a higher craze density. Since the craze densities are different, a conclusive correlation cannot be made, but since the thinner samples failed in a much more brittle manner than the thick samples it is generally believed that the residual ductility is lower for thinner samples.

A reduction in ductility implies a reduction in toughness. These results show that an aircraft transparency with as little as 1% relative craze density could experience greatly reduced impact toughness and fail in the event of a birdstrike. One consolation is the thickness effect that was observed. The thickness of an aircraft transparency is on the order of 25 mm, approximately four times as thick as the samples used in Figure 45.

The second conclusion agrees with the failure stress results, in that a crazing stress of 40 MPa is more detrimental to the durability of polycarbonate than a crazing stress of 45 or 50 MPa. To further investigate this observation, an attempt will now be made to correlate the magnitude of crazing stress to the microstructure of the crazes.

5.1.3.5 Effect of crazing stress on the microstructure of crazes

Figure 46 compares the microstructure of a typical craze formed at 40 MPa to one formed at 45 MPa. Both images were taken at a relative craze density of 10%. The area of the craze formed at 40 MPa was more than 2.5 times the area of the craze formed at 45 MPa. Similar results have been found in the literature [3]. Table 6 shows that the increased area is mostly the result of increased length. The craze formed at 40 MPa is more than twice as long as the other craze but is only about 25% wider.

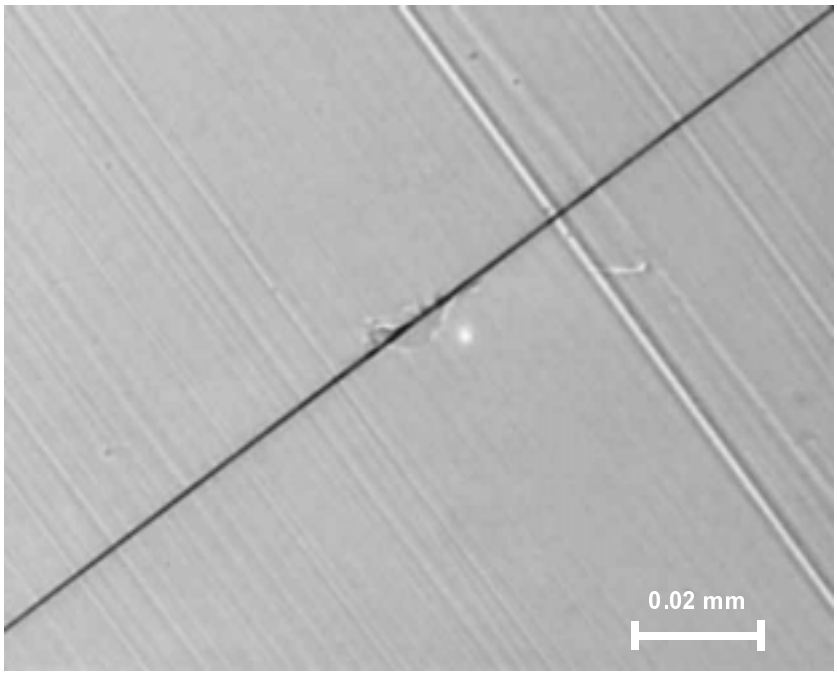

(a)

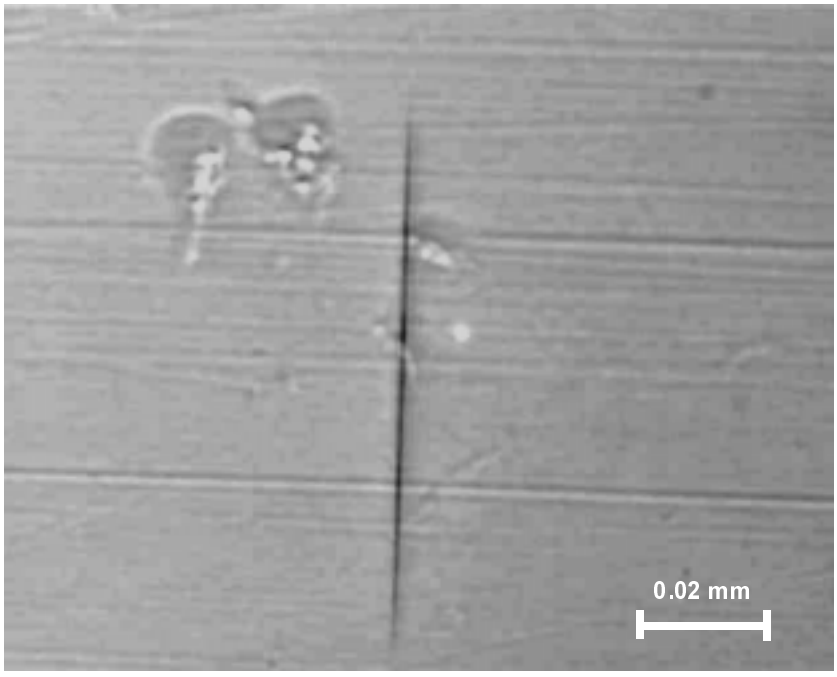

(b)

Figure 46: Micrograph of typical craze on samples crazed at (a) 40 MPa and (b) 45 MPa

Table 6: Dimensions of crazes formed at 40 and 45 MPa

Crazing Stress →	**40 MPa**	**45 MPa**
Area (mm^2)	5.7e-5	2.2e-5
Length (mm)	0.11	0.05
Width (mm)	6.8e-4	5.4e-4
Aspect Ratio (L/W)	162	93

One reason why the lower stress creates fewer, larger crazes could be that the crazes often form at microscopic flaws that produce stress concentrations. At the lower crazing stress, there are fewer flaws large enough to increase the local stress to the magnitude required for craze initiation. Fewer craze initiation sites means fewer crazes. This concept is illustrated in Figure 47.

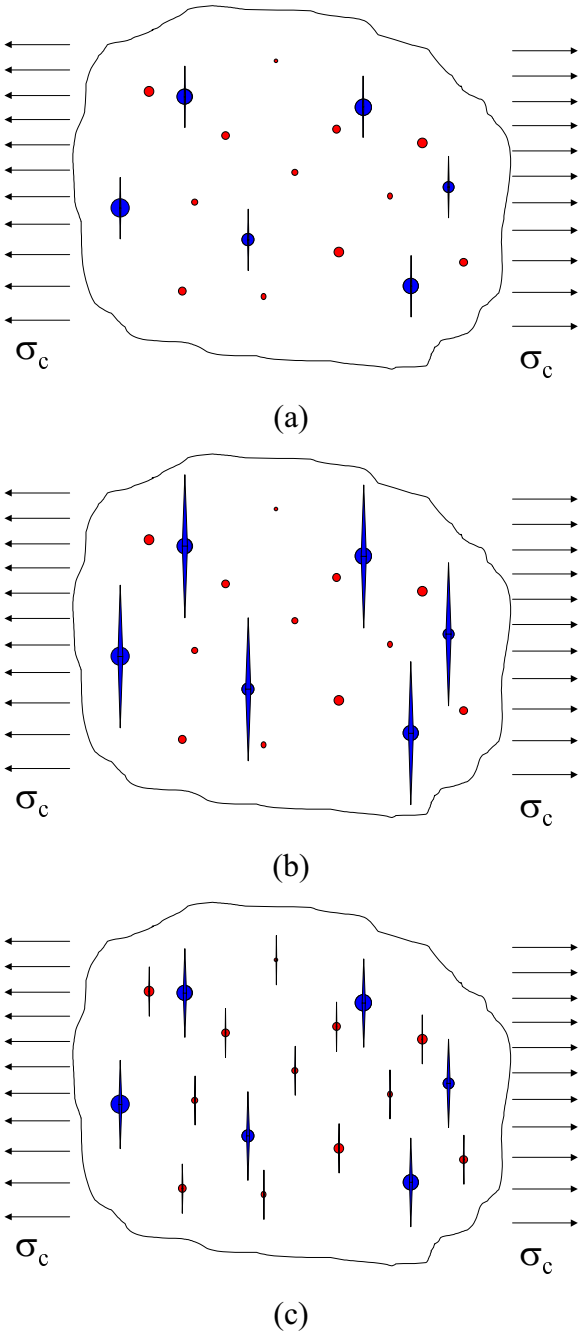

Figure 47: Microscopic model of a statistical distribution of flaws with (a) a crazing stress of 40 MPa held for 24 hrs containing 2% craze density, (b) a crazing stress of 40 MPa held for 100 hrs containing 10% craze density, and (c) a crazing stress of 45 MPa held for 24 hrs containing 10% craze density.

Figure 47 shows a microscopic region in the polycarbonate, with the red circles representing a distribution of flaws with stress concentrations too low to initiate crazes at 40

MPa but high enough to initiate crazes at 45 MPa. The blue circles represent a distribution of flaws with stress concentrations sufficient for craze initiation at 40 MPa. Figure 47(a) shows the region after 40 MPa has been held for 24 hours. By this time, the relative craze density has reached 2%, but the testing continues until 10% is obtained. Figure 47(b) shows the region under 40 MPa after 100 hrs. The red circles still do not have local stresses high enough for craze initiation, so the crazes on the blue circles are now very large, making up 10% relative craze density.

Figure 47(c) shows the region with a stress of 45 MPa held for 24 hrs. At this magnitude of stress, the red circles had a high enough magnitude of local stress to initiate crazes. Now the total relative craze density consists of many more crazes, reaching 10% much faster. Since more crazes are involved, the crazes on the blue circles were not grown as large as when the 40 MPa stress was applied. This model demonstrates that when polycarbonate is crazed to 10% with a stress of 40 MPa, the sample contains fewer, larger crazes than with a stress of 45 MPa.

Correlating the microstructure of crazes formed at 40 and 45 MPa to the residual failure strength and ductility described above shows that the larger crazes formed at the lower stress level cause a much larger decrease in the failure strength and ductility of polycarbonate. In other words, flaw size has a greater effect on the failure properties of polycarbonate than flaw quantity.

The craze density results reported in this dissertation are actually relative, depending on the amount of light reflected by the crazes. The average area of the crazes were calculated for the optical craze measurement procedure described in Chapter 3. The calculated areas are plotted as a function of crazing stress in Figure 48 with error bars showing one standard deviation.

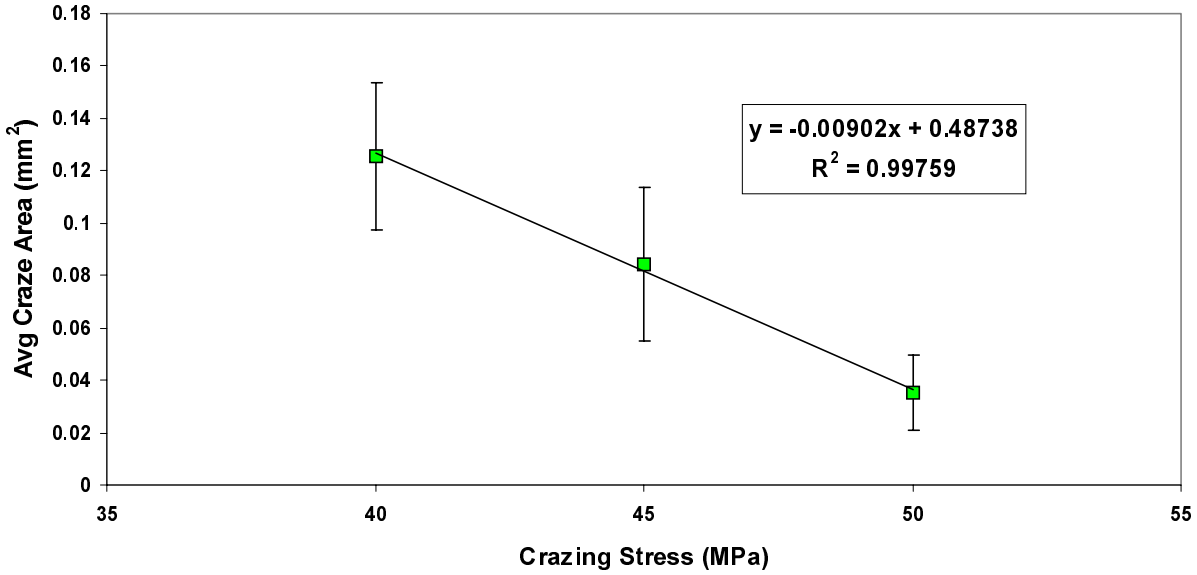

Figure 48: Effect of crazing stress on average craze area (24°C, 85% rh)

Comparing the areas of the light reflection in Figure 48 and the areas measured on an optical microscope in Table 6 shows that the light reflections are about three to four orders of magnitude larger, but follow the same trend of decreasing area with increasing crazing stress. The linear regression model for average craze area versus crazing stress using the technique developed for this dissertation is given by

$$\mathbf{A_c = -0.00902\ \sigma + 0.487} \qquad (5\text{-}1)$$

where A_c is the average area of the crazes in mm and σ is the crazing stress in MPa.

5.1.4 Effect of strain rate on pre-crazed polycarbonate

The data presented in Figure 49 through Figure 52 have been organized in a way to try to show the effect that the strain rate and relative craze density have on the yield stress, elastic modulus, failure stress, and ductility. The effect of strain rate on the mechanical properties of uncrazed polycarbonate has already been shown in Figure 37 through Figure 40. The analysis presented in this chapter will concentrate on identifying interactions between the strain rate and relative craze density or crazing stress.

5.1.4.1 Effect of strain rate on the yield stress of pre-crazed polycarbonate

Figure 49 shows the effect that the magnitude of strain rate and relative craze density have on the yield stress of polycarbonate. The data from the three different crazing stresses are plotted on separate graphs to decouple the effects of strain rate and crazing stress.

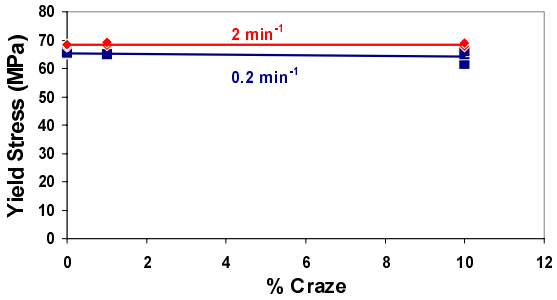

(a)

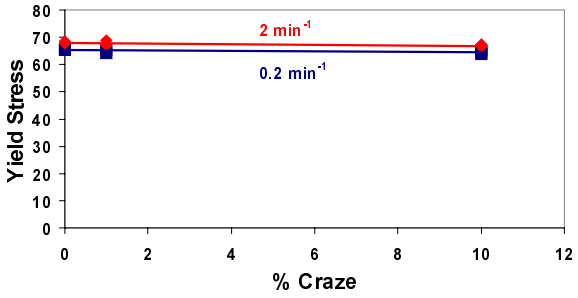

(b)

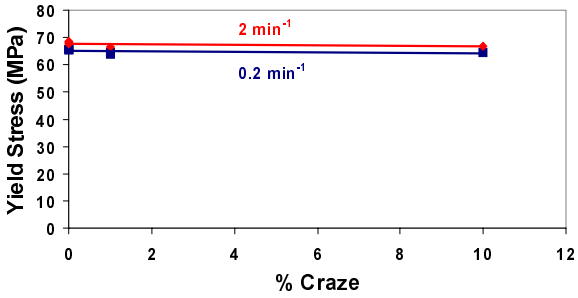

(c)

Figure 49: Effect of strain rate and relative craze density on the yield stress of polycarbonate crazed at (a) 40 MPa, (b) 45 MPa, and (c) 50 MPa

As expected from Figure 37 (11.3% rh), the yield stress is higher for the faster strain rate at all levels of relative craze density and crazing stress. The negative slope of the linear fit indicates a slight decrease in yield stress with increasing craze density. For the most part, the decrease occurs with as little as 1% relative craze density.

5.1.4.2 Effect of loading rate on the elastic modulus of pre-crazed polycarbonate

Figure 50 shows the effect that the magnitude of strain rate and relative craze density have on the elastic modulus of polycarbonate. The data from the three different crazing stresses are plotted on separate graphs to decouple the effects of strain rate and crazing stress.

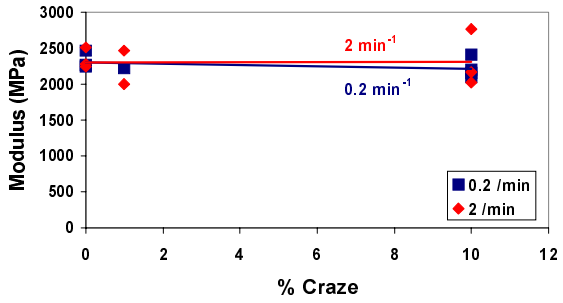

(a)

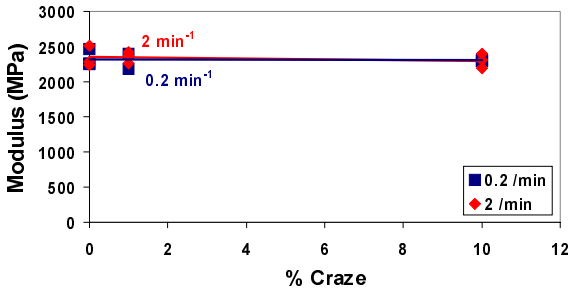

(b)

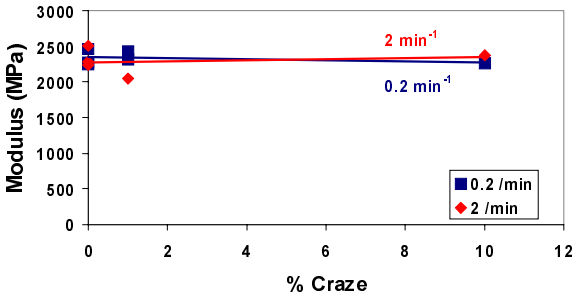

(c)

Figure 50: Effect of strain rate and relative craze density on the elastic modulus of polycarbonate crazed at (a) 40 MPa, (b) 45 MPa and (c) 50 MPa

Figure 50 shows that neither strain rate nor relative craze density has a significant effect on the elastic modulus of crazed polycarbonate. Also, there is no apparent interaction between strain rate and relative craze density with respect to their effect on elastic modulus.

5.1.4.3 Effect of strain rate on the failure stress of pre-crazed polycarbonate

Figure 51 shows the effect that the magnitude of strain rate and relative craze density have on the failure stress of polycarbonate. The data from the three different crazing stresses are plotted on separate graphs to decouple the effects of strain rate and crazing stress.

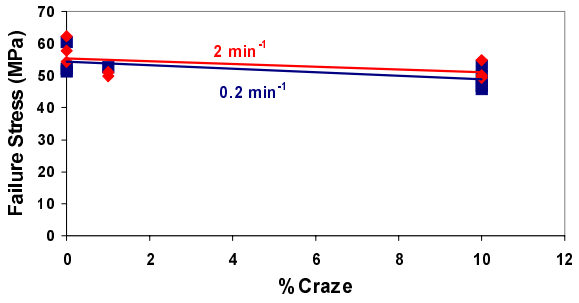

(a)

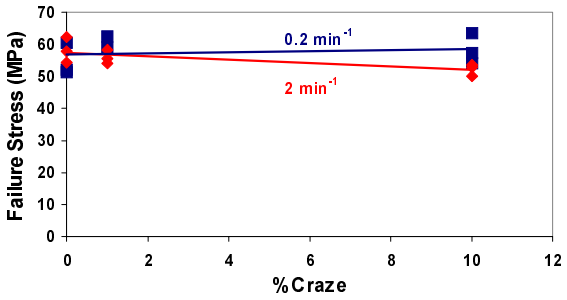

(b)

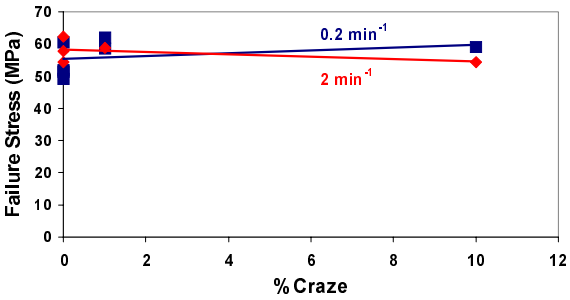

(c)

Figure 51: Effect of strain rate and relative craze density on the failure stress of polycarbonate crazed at (a) 40 MPa, (b) 45 MPa, and (c) 50 MPa

The most significant effect seems to be at the higher crazing stresses (45 and 50 MPa) and 10% relative craze density where the higher strain rate (2 min^{-1}) resulted in a much lower failure stress than the lower strain rate (0.2 min^{-1}). At the lower relative craze densities (≤1%), the changes in the failure stress at the two strain rates are statistically insignificant. Correlating this conclusion to the microstructure of the crazes implies that the failure stress of the samples with a large number of small crazes are much more effected by the strain rate than samples with a small number of large crazes.

5.1.4.4 Effect of strain rate on the ductility of pre-crazed polycarbonate

Figure 52 shows the effect that the magnitude of strain rate and relative craze density have on the ductility of polycarbonate. The data from the three different crazing stresses are plotted on separate graphs to decouple the effects of strain rate and crazing stress. Once again, the final length of the plastically deformed neck normalized to the gage length was taken to be the measure of ductility.

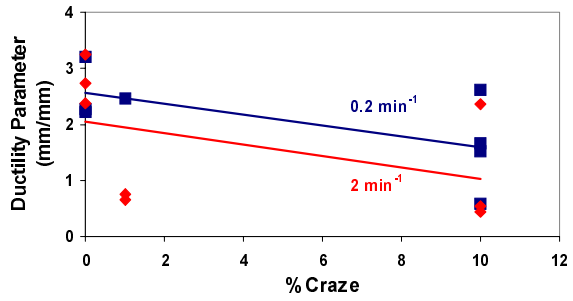

(a)

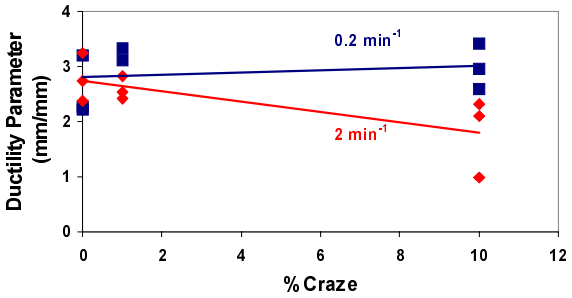

(b)

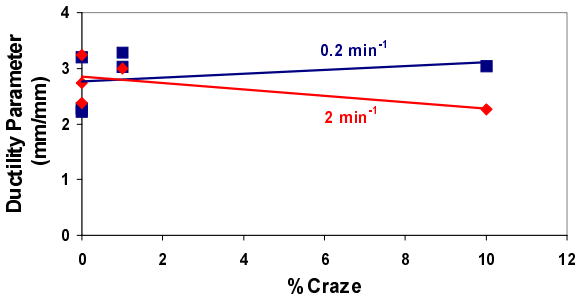

(c)

Figure 52: Effect of strain rate and relative craze density on the ductility of polycarbonate crazed at (a) 40 MPa, (b) 45 MPa, and (c) 50 MPa

The results presented in Figure 52 indicate that an increase in strain rate causes a decrease in ductility. Similar to Figure 51, this trend is most significant at the higher crazing stresses (45 and 50 MPa) and 10% relative craze density where the higher strain rate (2 min^{-1}) resulted in a much lower ductility than the lower strain rate (0.2 min^{-1}). At the lower relative

craze densities (≤1%), the changes in ductility at the two strain rates are much less significant, but in this case are in the same direction.

5.2 Development of a quantitative model using the Design of Experiments (DOE) approach with three factors

A Design of Experiments analysis was conducted to build a mathematical model for the residual mechanical properties of PC as a function of crazing stress, relative craze density, and strain rate. A computer program called DOE KISS [59] was used to analyze the results of the craze test matrix. The program coded the values to –1 for the low level and +1 for the high level (Table 7). For example, the stress level of 40 MPa corresponds to –1 while 45 MPa corresponds to +1. The orthogonal nature of the coded matrix allows efficient statistical calculations to be performed on the collected data.

Table 7: Coded values for DOE models

	Low (-1)	High (+1)
Crazing Stress (MPa)	40	45
Relative Craze Density (%)	1	10
Strain Rate (min^{-1})	0.2	2

The predictive model output of DOE KISS will be in the general form as described in Chapter 3 and shown in Equation 5-2.

$$\mathbf{Y = c_0 + c_1A + c_2B + c_3C + c_4AB + c_5AC + c_6BC} \quad (5\text{-}2)$$

where Y is the predicted value of a given residual mechanical property, the c's are coefficients, A is the coded stress level (-1, +1), B is the coded relative craze density (-1, +1), C is the coded strain rate (-1, +1), and multiplication of two main factors represents the interaction between the two main factors.

5.2.1 Three factor DOE model of residual yield stress

The first mechanical property of crazed polycarbonate to be considered was yield stress. Table 8 shows the test results for all three repetitions of the eight test runs. The mean and standard deviation of the three repetitions are also given.

Table 8: DOE test results for residual yield stress

(A) Crazing Stress (MPa)	(B) Relative Craze Density (%)	(C) Strain Rate (mm/min)	Y1 (MPa)	Y2 (MPa)	Y3 (MPa)	YBAR (MPa)	S (MPa)
40	1	0.2	65.1	65.7	65.6	65.5	0.348
40	1	2	68.1	69.2	68.6	68.6	0.570
40	10	0.2	61.6	65.2	66.3	64.3	2.44
40	10	2	68.4	67.9	69.1	68.5	0.561
45	1	0.2	64.2	65.4	64.9	64.8	0.573
45	1	2	67.5	67.0	68.8	67.8	0.943
45	10	0.2	65.4	64.0	64.4	64.6	0.735
45	10	2	66.6	67.0	67.4	67.0	0.385

Using the data in Table 8, the constant and coefficients for the predictive model for yield stress were calculated by the statistical software program in the manner shown in Equations 3-1 and 3-2. *P(2-tail)* and the standard deviation for each factor are also given in Table 9. *P(2-tail)* is described in Chapter 3 as the probability of placing an insignificant term in the predictive model [53]. The rule of thumb suggested in the literature is that if *P(2-tail)* is less than 0.1 then the term is significant [53].

Table 9: Original model for yield stress with all factors included in regression

FACTOR	COEFFICIENT FOR Y MODEL (MPa)	P(2 tail)	COEFFICIENT FOR S MODEL (MPa)
Constant	66.4	**0.000**	**0.820**
(A) Crazing Stress	-0.350	0.119	-0.161
(B) Relative Craze Density	-0.295	0.184	0.212
(C) Strain Rate	1.58	**0.000**	-0.205
AB	0.0312	0.885	-0.310
AC	-0.244	0.268	0.210
BC	0.0513	0.812	-0.353
ABC	-0.191	0.381	0.173

$R^2 = 0.796$

The only terms shown in Table 9 that have *P(2-tail)* < 0.1 are the constant and the strain rate. Therefore, the predictive model for yield stress of crazed polycarbonate will only contain these two terms, as shown by

$$\sigma_y = 66.4 + 1.58\ R \qquad (5\text{-}3)$$

where σ_y is the yield stress of the crazed sample in MPa and R is the coded strain rate.

These results correlate well with the qualitative results shown in Section 5.1. The previously reported qualitative results show that increasing the crazing stress from 40 to 45 MPa and increasing the relative craze density from 1 to 10% produces a very slight decrease, but overall insignificant effect on the yield stress. The previous results also showed that increasing the strain rate from 0.2 to 2 min^{-1} increased the yield stress on the order of 3 MPa. Equation 5-3 implies that an increase in the strain rate from 0.2 to 2 min^{-1} will increase the yield stress by 3.16

MPa since the coefficient shows the half effect of the factor. Therefore, Equation 5-3 provides a quantitative model to the qualitative results.

The relative importance of each factor are shown graphically in Figure 53. The absolute value of half of each differential effect is plotted as a function of the corresponding factor as described in Section 2.6.2.

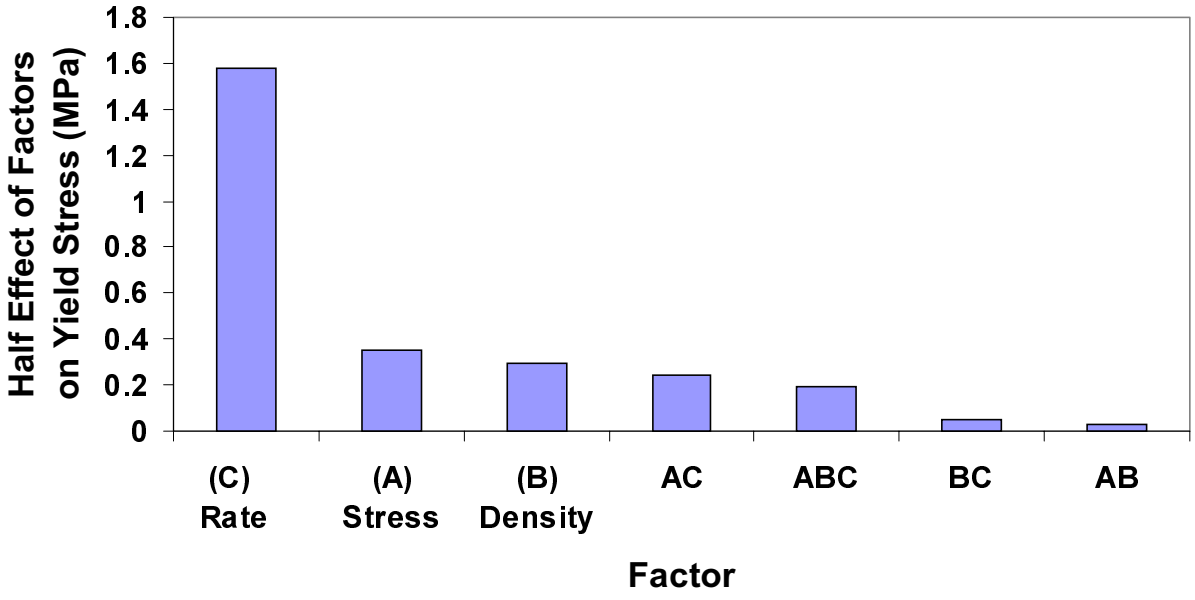

Figure 53: Pareto diagram showing relative factor importance for the yield stress model

The Pareto diagram shows graphically that the strain rate produces a much greater change in the yield stress than the other factors or interactions. Since it is obvious that the contribution of the interactions are insignificant, no interaction graphs will be displayed for yield stress.

5.2.2 Three factor DOE model of residual elastic modulus

The next mechanical property of crazed polycarbonate to be considered was elastic modulus. Table 10 shows the test results for all three repetitions of the eight test runs. The mean and standard deviation of the three repetitions are also given.

Table 10: DOE test results for residual elastic modulus

(A) Crazing Stress (MPa)	(B) Relative Craze Density (%)	(C) Strain Rate (min^{-1})	Y1 (MPa)	Y2 (MPa)	Y3 (MPa)	YBAR (MPa)	S (MPa)
40	1	0.2	2221	2177	2166	2188	29.1
40	1	2	1999	2471	2235	2235	236
40	10	0.2	2099	2197	2413	2236	161
40	10	2	2021	2162	2397	2193	190
45	1	0.2	2185	2398	2257	2280	108
45	1	2	2260	2371	2415	2349	79.9
45	10	0.2	2308	2300	2300	2303	4.62
45	10	2	2188	2310	2394	2297	104

Using the data in Table 10, the constant and coefficients for the predictive model for elastic modulus were calculated similarly to the yield stress calculations above and are shown in Table 11. The *P(2-tail)* and the effect of each factor on the standard deviation of the elastic modulus are also given.

Table 11: Original model for elastic modulus with all factors included in regression

FACTOR	COEFFICIENT FOR Y MODEL (MPa)	P(2 tail)	COEFFICIENT FOR S MODEL (MPa)
Constant	2260	**0.0000**	114
(A) Crazing Stress	47.0	0.109	-39.9
(B) Relative Craze Density	-2.75	0.922	0.684
(C) Strain Rate	8.42	0.765	38.3
AB	-4.42	0.875	-20.7
AC	7.42	0.792	-20.7
BC	-20.5	0.470	-6.27
ABC	2.00	0.943	38.1

$R^2 = 0.185$

The only term shown in Table 11 that has P(2-tail) < 0.1 is the constant. Therefore, the predictive model for elastic modulus of crazed polycarbonate will only contain the constant term, as shown in Equation 5-4.

$$\mathbf{E = 2260\ MPa} \tag{5-4}$$

where E is the elastic modulus of the crazed sample.

These results correlate well with the qualitative results shown in Section 5.1. The previously reported qualitative results show that increasing the crazing stress from 40 to 45 MPa and increasing the strain rate from 0.2 to 2 min^{-1} produces a very slight increase, but overall insignificant effect on the elastic modulus. No correlation was previously seen with relative craze density and elastic modulus. Since each of the factors appear to play an insignificant role in the behavior of the elastic modulus, no Pareto diagram will be shown for this model.

5.2.3 Three factor DOE model of residual failure stress

The previous two sections quantitatively modeled the effects of crazing stress, relative craze density, and strain rate on the elastic properties of polycarbonate. The following two sections attempt to model the failure properties of crazed polycarbonate. As mentioned before, crazing is expected to affect the failure properties more than the elastic properties. The first failure property to be considered is failure stress. Table 12 shows the test results for all three repetitions of the eight test runs. The mean and standard deviation of the three repetitions are also given.

Table 12: DOE test results for residual failure stress

(A) Crazing Stress (MPa)	(B) Relative Craze Density (%)	(C) Strain Rate (min^{-1})	Y1 (MPa)	Y2 (MPa)	Y3 (MPa)	YBAR (MPa)	S (MPa)
40	1	0.2	52.6	48.0	47.5	49.4	2.82
40	1	2	49.7	51.1	50.4	50.4	0.680
40	10	0.2	45.9	46.8	49.6	47.4	1.92
40	10	2	49.2	54.7	50.1	51.3	2.94
45	1	0.2	58.9	62.4	51.2	57.5	5.75
45	1	2	55.5	54.2	58.3	56.0	2.11
45	10	0.2	63.5	57.3	54.1	58.3	4.77
45	10	2	50.0	53.6	52.9	52.2	1.93

Using the data in Table 12, the constant and coefficients for the predictive model for failure stress were calculated similarly to the calculations above and are shown in Table 13. The *P(2-tail)* and the effect of each factor on the standard deviation of the failure stress are also given.

Table 13: Original model for failure stress with all factors included in regression

FACTOR	COEFFICIENT FOR Y MODEL (MPa)	P(2 tail)	COEFFICIENT FOR S MODEL (MPa)
Constant	52.8	**0.0000**	2.87
(A) Crazing Stress (MPa)	3.19	**0.0002**	0.775
(B) Relative Craze Density (%)	-0.503	0.460	0.0240
(C) Strain Rate (min^{-1})	-0.335	0.622	-0.950
AB	-0.259	0.702	-0.315
AC	-1.57	**0.0308**	-0.671
BC	-0.210	0.756	0.495
ABC	-0.935	0.179	-0.297

$R^2 = 0.664$

The only terms shown in Table 13 that have P(2-tail) < 0.1 are the constant, the crazing stress, and the interaction between the crazing stress and the strain rate. Therefore, the predictive model for the failure stress of crazed polycarbonate will only contain these three terms, as shown by

$$\sigma_f = 52.8 + 3.19\,\sigma_c - 1.57\,\sigma_c \bullet R \qquad (5\text{-}5)$$

where σ_f is the failure stress of the crazed sample in MPa, σ_c is the dimensionless coded crazing stress, and $\sigma_c \bullet R$ is the dimensionless interaction between the coded crazing stress and the coded strain rate.

These results correlate well with the qualitative results shown in Section 5.1. The previously reported qualitative results show that no strong correlations exist between relative craze density or strain rate and failure stress. They also showed a strong correlation between crazing stress and failure stress, in that a crazing stress of 40 MPa results in a failure stress

significantly lower than a crazing stress of 45 MPa. Another observation from Section 5.1 that could have easily been overlooked is that when increasing the crazing stress from 40 to 45 MPa, the effect that the strain rate has on the failure stress reverses. At the lower crazing stress, an increase in strain rate increases the failure stress, while at the higher crazing stress, an increase in the strain rate decreases the failure stress. Therefore, an interaction exists between crazing stress and strain rate. Equation 5-5 provides a quantitative model to the qualitative results previously reported.

The relative importance of each factor in Table 13 are shown graphically in Figure 54. The absolute value of each half effect is plotted as a function of the corresponding factor.

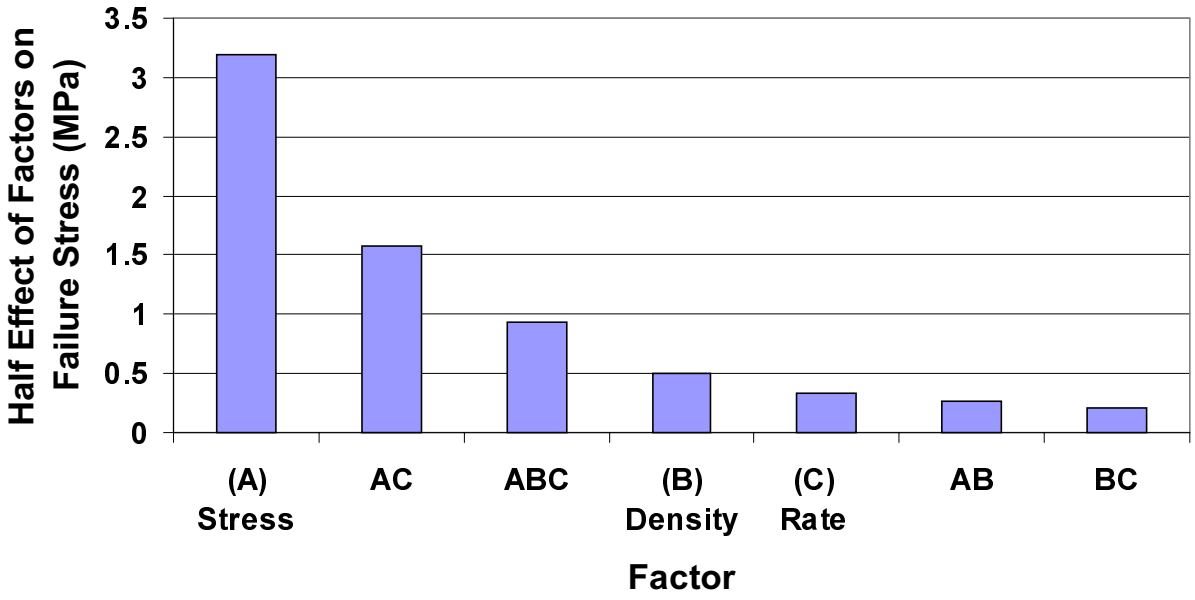

Figure 54: Pareto diagram showing relative factor importance for the failure stress model

The Pareto diagram shows graphically that the crazing stress and interaction between crazing stress and strain rate produce the greatest change in the failure stress compared to the other factors or interactions. Since the interactions are important in the failure stress model, interaction diagrams are shown in Figure 55.

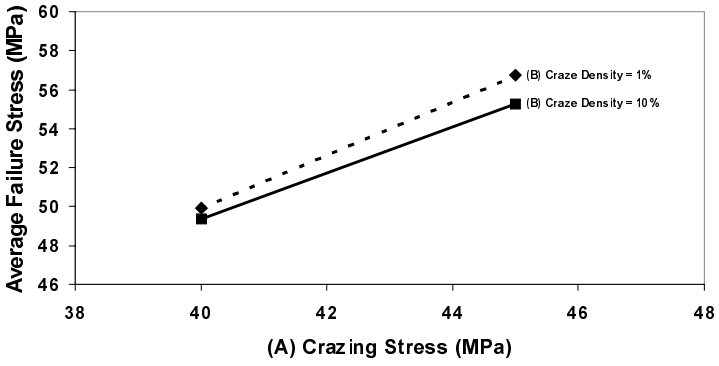

(a)

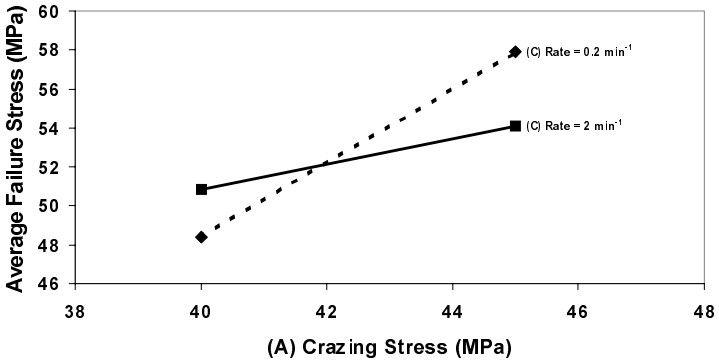

(b)

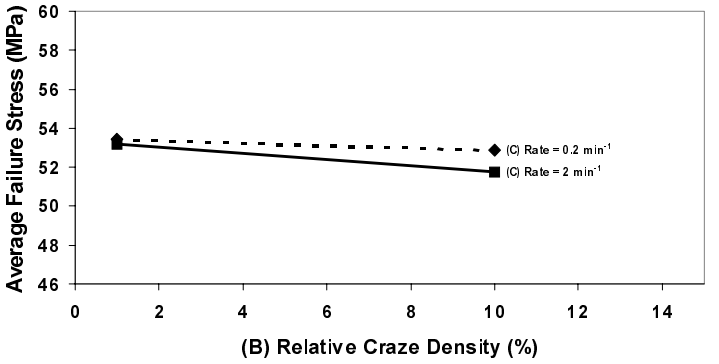

(c)

Figure 55: Failure stress interaction diagrams for factors (a) AB, (b) AC, and (c) BC

The fact that the curves in Figure 55a and c do not intersect indicate that there is no strong interaction between crazing stress and craze density or between craze density and strain

rate. The intersecting lines in Figure 55b indicate a strong interaction between crazing stress and strain rate. These results graphically verify the need to include the interaction in Equation 5-5.

5.2.4 Three factor DOE model of residual ductility

The next failure property to be considered is the ductility parameter defined as the ratio of the final length of the necked region of the fractured dogbone samples to the gage length of 50 mm. Table 14 shows the test results for all three repetitions of the eight test runs. The mean and standard deviation of the three repetitions are also given.

Table 14: DOE test results for residual ductility

(A) Crazing Stress (MPa)	(B) Relative Craze Density (%)	(C) Strain Rate (min^{-1})	Y1 (mm/mm)	Y2 (mm/mm)	Y3 (mm/mm)	YBAR (mm/mm)	S (mm/mm)
40	1	0.2	2.46	1.34	0.96	1.58	0.78
40	1	2	0.66	0.76	0.70	0.70	0.05
40	10	0.2	1.52	0.58	1.66	1.26	0.58
40	10	2	0.54	2.36	0.44	1.12	1.08
45	1	0.2	3.12	3.34	2.28	2.92	0.56
45	1	2	2.54	2.42	2.82	2.60	0.20
45	10	0.2	3.42	2.96	2.60	3.00	0.42
45	10	2	0.98	2.32	2.10	1.80	0.72

Using the data in Table 14, the constant and coefficients for the predictive model for the ductility parameter were calculated similarly to the calculations above and are shown in Table 15. The *P(2-tail)* and the effect of each factor on the standard deviation of the ductility measurement are also given.

Table 15: Original model for ductility with all factors included in regression

FACTOR	COEFFICIENT FOR Y MODEL (mm/mm)	P(2 tail)	COEFFICIENT FOR S MODEL (mm/mm)
Constant	1.87	**0.0000**	0.550
(A) Crazing Stress	0.706	**0.0000**	-0.0754
(B) Relative Craze Density	-0.080	0.5419	0.150
(C) Strain Rate	-0.316	**0.0253**	-0.0354
AB	-0.0984	0.455	-0.0592
AC	-0.0616	0.638	0.0236
BC	-0.0167	0.898	0.236
ABC	-0.202	0.136	-0.0702

$R^2 = 0.714$

The only terms shown in Table 15 that have *P(2-tail)* < 0.1 are the constant, the crazing stress, and the strain rate. Therefore, the predictive model for the final length of the necked region normalized to the gage length will only contain these three terms, as shown by

$$\mathbf{L_f/L_g = 1.87 + 0.706\ \sigma_c - 0.316\ R} \qquad (5\text{-}6)$$

where L_f is the final length of the necked region of the crazed samples in mm, L_g is the gage length of 50 mm, σ_c is the dimensionless coded crazing stress, and R is the dimensionless coded strain rate.

These results correlate well with the qualitative results shown in Section 5.1. The previously reported qualitative results show that no strong correlation exists between relative craze density between 1 and 10% and ductility. They also showed a strong correlation between crazing stress and ductility, in that a crazing stress of 40 MPa results in a significantly lower amount of ductility than a crazing stress of 45 MPa. A strong correlation was also qualitatively

displayed between strain rate and ductility. The ductility was seen to decrease with increasing strain rate. Equation 5-6 provides a quantitative model to the qualitative results previously reported.

The relative importance of each factor in Table 15 are shown graphically in Figure 56. The absolute value of each half effect is plotted as a function of the corresponding factor.

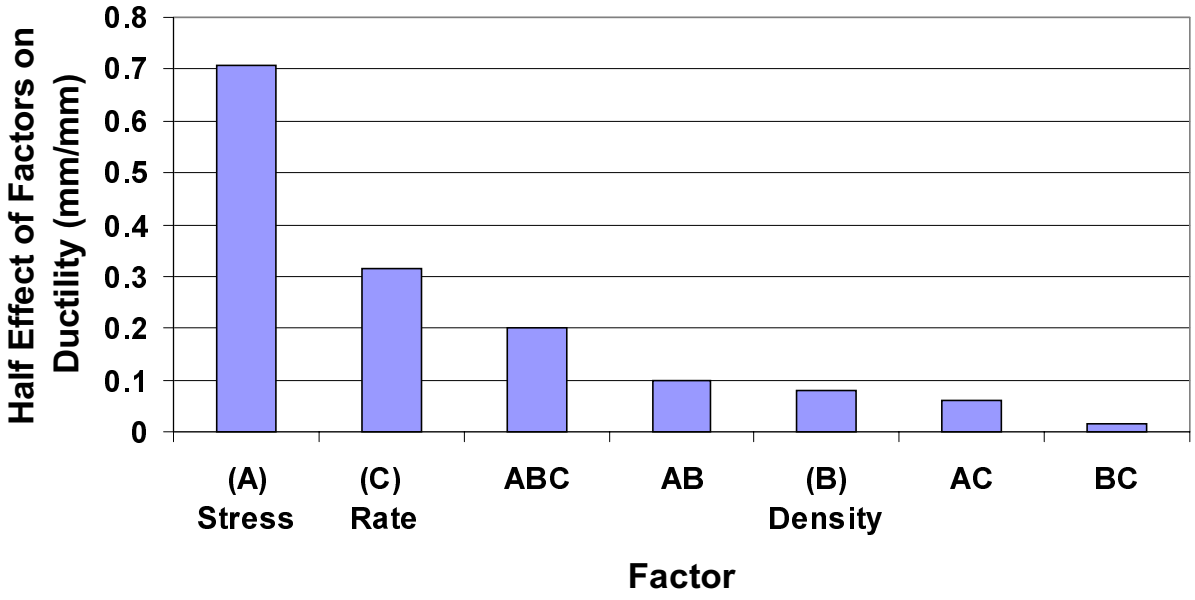

Figure 56: Pareto diagram showing relative factor importance for the ductility model

The Pareto diagram shows graphically that the crazing stress and strain rate produce much greater changes in the ductility than the other factors or interactions. The three-way interaction appears to be the third most significant term but only has a *P(2-tail)* value of 0.136. Since it is obvious that the contribution of the other interactions are insignificant, no interaction graphs will be displayed for ductility.

5.3 Development of a quantitative model using the Design of Experiments (DOE) approach with two factors

Consideration of Equations 5-3 through 5-6 shows that changing the relative craze density from 1 to 10% had no significant effect on the residual mechanical properties of crazed polycarbonate. On the other hand, the qualitative results of Section 5.1 show significant changes in the mechanical properties with an increase in relative craze density from 0 to 1%. For this reason, a DOE model for residual mechanical properties with a constant crazing stress of 40 MPa, a relative craze density from 0 to 1%, and a strain rate from 0.2 to 2 min^{-1} will be developed to quantify the effect of crazing. The two level, two factor coded values for the DOE model are shown in Table 16.

Table 16: Coded values for DOE models

	Low (-1)	High (+1)
Relative Craze Density (%)	0	1
Strain Rate (min^{-1})	0.2	2

Similar to the three factor DOE models above, the mechanical properties to be considered for the two factor modeling are yield stress, elastic modulus, failure stress, and ductility.

5.3.1 Two factor DOE model of residual yield stress

The first mechanical property of crazed polycarbonate to be considered in the two factor model was yield stress. Table 17 shows the test results for all three repetitions of the four test runs. The mean and standard deviation of the three repetitions are also given.

Table 17: DOE test results for residual yield stress

(A) Relative Craze Density (%)	(B) Strain Rate (min^{-1})	Y1 (MPa)	Y2 (MPa)	Y3 (MPa)	YBAR (MPa)	S (MPa)
0	0.2	65.3	65.8	65.6	65.6	0.252
0	2	67.6	68.3	68.6	68.2	0.513
1	0.2	65.1	65.7	65.6	65.5	0.321
1	2	68.1	69.2	68.6	68.6	0.551

Using the data in Table 17, the constant and coefficients for the predictive model for the yield stress of crazed polycarbonate were calculated similarly to the calculations above and are shown in Table 18. The *P(2-tail)* and the effect of each factor on the standard deviation of the yield stress are also given.

Table 18: Original model for yield stress with all factors included in regression

FACTOR	COEFFICIENT FOR Y MODEL (MPa)	P(2 tail)	COEFFICIENT FOR S MODEL (MPa)
Constant	67.0	**0.0000**	0.409
(A) Relative Craze Density	0.0917	0.4795	0.0268
(B) Strain Rate	1.44	**0.0000**	0.123
AB	0.142	0.285	-0.0080

The only terms shown in Table 18 that have *P(2-tail)* < 0.1 are the constant and the strain rate. Therefore, the predictive model for the yield stress of crazed polycarbonate will only contain these two terms, as shown by

$$\sigma_y = 67.0 + 1.44\ R \qquad (5\text{-}7)$$

where σ_y is the yield stress in MPa and R is the dimensionless coded strain rate.

These results correlate well with the qualitative results shown in Section 5.1. The previously reported qualitative results show that changing the relative craze density from 0 to 1% does not significantly effect the yield stress. They also showed a strong correlation between strain rate and yield stress, in that a strain rate of 2 min^{-1} results in a significantly higher yield stress than a strain rate of 0.2 min^{-1}. Equation 5-7 provides a quantitative model to the qualitative results previously reported.

The relative importance of each factor in Table 18 are shown graphically in Figure 57. The absolute value of each half effect is plotted as a function of the corresponding factor.

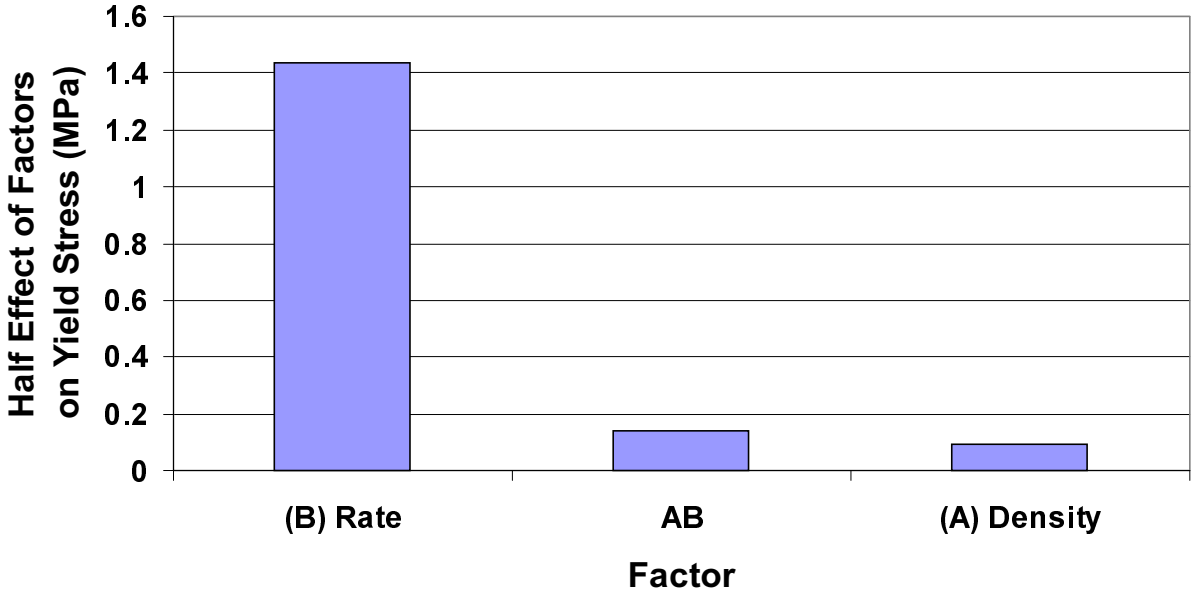

Figure 57: Pareto diagram showing relative factor importance for the yield stress model

The Pareto diagram shows graphically that changing the strain rate from 0.2 to 2 min^{-1} produces a much greater change in the yield stress than changing the relative craze density from 0 to 1%. Since it is obvious that the contribution of the interaction is insignificant, no interaction graph will be displayed for yield stress.

5.3.2 Two factor DOE model of residual elastic modulus

The next property of crazed polycarbonate to be considered in the two factor model was elastic modulus. Table 19 shows the test results for all three repetitions of the four test runs. The mean and standard deviation of the three repetitions are also given.

Table 19: DOE test results for residual elastic modulus

(A) Relative Craze Density (%)	(B) Strain Rate (min^{-1})	Y1 (MPa)	Y2 (MPa)	Y3 (MPa)	YBAR (MPa)	S (MPa)
0	0.2	2267	2465	2247	2326	121
0	2	2280	2241	2508	2343	144
1	0.2	2221	2166	2177	2188	29.1
1	2	1999	2471	2235	2235	236

Using the data in Table 19, the constant and coefficients for the predictive model for the elastic modulus of crazed polycarbonate were calculated similarly to the calculations above and are shown in Table 20. The *P(2-tail)* and the effect of each factor on the standard deviation of the elastic modulus are also given.

Table 20: Original model for elastic modulus with all factors included in regression

FACTOR	COEFFICIENT FOR Y MODEL (MPa)	P(2 tail)	COEFFICIENT FOR S MODEL (MPa)
Constant	2273	**0.0000**	132
(A) Relative Craze Density	-61.6	0.1969	0.095
(B) Strain Rate	15.9	0.7254	58
AB	7.58	0.8667	46

Similar to the three factor DOE model, the only term shown in Table 20 that has *P(2-tail)* < 0.1 is the constant. Therefore, the predictive model for elastic modulus of crazed polycarbonate will only contain the constant term, as shown by

$$\mathbf{E = 2273\ MPa} \tag{5-8}$$

where E is the elastic modulus.

These results correlate well with the qualitative results shown in Section 5.1. The previously reported qualitative results show that changing the relative craze density from 0 to 1% and changing the strain rate from 0.2 to 2 min^{-1} do not produce significant changes in the elastic modulus of polycarbonate. Since each of the factors appear to play an insignificant role in the behavior of the elastic modulus, no Pareto diagram or interaction plot will be shown for this model.

5.3.3 Two factor DOE model of residual failure stress

The failure stress will now be considered in the two factor model. As stated before, crazing is expected to play a more significant role in the failure properties of polycarbonate than it did in the elastic properties. Table 21 shows the test results for all three repetitions of the four test runs. The mean and standard deviation of the three repetitions are also given.

Table 21: DOE test results for residual failure stress

(A) Relative Craze Density (%)	(B) Strain Rate (min^{-1})	Y1 (MPa)	Y2 (MPa)	Y3 (MPa)	YBAR (MPa)	S (MPa)
0	0.2	60.5	51.4	51.9	54.6	5.12
0	2	54.3	62.3	57.8	58.1	4.01
1	0.2	52.6	48.0	47.5	49.4	2.81
1	2	49.7	51.1	50.4	50.4	0.70

Using the data in Table 21, the constant and coefficients for the predictive model for the failure stress of crazed polycarbonate were calculated similarly to the calculations above and are shown in Table 22. The *P(2-tail)* and the effect of each factor on the standard deviation of the failure stress are also given.

Table 22: Original model for failure stress with all factors included in regression

FACTOR	COEFFICIENT FOR Y MODEL (MPa)	P(2 tail)	COEFFICIENT FOR S MODEL (MPa)
Constant	53.1	**0.0000**	3.16
(A) Relative Craze Density	-3.24	**0.0135**	-1.40
(B) Strain Rate	1.14	0.2987	-0.804
AB	-0.625	0.5598	-0.252

The only terms shown in Table 22 that have *P(2-tail)* < 0.1 are the constant and the relative craze density. Therefore, the predictive model for the failure stress of crazed polycarbonate will only contain these two terms, as shown by

$$\sigma_F = 53.1 - 3.24\ D \qquad (5\text{-}9)$$

where σ_F is the failure stress in MPa and D is the dimensionless coded relative craze density.

These results correlate well with the qualitative results shown in Section 5.1. The previously reported qualitative results show that changing the relative craze density from 0 to 1% at a crazing stress of 40 MPa decreases the failure stress significantly. They also show that increasing the strain rate from 0.2 to 2 min^{-1} does not produce significant changes in the failure stress of polycarbonate. Equation 5-9 provides a quantitative model to the qualitative results previously reported.

The relative importance of each factor in Table 22 are shown graphically in Figure 58. The absolute value of each half effect is plotted as a function of the corresponding factor.

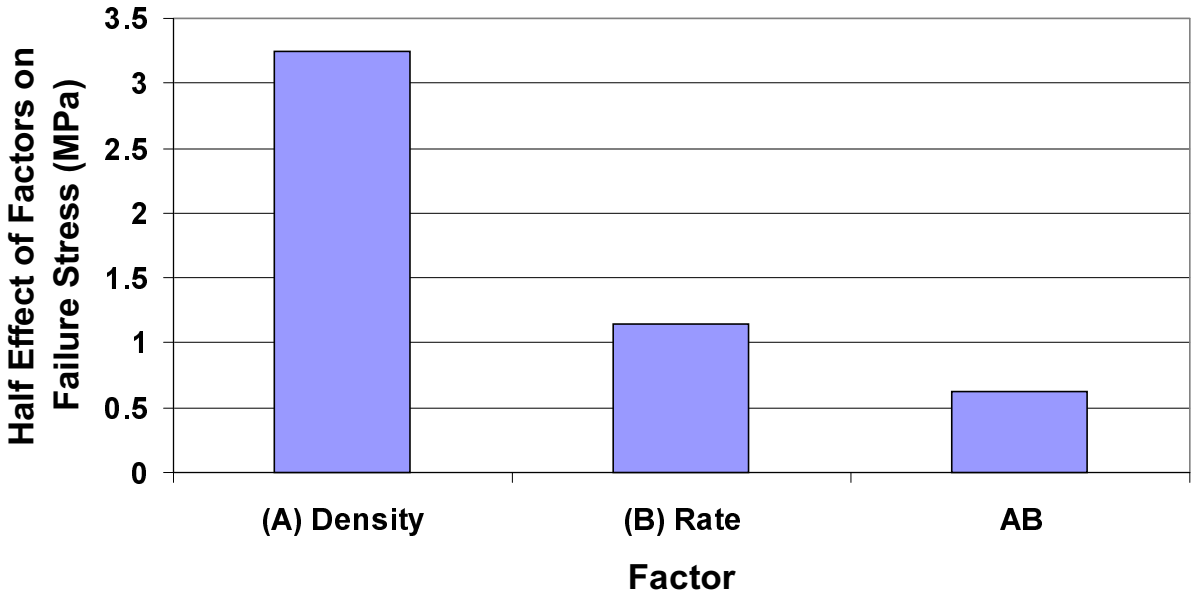

Figure 58: Pareto diagram showing relative factor importance for the failure stress model

The Pareto diagram shows graphically that changing the relative craze density from 0 to 1% produces a much greater change in the failure stress than changing the strain rate from 0.2 to 2 min^{-1}. Since it is obvious that the contribution of the interaction is insignificant, no interaction graph will be displayed for failure stress.

5.3.4 Two factor DOE model of residual ductility

The next property of crazed polycarbonate to be considered in the two factor model was ductility. The measure of ductility was the ratio of the final length of the necked region of the fractured polycarbonate samples to the gage length of 50 mm. Table 23 shows the test results for all three repetitions of the four test runs. The mean and standard deviation of the three repetitions are also given.

Table 23: DOE test results for residual ductility

(A) Relative Craze Density (%)	(B) Strain Rate (min^{-1})	Y1 (mm/mm)	Y2 (mm/mm)	Y3 (mm/mm)	YBAR (mm/mm)	S (mm/mm)
0	0.2	3.2	2.22	2.28	2.56	0.54
0	2	2.38	3.24	2.74	2.78	0.44
1	0.2	2.46	1.34	0.96	1.58	0.78
1	2	0.66	0.76	0.70	0.70	0.06

Using the data in Table 23, the constant and coefficients for the predictive model for the ductility of crazed polycarbonate were calculated similarly to the calculations above and are shown in Table 24. The *P(2-tail)* and the effect of each factor on the standard deviation of the ductility measurement are also given.

Table 24: Original model for ductility with all factors included in regression

FACTOR	COEFFICIENT FOR Y MODEL (mm/mm)	P(2 tail)	COEFFICIENT FOR S MODEL (mm/mm)
Constant	1.92	**0.0000**	0.46
(A) Relative Craze Density	-0.76	**0.0010**	-0.040
(B) Strain Rate	-0.16	0.3073	-0.22
AB	-0.28	0.1067	-0.16

The only terms shown in Table 22 that have *P(2-tail)* < 0.1 are the constant and the relative craze density. Therefore, the predictive model for the ductility parameter will only contain these two terms, as shown by

$$\mathbf{L_F/L_g = 1.92 - 0.76\ D} \qquad (5\text{-}10)$$

where L_F is the final length of the necked region of the sample in mm, L_g is the gage length of 50 mm, and D is the dimensionless coded relative craze density.

These results correlate well with the qualitative results shown in Section 5.1. The previously reported qualitative results show that changing the relative craze density from 0 to 1% at a crazing stress of 40 MPa decreases the ductility significantly. They also show that increasing the strain rate from 0.2 to 2 min^{-1} does not produce significant changes in the ductility of polycarbonate. Equation 5-10 provides a quantitative model to the qualitative results previously reported.

The relative importance of each factor in Table 24 are shown graphically in Figure 59. The absolute value of each half effect is plotted as a function of the corresponding factor.

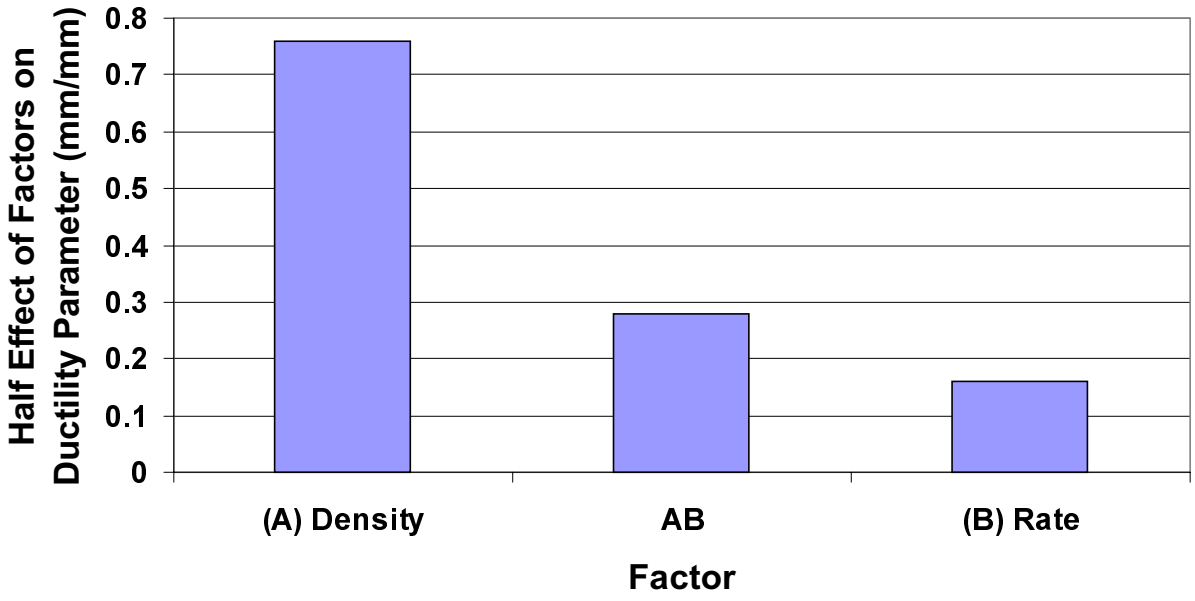

Figure 59: Pareto diagram showing relative factor importance for the ductility model

The Pareto diagram shows graphically that changing the relative craze density from 0 to 1% produces a much greater change in the ductility than changing the strain rate from 0.2 to 2 min^{-1}. Since it is obvious that the contribution of the interaction is insignificant, no interaction graph will be displayed for failure stress.

5.4 Confirmation of DOE Models

As with any new model development, confirmation tests are necessary to validate the model at non-endpoint conditions. For this dissertation, the accuracy of both the three factor and the two factor DOE predictions will be determined. First, the three factor DOE model will be evaluated with yield stress as a function of strain rate, failure stress as a function of crazing stress and strain rate, and ductility as a function of crazing stress and strain rate. Next, the two factor DOE model will be evaluated with yield stress as a function of strain rate, failure stress as a function of craze density, and ductility as a function of craze density. The modulus model will not be assessed since none of the factors were correlated to the elastic modulus in either DOE model.

5.4.1 Confirmation of three factor DOE model

The three factor DOE model was developed to predict the mechanical properties of polycarbonate with relative craze densities from 1 to 10%, crazing stresses from 40 to 45 MPa, and strain rates from 0.2 to 2 min^{-1}. The first confirmation tests were conducted to determine the accuracy of the yield stress model shown in Equation 5-3. The only factor found to correlate to yield stress was strain rate. Figure 60 shows the yield stress as a function of strain rate, with the solid line representing the predictive model and the data points depicting the average value of the confirmation tests. The endpoints represent the test conditions used to build the model with error bars showing one standard deviation of the data collected at each point.

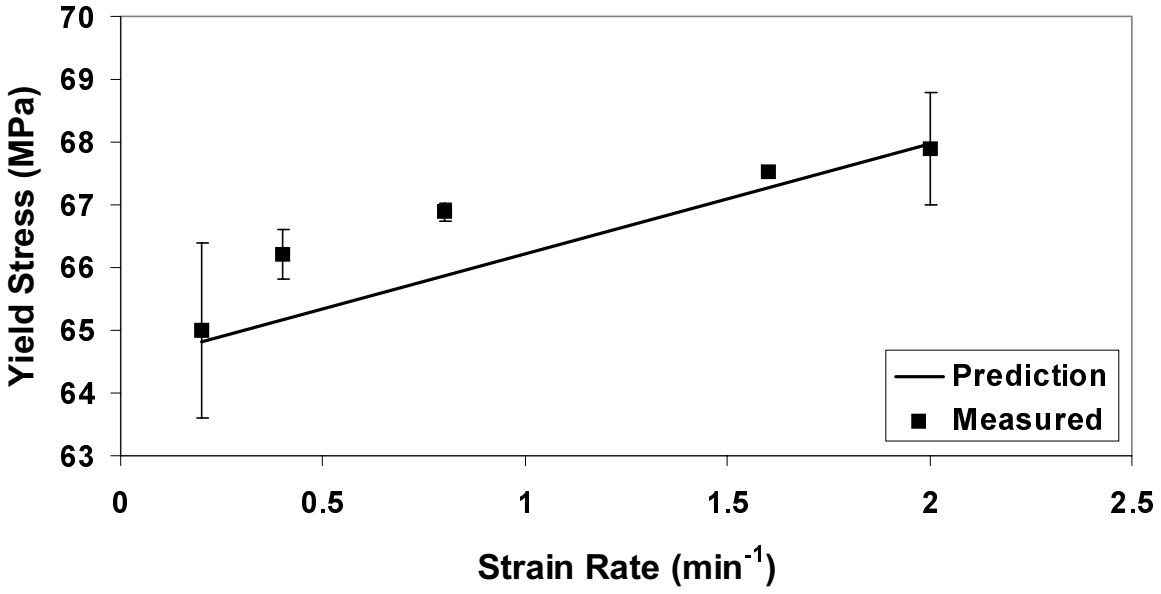

Figure 60: Confirmation of 3-factor yield stress model

As expected, the endpoints fit well to the predictive model since they were used to build the model. The yield stress at 0.4, 0.8, and 1.6 min^{-1} are shown to be higher than predicted with the largest difference between the predicted and measured values being about 1 MPa. These results show that the model slightly underestimates the yield stress, which is more desirable than overestimation.

Since the model shows that strain rate is the only important factor in predicting the yield stress of crazed polycarbonate, the Eyring stress-rate model for thermally activated deformation processes will now be revisited. The Eyring model was presented in Chapter 2 describing the effect of an applied stress on the deformation rate of a polymer as shown by

$$\dot{e} \approx \frac{\dot{e}_o}{2} \exp\left(-\frac{\Delta H - \nu\sigma}{RT}\right) \tag{5-11}$$

where $\dot{e}$ is the strain rate, $\dot{e}_o$ is a constant, ν is an activation volume, ΔH is the activation energy, R is the gas constant, T is the absolute temperature, and σ is the applied stress. Solving for stress in Equation 5-11 and applying the model to the yielding behavior of polycarbonate produces

$$\sigma_y = \left.\frac{RT}{\nu}\right|_y \left(\frac{\Delta H_y}{RT} + \ln\frac{2\dot{e}_y}{\dot{e}_{o\,y}}\right) \tag{5-12}$$

where σ_y is the yield stress, R is the gas constant, T is the temperature, ν_y is an activation volume associated with yielding, ΔH_y is the activation energy associated with yielding, $\dot{e}_y$ is the strain rate associated with yielding, and $\dot{e}_{o\,y}$ is a constant. A plot of Equation 5-12 is of the general shape shown in Figure 61.

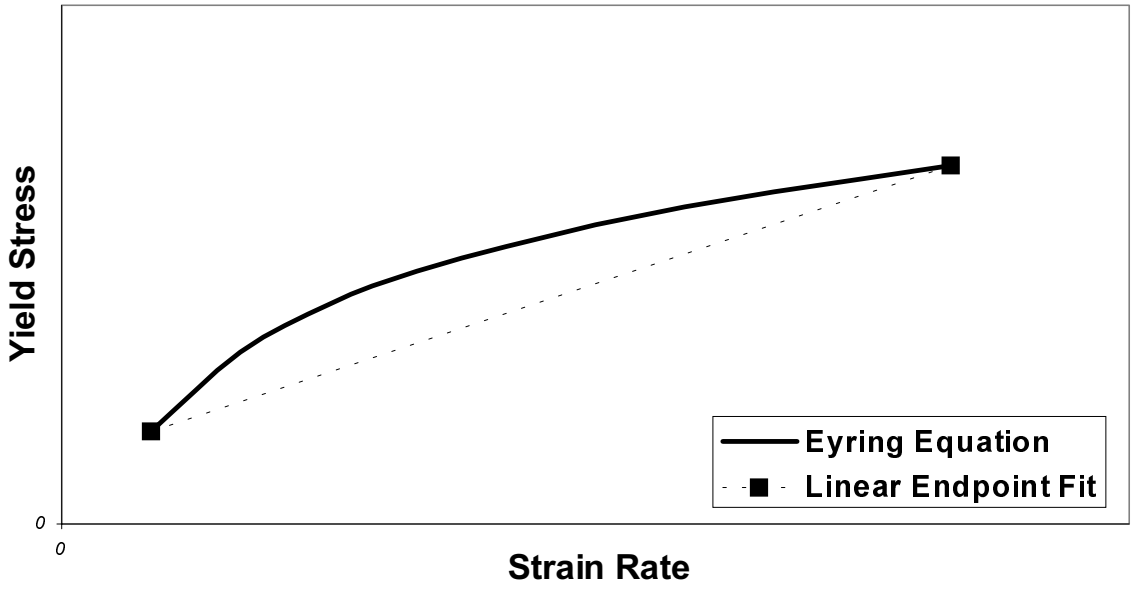

Figure 61: Shape of Eyring stress-rate equation

Since the confirmation data for yield stress shown in Figure 60 have the same shape as the Eyring stress-rate model shown in Figure 61, the yield stress is shown to follow the Eyring stress-rate model and a linear DOE model should not be expected to provide a good fit to the data. If the presence of crazes affected the yielding behavior of polycarbonate, the Eyring model would need to be modified to account for the effect of crazing, but crazing was not shown to play a significant role in yielding.

Next, the three factor DOE model for failure stress prediction will be evaluated. Both crazing stress and the interaction between crazing stress and strain rate were found to correlate to the failure stress, as shown in Equation 5-5. Table 25 shows the predicted values and the average of the measured values of failure stress at various crazing stresses and strain rates. The conditions of (40 MPa, 0.2 min^{-1}), (40 MPa, 2 min^{-1}), (45 MPa, 0.2 min^{-1}), and (45 MPa, 2 min^{-1}) represent the endpoints used to build the model.

Table 25: Confirmation of 3-factor failure stress model

Crazing Stress (MPa)	Strain Rate (min^{-1})	Predicted Failure Stress (MPa)	Measured Failure Stress (MPa)
40	0.2	48.0	46.7
40	2	51.2	51.0
41	1.6	51.4	52.3
42.5	0.8	52.8	55.1
44.5	0.4	56.3	60.0
45	0.2	57.6	59.2
45	2	54.4	54.1

The average difference between the predicted and measured values of failure stress in Table 25 was found to be approximately 1.5 MPa. Also, the measured values for failure stress at all three non-endpoint conditions are slightly higher than the predicted values, showing an underestimation of failure stress similar to what was seen in the yield stress model. Once again, underestimation of the failure stress is more desirable than overestimation.

The Eyring model has previously been applied to the fracture of polymers [5], similar to the yield stress as shown above. In this case, the failure stress has been shown to be a function of both crazing stress and strain rate, so the Eyring rate influence would be expected to predict failure stress values higher than the linear fit of the DOE model.

The accuracy of the ductility model will now be evaluated. The ductility parameter was found to correlate to both the crazing stress and the strain rate, as shown in Equation 5-6. Figure 62 shows a contour plot of the predictive model for ductility as a function of both important factors. The plot is broken up into three regions of 40 mm increments, shown by the solid lines. The four endpoint conditions used to build the model are shown on the four corners of Figure 62, along with four non-endpoint conditions.

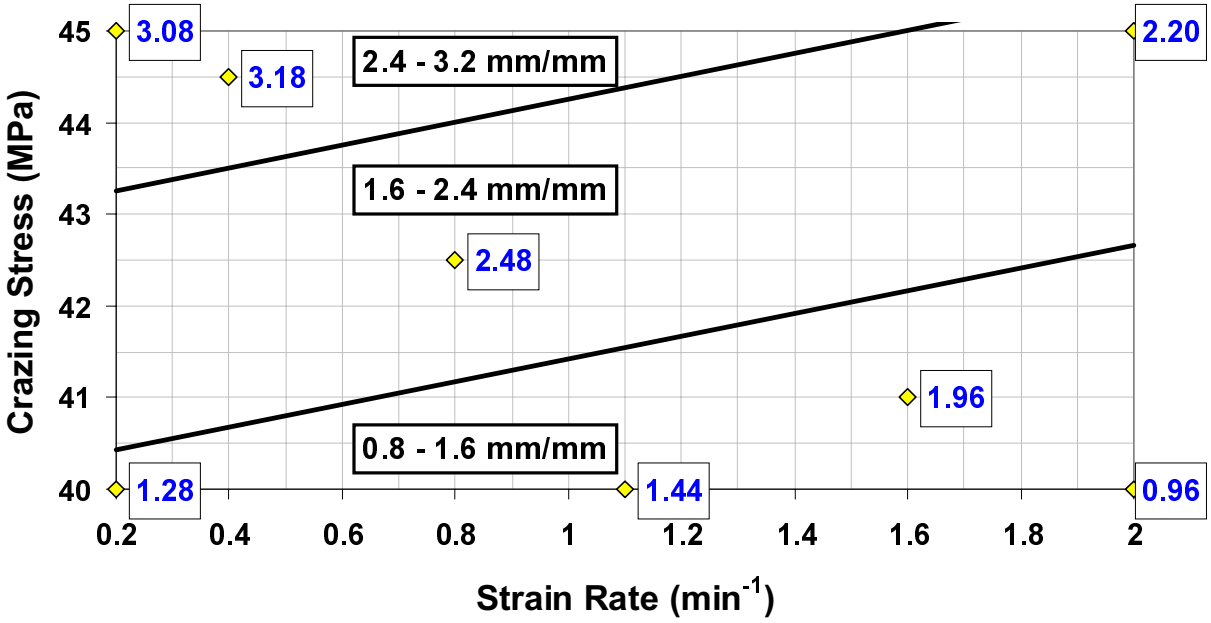

Figure 62: Confirmation of 3-factor ductility model with framed values of ductility parameter in mm/mm

As expected, the four endpoints fit well into the predictive model. The four non-endpoint conditions are shown to follow the correct trend, but three of the four measured values are slightly higher than the predicted values. These results show that the model slightly underestimates the final length of the necked region of crazed polycarbonate. As will be shown in the next section of this dissertation, wide scatter exists in the ductility data due to the nature of the fracture dependence on flaw size and distribution. This wide scatter is believed to be one of the causes of the differences shown in Figure 62. Also, taking into consideration the Eyring rate effect, the failure stress at a given non-endpoint strain rate would be expected to be higher than predicted by a linear fit. The final length of the necked region normalized to the gage length follows the same behavior as the failure stress and should be expected to be higher than a linear prediction due to the rate effect. Once again, an underestimation of the ductility is much more desirable than an overestimation.

5.4.2 Confirmation of two factor DOE model

The two factor DOE model was developed to predict the mechanical properties of polycarbonate with relative craze densities from 0 to 1% and strain rates from 0.2 to 2 min^{-1}. The first confirmation tests were conducted to determine the accuracy of the yield stress model shown in Equation 5-7. The strain rate was the only factor found to correlate with yield stress. Figure 63 shows the yield stress as a function of strain rate, with the solid line representing the predictive model and the data points depicting the average value of the confirmation tests. The endpoints represent the test conditions used to build the model with error bars showing one standard deviation of the data collected at each point.

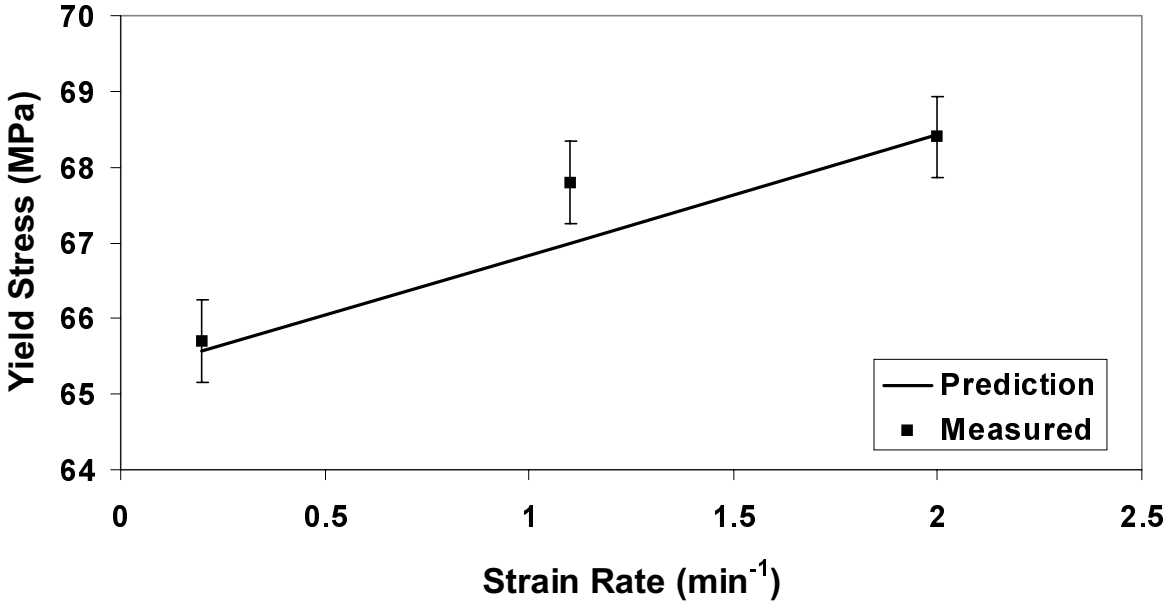

Figure 63: Confirmation of 2-factor yield stress model

As expected, the endpoints fit well to the predictive model since they were used to build the model. The yield stress at the midpoint is shown to be higher than predicted with the difference between the predicted and average measured values being 0.8 MPa. These results are expected as shown in the three-factor DOE yield stress prediction above in which the Eyring rate effect produces the shape of the curve shown in Figure 63. These results show that the model

produces a good prediction of the yield stress of crazed polycarbonate at the endpoints, with a slight underestimation at non-endpoint conditions, which is more desirable than overestimation.

Next, the accuracy of the two-factor DOE model for failure stress will be evaluated. The only factor found to correlate to the failure stress of crazed polycarbonate was relative craze density, as shown in Equation 5-9. Figure 64 shows the failure stress as a function of relative craze density, with the solid line representing the predictive model and the data points depicting the average value of the confirmation tests. The endpoints represent the test conditions used to build the model with error bars showing one standard deviation of the data collected at each point.

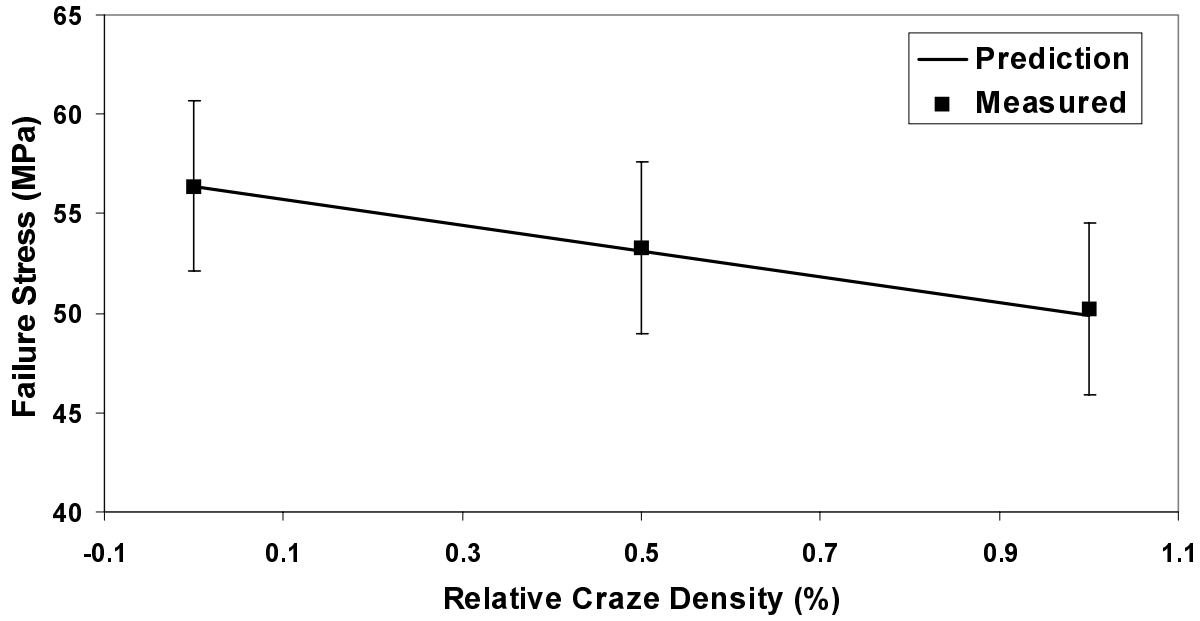

Figure 64: Confirmation of 2-factor failure stress model

Figure 64 shows that the model developed for this dissertation accurately predicts the effect of relative craze density on the failure stress of crazed polycarbonate. The average value for both the endpoint conditions and the midpoint fit well with the prediction, but the magnitude of the error bars show that there is significant scatter in the data with respect to the overall decrease in failure stress. This scatter is a result of the fact that failure properties depend on the distribution of flaws of various sizes and amounts which is increased with increased crazing, but

is highly variable from sample to sample. It should be noted that the Eyring rate effect is not seen in this model since strain rate was not found to be a significant factor and crazing dominates the failure behavior. For this reason, a linear model is appropriate.

Finally, the accuracy of the two-factor ductility model will be evaluated. The only factor found to correlate to the ductility parameter of crazed polycarbonate was relative craze density, as shown in Equation 5-10. Figure 65 shows the ductility as a function of relative craze density, with the solid line representing the predictive model and the data points depicting the average value of the confirmation tests. The endpoints represent the test conditions used to build the model with error bars showing one standard deviation of the data collected at each point.

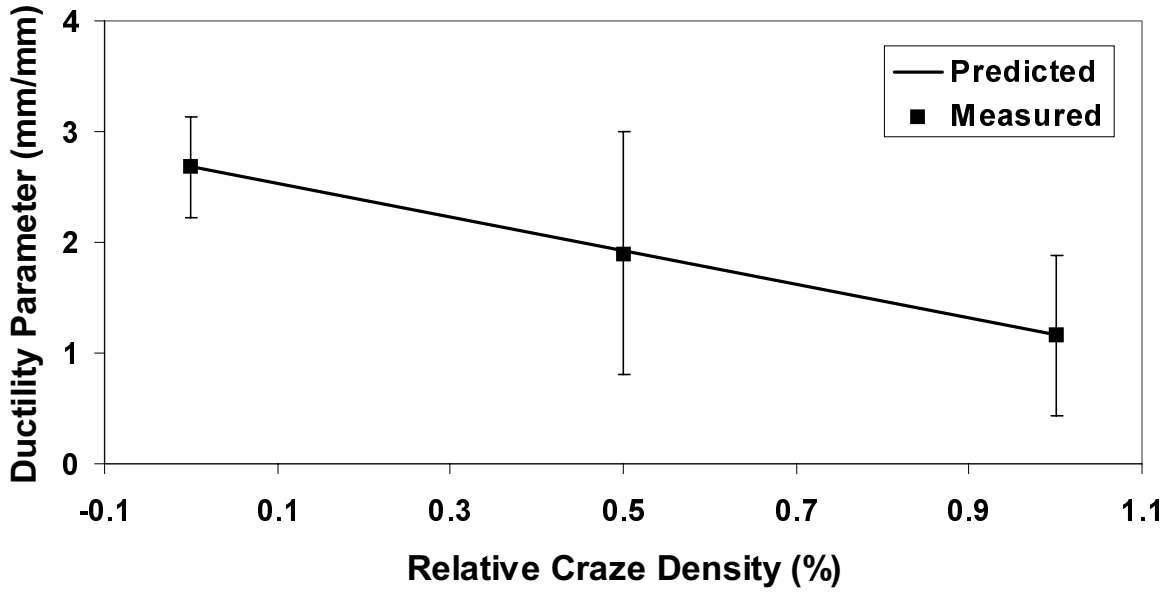

Figure 65: Confirmation of 2-factor ductility model

Figure 65 shows that the model developed for this dissertation accurately predicts the effect of relative craze density on the ductility of crazed polycarbonate. The average value for both the endpoint conditions and the midpoint fit well with the prediction, but the magnitude of the error bars show that there is a very large amount of scatter in the data with respect to the overall decrease in ductility. Similar to the failure stress model, this scatter is a result of the fact that failure properties depend on the highly variable distribution of flaws. Special care should be

taken when using this model to predict the ductility or to set design loads for a crazed aircraft transparency. The large scatter at the midpoint shows that the actual value for the final length of the necked region of crazed polycarbonate could possibly be as small as one-third of the predicted value.

5.5 Polymer Degradation

It is well known that the mechanical properties of polymers degrade over time [60 - 62]. Free volume theories have been developed to describe this behavior on a molecular level [63]. For this dissertation, it is a concern that part of the decrease in mechanical integrity may be attributed to physical aging or some other form of polymer degradation instead of crazing. The material was characterized before and after the craze tests to determine the extent that degradation has occurred. The characterization techniques were differential scanning calorimetry (DSC), thermogravimetric analysis (TGA), and gel permeation chromatography (GPC).

5.5.1 Differential scanning calorimetry

DSC was performed on both as-received polycarbonate samples and polycarbonate samples that were craze tested for 110 hours at 40 MPa. Physical aging can be detected by shifts and endothermic peaks in the glass transition region. Figure 66 shows the DSC scans of two as-received samples and two crazed samples.

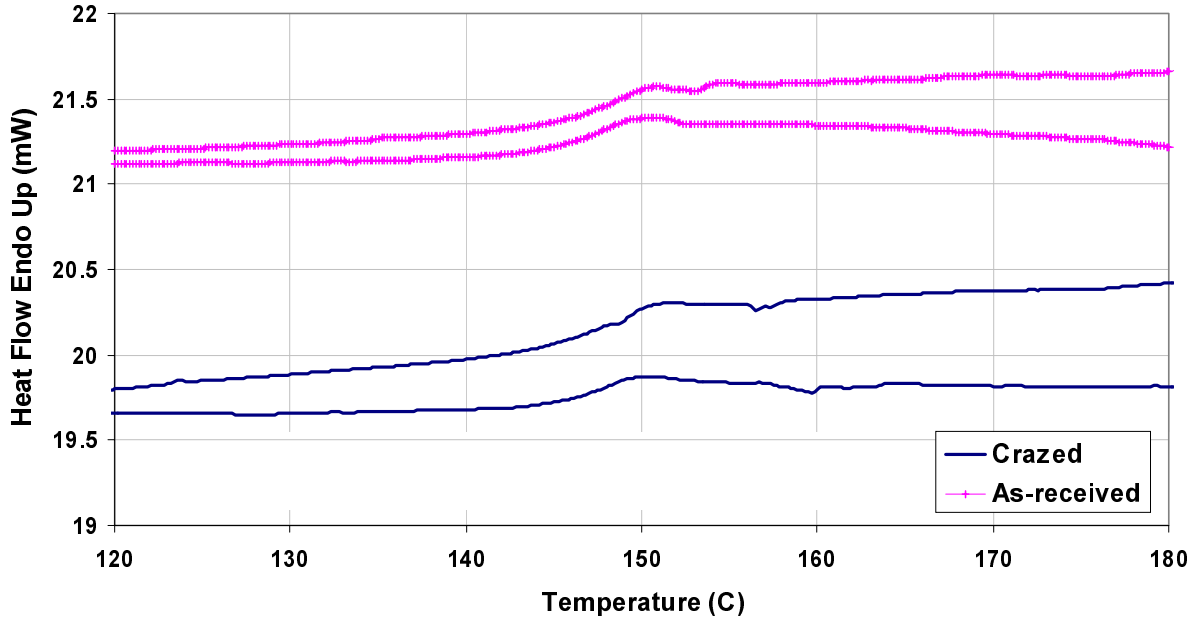

Figure 66: DSC scan of as-received and crazed (110 hr, 40 MPa) polycarbonate

Figure 66 qualitatively shows that there are no apparent differences in the thermal response of crazed and as-received polycarbonate. To more quantitatively investigate the DSC results, the glass transition temperatures were calculated by finding the temperature at which half of the increase in heat capacity was complete. The average T_g for four crazed and four as-received samples are shown in Table 26.

Table 26: Average glass transition temperature for as-received and crazed polycarbonate

	Average Tg (°C)	Standard Deviation (°C)
As-received	147.05	0.947
Crazed	147.10	0.816

These results along with the absence of an endothermic peak in the glass transition region show that no physical aging is apparent with DSC thermal characterization. This leads to the

conclusion that the long term craze tests at 40 MPa, 25°C, and 85% rh do not cause physical aging that would lead to degradation of the mechanical properties.

5.5.2 Thermogravimetric analysis

It is believed that differences in the TGA transition between as-received and crazed polycarbonate would indicate polymer degradation during craze testing [6]. The metrics to determine the location of the transition are the initial and final temperature of the transition determined by the double tangent technique shown in Chapter 3. The longest craze tests that were performed for this study took on the order of 100 hours to complete. To detect changes in transitions, TGA analyses were performed on two as received samples and two samples that were craze tested for 110 hours. The results are shown in Figure 67.

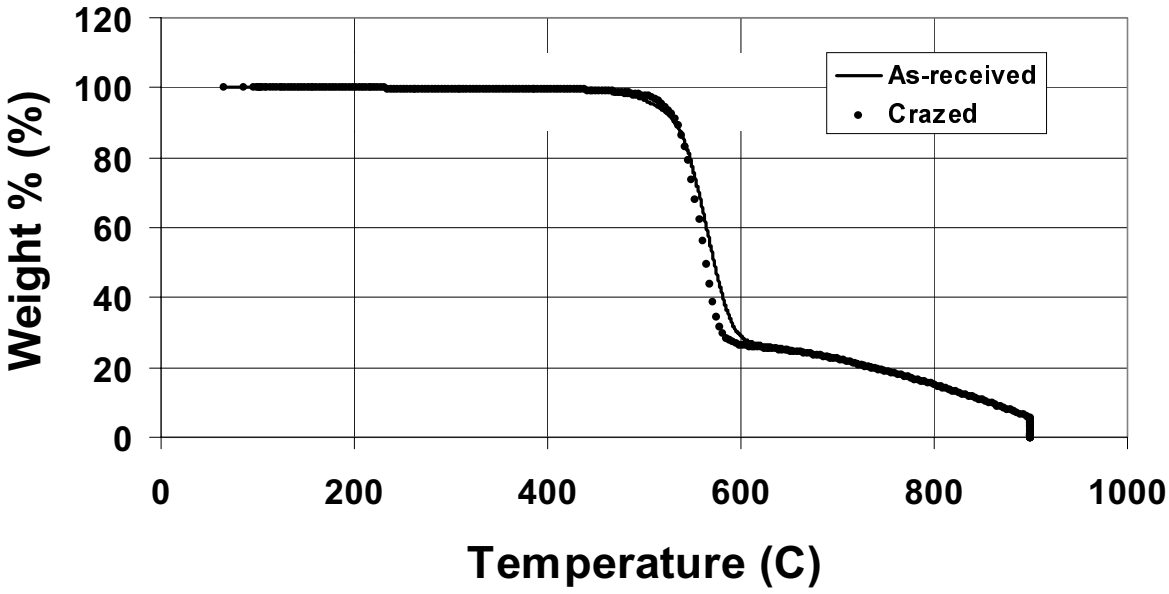

Figure 67: TGA results of crazed and as-received polycarbonate

Figure 67 qualitatively shows that the transition of the crazed polycarbonate sample is at the same location as the transition of the as-received sample. The initial and final transition temperatures were measured for two as-received and two crazed samples and shown in Table 27.

Table 27: TGA transition results for as-received and crazed polycarbonate

	Initial Transition Temperature (°C)	Final Transition Temperature (°C)
As-received	537	588
As-received	535	577
Crazed	535	582
Crazed	535	591

These results quantitatively show that the transition of the crazed and as-received samples occur at the same location, within experimental scatter. It is concluded that there are no chemical reactions causing polymer degradation that are detectable by TGA.

5.5.3 Gel permeation chromatography

GPC is a size exclusion technique to determine the molar mass distribution of polymers. If molecular rearrangements or chain scission are occurring during long term craze tests, these changes would show up as changes in the molar mass distribution. The relative molar mass distributions of as-received polycarbonate and polycarbonate crazed for 110 hours are shown in Figure 68 as the relative response (normalized count) versus the retention volume.

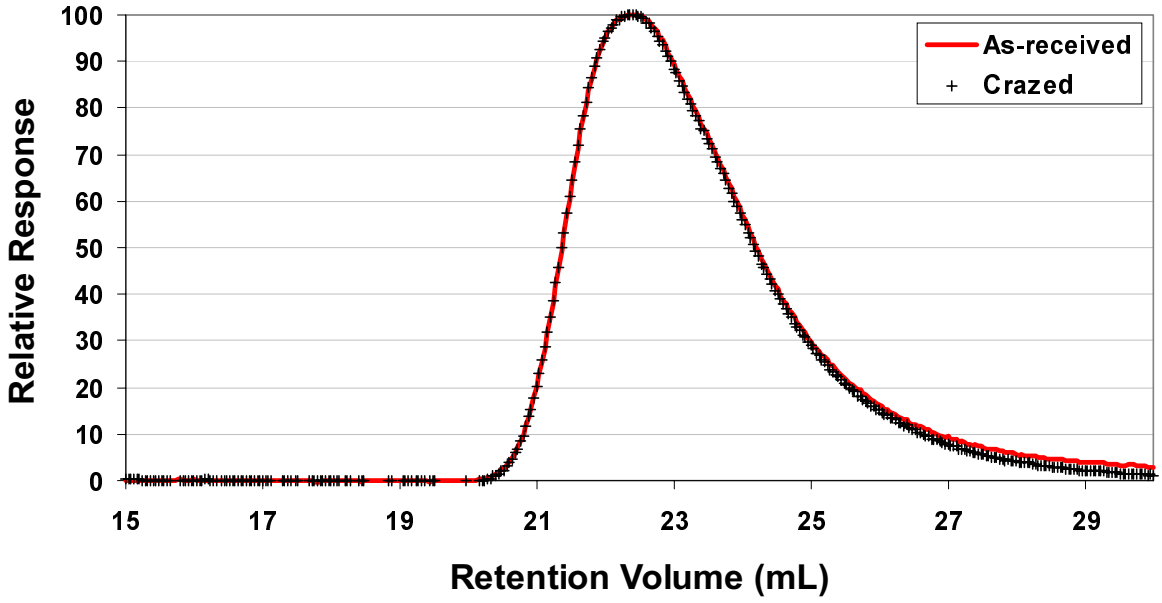

Figure 68: GPC chromatogram of as-received and crazed polycarbonate

Figure 68 qualitatively shows that the changes in the polycarbonate molar mass distribution between the as-received and crazed samples fall within experimental scatter for the GPC. To more quantitatively investigate changes in molar mass, the number average and weight average molecular weights for each of the samples shown in Figure 68 have been calculated with a universal calibration. These results are shown in Table 28.

Table 28: Number average and weight average molecular weights of as-received and crazed polycarbonate

	M_n (g/mol)	M_w (g/mol)
As-received	18,200	42,400
As-received	20,700	44,300
Crazed	17,300	42,300
Crazed	19,000	43,200

Table 28 quantitatively shows that the average molar masses of the as-received and crazed samples are the same, within experimental scatter. These results combined with the TGA results lead to the conclusion that craze testing for as long as 100 hrs at 40 MPa, 25°C and 85%rh does not cause polymer degradation caused by molecular rearrangement or chain scission. Therefore, the changes in mechanical properties that are reported in this dissertation can be attributed to crazing and not to physical aging or chemical degradation during testing.

Chapter 6 Conclusions

Polycarbonate is likely to be the material selected for use in the Air Force Research Laboratory's Next Generation Transparency program in which the technology is being developed to injection mold a large, one-piece aircraft canopy in a single shot. Crazing is a common problem with polycarbonate that could affect the mechanical durability of the canopy. Historically, the models developed for crazing in polymers predicted only the onset of crazing as a function of stress, strain, temperature, molecular weight, and solvent exposure. Previously, very little work has been done to determine the effect of crazing amount on the mechanical properties of polycarbonate.

Due to the lack of a standardized craze quantification technique, a new technique was developed for this study that is an *in-situ*, quantitative, non-subjective, direct measurement of relative craze density. This new method has been shown to produce repeatable results that follow the theoretical trends of crazing with respect to stress and temperature. At relative craze densities greater than 1%, it was found that the measured value of craze density was higher when taken at a stress of 14 MPa than when taken at 7 MPa. The readings at 3.5 and 7 MPa are essentially the same. At relative craze densities less than 1%, the measurement is not a function of stress. For this reason, any data reported using the newly developed technique must report the measurement stress with the relative craze density. During the development of this new technique, it was also found that extreme caution should be used in materials handling to avoid exposure of uncoated polycarbonate to possible craze accelerating agents such as skin oils and other plasticizers. In application, a polycarbonate aircraft transparency is only put into service after protective coatings are applied to the surface. These coatings are expected to limit the solvent exposure in service.

After the new technique was validated, the next step in determining the effect of crazing amount on the mechanical properties of polycarbonate was to measure the craze growth rate as a function of stress level. Testing performed at 24°C and 85% rh showed that the craze growth rate increased exponentially from an average value of 0.4%/hr at 40 MPa to 24%/hr at 50 MPa. This behavior has been shown to follow the Eyring stress-rate model describing the effect of

stress on thermally activated deformation processes, leading to the conclusion that craze growth in polycarbonate is a thermally activated process.

It has also been shown that the time to craze initiation and the time to 1% relative craze density decrease with increasing stress level. For this technique, in the range of stress tested, the time to 1% relative craze density provided a much better metric for the time dependence of crazing than the time to craze initiation. This is due to the fact that the initiation occurs on a very small time scale and produces large scatter in the data with respect to the magnitude of measured time.

The final conclusion in the craze growth study was that a competition between crazing and shear yielding exists at a crazing stress of 50 MPa for the test material. It has been shown that both the yielding and crazing behavior have certain potential energy barriers which must be overcome before deformation will occur. Locally, the energy barrier for crazing is overcome at fairly low bulk stress levels due to localized stress concentrations such as pre-existing flaws. The energy barrier for yielding is eventually overcome as the magnitude of the bulk stress is increased to a high enough level.

The draw stress for this material determined from the stress-strain curves at ambient conditions and a strain rate of 0.2 min^{-1} was found to be between 46 and 48 MPa. This leads to the conclusion that the draw stress acts as a lower bound below which delayed necking will not occur in a reasonable time frame. The magnitude of the draw stress is believed to provide the energy needed to overcome the potential energy barrier for macrodeformation.

Next, the effect of moisture and strain rate on as-received polycarbonate was determined, to be used as a baseline for the crazing study. These results showed that increasing the strain rate from 0.2 to 2 min^{-1} increased the yield stress by 3 MPa and did not significantly affect the elastic modulus, failure stress, or ductility. It was also shown that increasing the relative humidity from 11.3 to 100% decreased the yield stress by 1 MPa, decreased the elastic modulus by 100 MPa, and did not significantly affect the failure stress or ductility. These results show that the elastic properties of polycarbonate are more affected by moisture and rate than the failure properties. It is believed that the strain rate effect is due to the polycarbonate chains not having sufficient time to relax at the higher rate, and the moisture effect is a result of plasticization increasing the molecular mobility which would decrease the yield stress and elastic modulus.

Finally, two separate design of experiments analyses were performed to determine the effect of crazing on the mechanical properties of polycarbonate. The first analysis included experimental factors of crazing stress, relative craze density, and strain rate.

Two general conclusions can be drawn from the results. First, crazing affects the failure properties of polycarbonate much more than the elastic and yielding properties. This is because the yield stress and elastic modulus involve the coordinated motion of the polymer chains in the entire bulk region of the gage section, of which crazing is a very small part. The failure properties are governed by the statistical distribution of flaws, which is much higher for a crazed sample than an uncrazed sample.

Specifically, a crazing stress of 40 MPa decreased the failure stress and ductility much more than a crazing stress of 45 MPa. In correlating these results to the craze microstructure, it was found that the crazes formed with the lower crazing stress were more than 2.5 times as large as the crazes formed at the higher crazing stress. It is believed that flaw size has a greater effect on the failure properties of polycarbonate than flaw quantity.

The second general conclusion that can be drawn is that increasing the relative craze density from 1 to 10% does not significantly affect the mechanical properties. For this reason, a second design of experiments analysis was performed with only two factors: relative craze density and strain rate. For the second analysis, the relative craze density was increased from 0 to 1% to show the change in properties from as-received material to crazed material.

It can be concluded that increasing the relative craze density from 0 to 1% significantly decreases both the failure stress and ductility. This conclusion shows that the presence of crazing on a military aircraft transparency could result in catastrophic failure in the event of a birdstrike, even in a transparency that passed the birdstrike requirement when it was put into service. The fact that the yield stress and elastic modulus are not affected by the presence of crazes means that the static structural properties of a crazed aircraft transparency can be designed to the appropriate yield criterion, ignoring crazing amounts at least up to 10% relative craze density.

Some conclusions can also be drawn about application of the DOE models outside of the testing ranges. Any of the properties that are shown to be a function of strain rate follow the nonlinear Eyring model, and extrapolation of the DOE model outside of the original strain rates of 0.2 to 2 min^{-1} will likely result in large discrepancies between the predicted and measured

values. Also, the model is not expected to be valid above a stress of 45 MPa since the deformation mechanism has been shown to change from crazing to shear yielding between 45 and 50 MPa. No fundamental reason has been shown to imply that extrapolation to below 40 MPa would create large amounts of error.

Although it is common to see statements in the literature like "the crazing stress decreases with increasing temperature", the results from this study indicate that there is more to it than that. Crazing is a viscoelastic response, meaning it exhibits time-dependent behavior. What is probably meant by "crazing stress" is the stress at which a visible amount of crazing is seen "instantaneously" upon load application. The visibility of crazing is even dependent on the sensitivity of the measurement technique. It has been concluded that the appropriate reporting technique in a constant load craze study is to state the craze initiation time and growth rate as a function of time under load, temperature, and stress. It is believed that there is no true lower limit for stress below which crazing will not occur. If the stress is held long enough, crazes will eventually grow to detectable sizes. The issue to consider is whether these crazes will form and grow to significant size within the lifetime of the part. It has been determined, however, that there is an upper limit of stress above which a transition from crazing to ductile yielding occurs.

Chapter 7 Future Work

The goals of this research study have been satisfactorily accomplished, but the work performed for this project has paved the way for many new studies in the future. With the use of the newly developed craze quantification technique, craze criteria can now be based on crazing amount instead of just craze initiation. Craze growth studies could be performed that combine the effects of stress level with external factors such as temperature, solvent exposure, ultraviolet exposure and humidity. Material properties such as molecular weight, chemical structure, and molecular orientation could also be included as experimental variables. Another important factor to consider is the effect of coatings on the crazing properties of polycarbonate. In practice, uncoated polycarbonate is never used in aircraft transparencies due to polycarbonate low scratch resistance. Once coatings have been selected for a particular application, a study similar to this dissertation should be performed on the polymer/coating system as it will be used in service.

After a database has been built to correlate crazing amount to residual strength, another valuable project would be to convert the experimental equipment into a portable measurement tool that could be used on the flightline. A tool that could quantify the amount of crazing on an aircraft transparency while in-service could give the United States Air Force more confidence to accept or reject the part during inspection based on mechanical durability.

Overall, the results of this study show that the failure properties of polycarbonate are negatively affected by crazing. Another crazing issue to consider is pilot visibility. At certain angles of sunlight, crazes reflect the light and greatly reduce the visibility of the pilot. This can greatly reduce the mission success rate and could be very costly in both aircraft and life. With the new technique, the relative craze density could be measured at various camera and light angles to quantify the glaring that negatively affects pilot visibility. These results could be used during the inspection process along with the mechanical durability database.

Another valuable study would be to determine the effect of multiaxial stress on the crazing properties of polycarbonate since this study was limited to uniaxial stress. A new fixture has already been invented to convert a uniaxial stress on a universal testing machine to a biaxial stress in a flat plate [64]. A schematic diagram of the test fixture is shown in Figure 69.

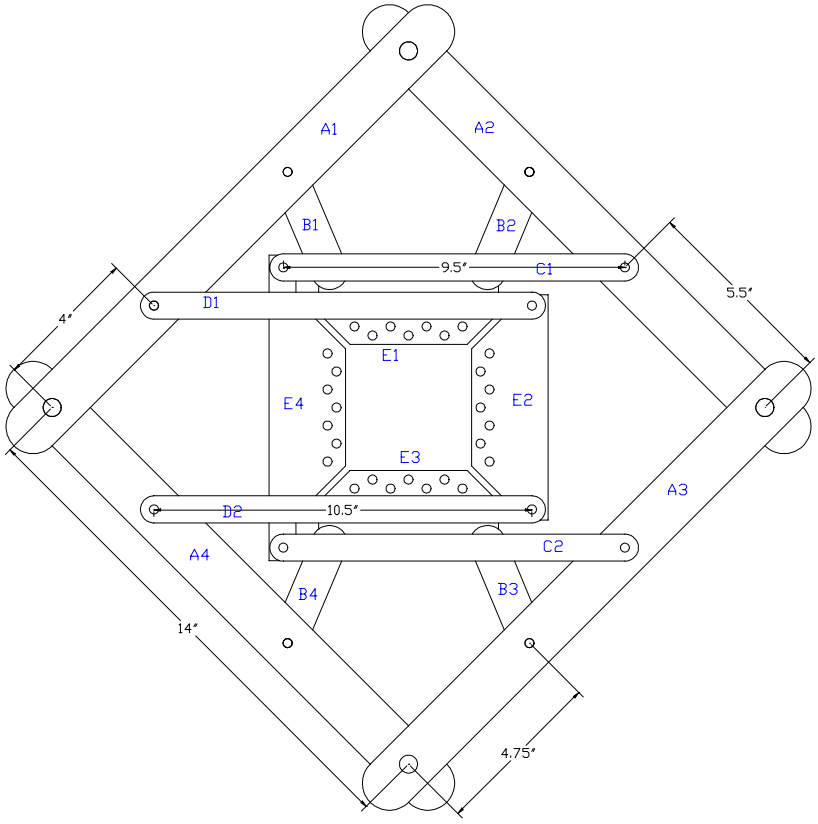

Figure 69: Biaxial testing apparatus

Finally, the results in this study could also be used to develop a thermal craze map as shown below in Figure 70. The time to reach 0.1, 1, 10, and 100% craze density was found and plotted for each test temperature using the experimental data shown in Figure 29.

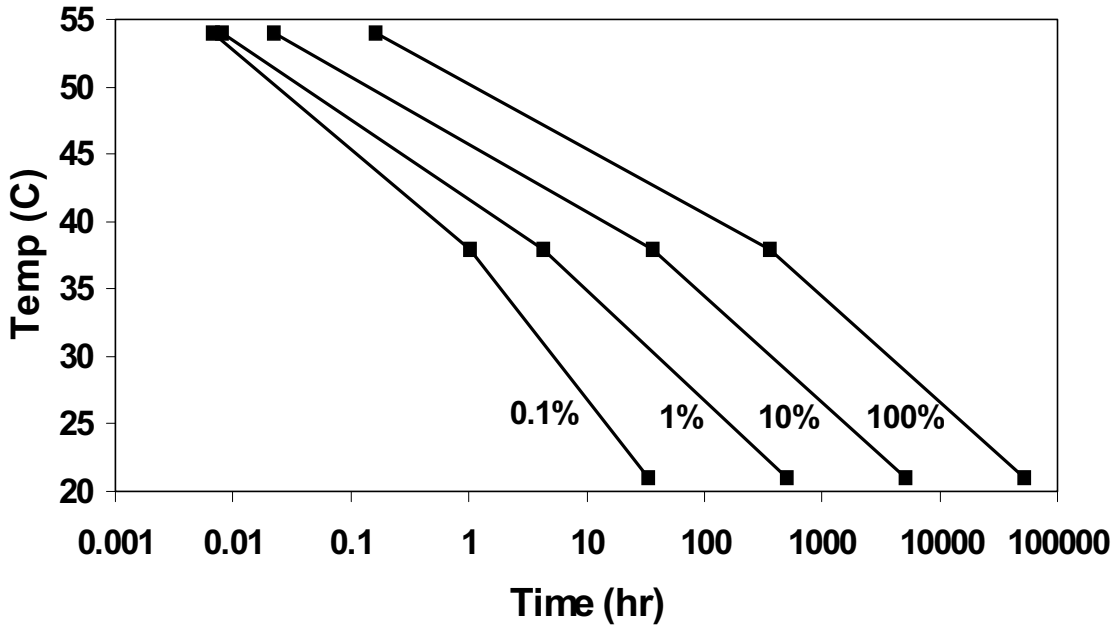

Figure 70: Thermal craze map of 3 mm thick Rohm and Haas polycarbonate under creep load of 28 MPa at 50% rh

The simplicity of thermal craze maps make them useful tools for design. Similar maps could be developed for other factors such as stress, humidity, solvent exposure, ultraviolet exposure, etc.

REFERENCES

1 L. Bottenbruch, *Engineering Thermoplastics: Polycarbonate, Polyacetals, Polyesters, Cellulose Esters*, Hanser Publishers, NY, 165, (1996)

2 M. Ishikawa, Y. Sato, and H. Higuchi, "Effect of intermolecular interactions on the plastic deformation of glassy polymers," *Polymer*, **37**, n7, 1177 (1996)

3 R. P. Kambour, "A review of crazing and fracture in thermoplastics," *Journal of Polymer Science: Macromolecular Reviews*, **7**, 1 (1973).

4 T. C. B. McLeish, C. J. G. Plummer, and A. M. Donald, "Crazing by disentanglement: non-diffusive reptation," *Polymer*, **30**, 1651 (1989).

5 I. M. Ward and D. W. Hadley, *An Introduction to the Mechanical Properties of Solid Polymers*, John Wiley & Sons, Inc., New York (1993)

6 L. H. Sperling, *Introduction to Physical Polymer Science, 2nd edition*, John Wiley & Sons, Inc., New York (1992)

7 J.C. Arnold, "Environmental stress crack initiation in glassy polymers," *Trends in Polymer Science (UK)*, **4**, n12, 403 (1996)

8 M. Ishikawa and H. Takahashi, "Crazing mechanism based on plastic instability," *Journal of Materials Science*, **26**, 1295 (1991)

9 J. Liu and A.F. Yee, "Effect of local conformational transition on craze initiation in polyestercarbonates containing cyclohexylene linkages," *Macromolecules*, **33**, 1338 (2000)

10 A.L. Volynskii and N.F. Bakeev, *Solvent Crazing of Polymers*, Elsevier, NY (1995)

11 G.J. Salomons, M.A. Singh, T. Bardouille, W.A. Foran, and M.S. Capel, "Small-angle x-ray scattering study of craze formation and dynamics in thermoplastics," *Macromolecules*, **32**, 1264 (1999)

12 H.Z.Y. Han, T.C.B. McLeish, R.A. Duckett, N.J. Ward, A.F. Johnson, A.M. Donald, and M. Butler, "Experimental and theoretical studies of the molecular motions in polymer crazing. 1. Tube model," *Macromolecules*, **31**, 1348 (1998)

13 S. S. Sternstein and L. Ongchin, "Yield criteria for plastic deformation of glassy high polymers in general stress fields," *Polymer Preprints*, American Chemical Society, Division of Polymer Chemistry, **10**, n2, 1117 (1969)

14 A. N. Gent, "Hypothetical mechanism of crazing in glassy plastics," *Journal of Materials Science*, **5**, 925 (1970)

15 J.C. Arnold and J.E. Taylor, "Improved thermodynamic approach for predicting the ESC behavior of polycarbonate in binary liquid mixtures," *Journal of Applied Polymer Science (USA)*, **71**, n13, 2155 (1999)

16 J.C. Arnold, "The effects of diffusion on environmental stress crack initiation in PMMA," *Journal of Materials Science (UK)*, **33**, n21, 5193 (1998)

17 X. Qin and W.V. Chang, "The role of interfacial free energy in wettability, solubility, and solvent crazing of some polymeric solids," *Journal of Adhesion Science and Technology (Netherlands)*, **10**, n10, 963 (1996)

18 R. P. Kambour, "Crazing," *Concise Encyclopedia of Polymer Science and Engineering,* ed. J. I Kroschwitz, Wiley-Interscience, NY (1990) 210-211

19 M. Kotoul, "Micromechanical and thermodynamical aspects of environmental crazing," *Journal of Materials Science (UK)*, **31**, n13, 3333 (1996)

20 K. Iisaka, M. Hayama, and A. Fukami, "Dependence of solvent crazing in bisphenol-A polycarbonate on molecular weight of organic liquids," *Journal of Macromolecular Science - Physics,* **B27**, n4, 385 (1988).

21 L. Josserand, R. Schirrer, and P. Davies, "Influence of water on crack propagation in polymethyl methacrylate: craze stress and craze fibril lifetime," *Journal of Materials Science*, **30**, 1772 (1995)

22 M. Notomi, K. Kishimoto, T. Shibuya, and T. Koizumi, "Effects of moisture absorption on fracture behaviors of acrylonitrile-butadiene-styrene resin," *Journal of Applied Polymer Science*, **72**, 435 (1999)

23 J. C. Devins and C. W. Reed, "Crazing of glassy polymers in oil-impregnated cables," *1970 Annual Report Conference on Electrical Insulation and Dielectric Phenomena*, National Academy of Sciences, Washington, D.C., 86 (1971)

24 M. M. Qayyum and J. R. White, "Weathering of injection-moulded glassy polymers: changes in residual stress and fracture behavior," *Journal of Materials Science*, **20**, 2557 (1985)

25 A. Ram, O. Zilber, and S. Kenig, "Residual stresses and toughness of polyethylene plastics," *Polymer Engineering and Science*, **25**, 577 (1985)

26 M. M. Qayyum and J. R. White, "Effect of water absorption and temperature gradients on polycarbonate injection moldings," *Journal of Applied Polymer Science*, **43**, 129 (1991)

27 C. J. G. Plummer, and A. M. Donald, "The deformation behavior of polyethersulfone and polycarbonate," *Journal of Polymer Science: Part B: Polymer Physics*, **27**, 325 (1989).

28 G. O. Shonaike and P. E. Reed, "The effect of cold rolling on crazing of polycarbonate," *Materials Science and Engineering*, **A119**, 231 (1989).

29 S.A. Xu and S.C. Tjong, "Tensile deformation mechanisms of the blends of polycarbonate with poly(methyl methacrylate)," *European Polymer Journal (USA)*, **34**, n8, 1143 (1998)

30 C.Y. Tang, L.C. Chan, M. Jie, and C.H. Yu, "Prediction of the effect of craze damage on apparent elastic properties of polystyrene by FEM," *Key Engineering Materials (Switzerland)*, **145-149**, n1, 249 (1998)

31 D.A. Skoog and J.J. Leary, *Principles of Instrumental Analysis, 4th ed.*, Harcourt Brace College Publishers, NY, 568 (1992)

32 P. C. Hiemenz, *Polymer Chemistry: The Basic Concepts*, Marcel Dekker, Inc. NY (1984)

33 H. Marand, *Physical Chemistry of Polymers* class notes (2000)

34 P. Rempp and E.W. Merrill, *Polymer Synthesis*, Huthig and Wepf Verlag, Postfach, Germany (1986)

35 http://www.technika.com/hum.htm (2000)

36 http://www.natmus.dk/cons/tp/satslt/satsol.hum (2000)

37 L. Greenspan, "Humidity fixed points of binary saturated aqueous solutions," *Journal of Research of the National Bureau of Standards – A. Physics and Chemistry*, **81A**, n1, 89, Jan-Feb (1977)

38 D. G. Legrand, "Thermochemical stress crazing and cracking of thermoplastics," *Journal of Applied Polymer Science*, **52**, 1933 (1994).

39 H. Cornèlis and R. G. Kander, "A new method to evaluate solvent stress cracking," *Polymer Engineering and Science*, **36**, n 6, 869 (1996).

40 G.M. Gusler and G.B. McKenna, "The effect of physical aging on the crazing behavior of polystyrene," *ACS Polymer Preprints (USA)*, **36**, n2, 63 (1995)

41 C. J. G. Plummer, C. L. Soles, C. Xiao, J. Wu, H.-H. Kausch, and A. F. Yee, "Effect of limiting chain mobility on the yielding and crazing behavior of bisphenol-A polycarbonate derivatives," *Macromolecules*, **28**, 7157 (1995).

42 H. Kawabe, Y. Natsume, Y. Higo, and S. Nunomura, "Non-destructive evaluation of the micromechanism of the deformation process during tensile tests on polymers by the elastic-wave transfer function method," *Journal of Materials Science*, **29**, 1004 (1994).

43 H.X.Y. Han, R.A. Duckett, T.C.B. McLeish, N.J. Ward, and A.F. Johnson, "A molecular model for crazing mechanisms in glassy polymers," ACS *Conference: Polymeric Materials Science and Engineering*, Spring Meeting, San Francisco, **76**, 257 (1997)

44 H. A. Hristov, A. F. Yee, and D. W. Gidley, "Fatigue craze initiation in polycarbonate: study by transmission electron microscopy," *Polymer*, **35**, n17, 3607 (1994).

45 J. E. Taylor and J. C. Arnold, "Environmental stress cracking of polycarbonate in mixed environments," *Key Engineering Materials*, **118-119**, 59 (1996).

46 C. Hockings, "Crazing inspection of acrylic cabin windows – A practical approach," presented to the Air Transport Association of America Non-Destructive Testing Forum, Albuquerque, New Mexico, Nov. 1-3, 1994.

47 H. L. Task, U. S. Patent # 5,557,403 "System and method for measuring crazing in a transparency," (1996).

48 J. C. Arnold, "The influence of liquid uptake on environmental stress cracking of glassy polymers," *Materials Science and Engineering*, **A197**, 119 (1995).

49 J. C. Arnold, "Craze initiation during the environmental stress cracking of polymers," *Journal of Materials Science (UK)*, **30**, n3, 655 (1995).

50 ASTM Standard D638-95, "Standard test method of tensile properties of plastics," *Annual Book of ASTM Standards*, **08.01**, 47 (1996)

51 *SigmaScan Pro User's Manual*, Jandel Corporation, San Rafael, CA (1995).

52 S. B. Clay, *Effect Of Ultraviolet Exposure On The Durability Of Polycarbonate*, Master's Thesis, Virginia Polytechnic Institute, (1995)

53 S. R. Schmidt and R. G. Launsby, *Understanding Industrial Designed Experiments*, Air Academy Press, Colorado Springs, Colorado (1994)

54 *Specifications for the Delta Series Thermal Analysis System*, Perkin Elmer DSC manual, Norwalk, CT

55 *Pyris 1 Differential Scanning Calorimeter*, Perkin Elmer pamphlet L-1893, Norwalk, CT (1995)

56 *Perkin-Elmer Delta Series TGA7* Instruction Manual

57 A. A. Gorbunov and A. M. Skvortsov, "Separating power of gel permeation chromatography," *Polymer Science USSR*, **32**, 567 (1990)

58 D. W. Shortt, "Differential molecular weight distributions in high performance liquid chromatography columns," *Journal of Liquid Chromatography*, **16**, 3371 (1993)

59 *DOE Kiss: Keeping it Simple Statistically User's Guide*, Air Academy Press, Colorado Springs, Colorado (1994)

60 T. Ricco and T. L. Smith, "Rate of physical aging of polycarbonate at a constant tensile strain," *Journal of Polymer Science: Part B: Polymer Physics*, **28**, 513 (1990)

61 A. J. Hill, K. J. Heater, and C. M. Agrawal, "The effects of physical aging in polycarbonate," *Journal of Polymer Science: Part B: Polymer Physics*, **28**, 387 (1990)

62 D. E. Nikles and C. E. Forbes, "Accelerated aging studies for polycarbonate optical disk substrates," *Optical Data Storage*, **1499**, 39 (1991)

63 J. D. Ferry, *Viscoelastic Properties of Polymers*, John Wiley and Sons, NY (1980)

64 S. B. Clay, U. S. Patent # 5,905,205 "Biaxial testing apparatus," (1996).

VITA

Stephen Brett Clay was born to Jim and Sharon Clay on December 12, 1969 in Huntington, West Virginia. He graduated from high school in 1988 at Barboursville High School in Barboursville, West Virginia.

Upon graduation from high school, Mr. Clay enrolled at West Virginia Institute of Technology in Montgomery, West Virginia. He graduated with a Bachelor of Science degree in Mechanical Engineering in 1992. He went on to work at INCO Alloys International in Huntington, West Virginia as a laboratory technician in the mechanical testing laboratory.

In the fall of 1993, Mr. Clay entered the Palace Knight program as a civilian employee of the United States Air Force. While in the program, Mr. Clay earned a Master of Science degree in Engineering Mechanics from Virginia Polytechnic Institute and State University in 1995. He went on to work in the Air Force Research Laboratory at Wright Patterson Air Force Base in Dayton, Ohio until 1998 when he returned to Virginia Polytechnic Institute for doctoral work in Engineering Mechanics.

Mr. Clay is married to the former Terry Aretta Legg of Barboursville, West Virginia. He has two wonderful children, Joshua Daniel and Sarah Grace. They plan to live in the Dayton, Ohio area where he will conduct research for the Air Force Research Laboratory at Wright Patterson Air Force Base.

The most important aspect of Mr. Clay's life is God. After accepting Jesus Christ as his personal Savior, he became a member of Antioch Baptist Church in Ona, West Virginia. While in college, he attended and served God at Gateway Baptist Church in Blacksburg, Virginia.